CWI
P.O. Box 94079, 1090 GB Amsterdam, The Netherlands
Telephone + 31 - 20 592 9333
Telefax + 31 - 20 592 4199
WWW page http://www.cwi.nl/publications_bibl/

CWI is the nationally funded Dutch institute for research in Mathematics and Computer Science.

Numerical methods for steady viscous free-surface flows

E.H. van Brummelen

2000 Mathematics Subject Classification:
Primary: 65N12.
Secondary: 35L65, 35R35, 49M29, 76D05, 76D27, 76T10.

ISBN 90 6196 518 7
NUGI-code: 811

Preface

This tract records the research that I conducted between 1997 and 2001, as a member of the Modelling, Analysis and Simulation group at the Centre for Mathematics and Computer Science (CWI) in Amsterdam. The research presented in this treatise was financially supported by the Maritime Research Institute Netherlands (MARIN) and was performed in a collaboration between CWI and MARIN.

Many people have contributed to the realization of this tract. In particular, I wish to express my gratitude to my promotor Piet Hemker for his helpful critique and for his stimulating zest for work. My supervisor Barry Koren has been very supportive, and I thank him for his understanding as well as our pleasant collaboration. I am grateful to Hoyte Raven of MARIN for his patience in forging our different perspectives into synergy, and the resulting fruitful collaboration. I am indebted to the members of the resistance-and-propulsion group at MARIN for providing valuable help when I adapted their codes for my purposes. I thankfully acknowledge Guus Segal's help in performing the numerical experiments of Chapter 5.

My sojourn at CWI has been a most pleasant one owing to the company of many friendly colleagues.

Delft, December 2002 Harald van Brummelen

Contents

Chapter 1
Introduction

1.1 Motivation

Flows of two distinct adjacent fluids occur in a wide variety of physical systems and engineering applications. The interaction of the fluids at their mutual interface gives rise to a multitude of complex phenomena. In many cases, however, one of the fluids exerts negligible stress on the interface, so that the other fluid can be considered separately. The interface then acts as a free surface, i.e., a boundary of which the position depends on the behavior of the enclosed flow. A specific instance of such a free-surface flow, that is of great practical relevance, is the flow of water underlying air. Accurate prediction of the behavior of free-surface flows is therefore important, e.g., in the assessment and design of immersed structures and vessels, such as ships.

Predictions of the behavior of free-surface flows are made on the basis of models. These models can be constructed at various levels of approximation. A particularly reliable mathematical model of fluid flow is a system of nonlinear partial differential equations, referred to as the Navier–Stokes equations. These equations were formulated independently by Navier (1822) and Stokes (1845). Unfortunately, these equations are too complicated to explicitly extract their solution. It is, however, possible to construct discrete approximations to the solution. The discretization of the differential equations yields a system of nonlinear algebraic equations. The solution of the algebraic system can be formulated in terms of recurrence relations, which are ideally suited to treatment by computers. Consequently, the prosperous development of computers has made it possible to consider increasingly complex flow problems. The investigation of flow problems by means of a computer is called Computational Fluid Dynamics (CFD). Figure 1.1 on the following page displays the steps in the solution of a flow problem by CFD, including some examples.

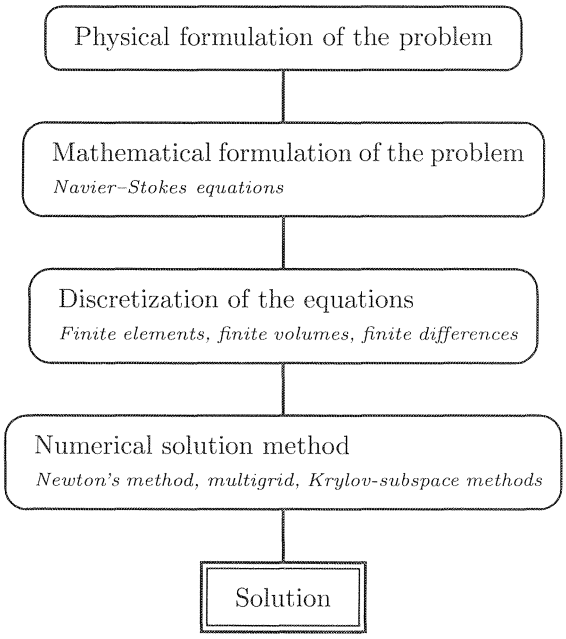

Figure 1.1: Steps in the solution of a flow problem by means of CFD.

The numerical solution of the Navier–Stokes equations with a free boundary has only recently become tractable. Previously, one had to revert to simpler models, for instance, the free-surface potential-flow equations. The free-surface potential flow equations already describe many of the prominent features of free-surface flow. The numerical techniques for these potential-flow equations are well developed, and they are routinely used in the investigation of practical flow problems. However, to include viscous effects, e.g., the interaction between the viscous boundary layer and the free surface near a surface-penetrating object, it is necessary to progress to the Navier–Stokes equations. Unfortunately, many of the numerical techniques for free-surface potential flow cannot be extended straightforwardly to the free-surface Navier–Stokes equations.

An important class of problems for which efficient numerical techniques are available for the potential-flow equations, but not for the Navier–Stokes equations, are *steady* free-surface flows. An example of such a steady free-surface flow is the wave pattern carried by a ship at forward speed in still water. In the field of ship hydrodynamics, dedicated techniques have been developed for solving the steady free-surface potential-flow equations. In contrast, methods for the Navier–Stokes equations typically continue a transient process until a steady state is reached. This time-integration method is often computationally inefficient, due to the specific transient behavior of free-surface flows. Alternative solution methods for

the steady free-surface Navier–Stokes equations exist. However, the performance of these methods usually depends sensitively on the parameters in the problem, or their applicability is too restricted. In general, the numerical solution of the steady free-surface Navier–Stokes equations by current computational methods is prohibitively expensive in actual design processes.

The need for efficient numerical techniques for the steady free-surface Navier–Stokes equations in practical applications, and the inadequacy of available methods, provide the motivation for the research presented in this tract.

1.2 Outline

The contents of this tract are organized as follows:

In Chapter 2 we present the mathematical formulation of free-surface flow. The Navier–Stokes equations are introduced. In addition, we discuss boundary conditions and initial conditions and their relevance for well-posedness of the corresponding initial boundary value problem. Furthermore, we state the interface conditions for two contiguous fluids and we derive the free-surface conditions as a special case.

Chapter 3 contains an analysis of the free-surface Navier–Stokes equations in primitive variables, by means of perturbation methods and Fourier techniques. In contrast to the classical analyses of free-surface flows (e.g., Refs. [42, 46, 65]), we adhere to a formulation of the equations in primitive variables, instead of a vorticity-based formulation. By virtue of the formulation in primitive variables, the analysis can serve in the investigation of numerical methods for the free-surface Navier–Stokes equations, if the differential operators in the continuum equations are replaced by their difference approximation. Moreover, the formulation in primitive variables permits a convenient treatment of the practically relevant case of three spatial dimensions, whereas the classical analyses are restricted to two spatial dimensions due to the properties of the vorticity formulation. The analysis yields important information on the properties of viscous free-surface flows in two and three spatial dimensions, e.g., on the dispersive behavior of surface gravity waves, the asymptotic temporal behavior of wave groups and the structure of the free-surface boundary layer.

In Chapter 4 we propose a novel iterative solution method for solving the steady free-surface Navier–Stokes equations. Moreover, we prove that the usual time-integration approach is generally inappropriate for solving steady free-surface flows. The proposed iterative solution method is analogous to methods for solving steady free-surface potential-flow problems. The method alternatingly solves the steady Navier–Stokes equations with a so-called quasi free-surface condition imposed at the free surface, and adjusts the free surface on the basis of the computed solution. The quasi free-surface condition ensures that the disturbance induced by the subsequent displacement of the boundary is negligible. Each surface adjustment then yields an improved approximation to the actual free-boundary position.

To establish the efficiency of the method, we show that its convergence behavior is asymptotically independent of the mesh width of the applied grid. The asymptotic computational complexity (computational cost per grid point) of the method deteriorates only moderately with decreasing mesh width. Mesh width independence of the computational complexity can be achieved by means of nested iteration. Numerical experiments and results are presented for a two-dimensional test case.

In Chapter 5 we consider an alternative approach to solving steady free-surface flow problems, viz., the optimal shape design method. A general characteristic of free-boundary problems is that the number of free-boundary conditions is one more than the number of boundary conditions required by the governing boundary value problem. A free-boundary problem can therefore be reformulated into the equivalent shape optimization problem of finding the boundary that minimizes a norm of the residual of one of the free-surface conditions, subject to the boundary value problem with the remaining free-surface conditions imposed. Such optimal shape design problems can in principle be solved efficiently by means of the adjoint method. Chapter 5 investigates the suitability of the adjoint shape optimization method for solving steady free-surface flow problems. Because inviscid, irrotational flow adequately describes the prominent features of free-surface flow, we base our investigation on the free-surface potential-flow equations. The adjoint shape optimization method is equally applicable to the free-surface Navier–Stokes equations, but the specifics of the method are in that case much more involved. Our investigation serves as an indication of the properties of the adjoint shape optimization method for steady free-surface flows. We formulate the optimal shape design problem associated with steady free-surface potential flow, and we examine the properties of the optimization problem. In addition, we analyze the convergence behavior of the adjoint method, by means of Fourier techniques. Motivated by the results of the analysis, we address preconditioning for the optimization problem. Numerical experiments and results are presented for a two-dimensional model problem.

Chapter 6 presents a preliminary investigation of the interface capturing approach to solving free-surface flow problems. Free-surface flows form a specific class of two-fluid flow. If the objective is the numerical solution of a free-surface flow problem, then it can be attractive to adhere to the underlying two-fluid flow formulation. In the absence of viscosity, two-fluid flow is described by a system of hyperbolic conservation laws. The numerical techniques for such systems of hyperbolic conservation laws are well developed and, in particular, efficient algorithms are available for solving steady hyperbolic problems. In Chapter 6 we present the prerequisites for a Godunov-type interface capturing method. We consider an Osher-type approximate Riemann solver and we elaborate its application to two-fluid flows. Moreover, we address the spurious pressure oscillations that are commonly incurred by conservative discretizations of two-fluid flows, and we construct a non-oscillatory conservative discretization. The implementation of the interface capturing approach with efficient techniques for steady problems is deferred to future research.

Chapter 2
Mathematical Description of Free-Surface Flow

2.1 Introduction

Flows of two distinct, contiguous fluids are encountered in many practical applications. A free-surface flow is a particular instance of such a two-fluid flow, in which the properties of the fluids are such that one fluid exerts negligible stress on the other. A model for free-surface flow is therefore included in a model for two-fluid flow. The mathematical model for two-fluid flow comprises governing equations for fluid flow and interface conditions, which describe the interaction of contiguous fluids at their interface. In this chapter we present the governing equations for fluid flow and the interface conditions for two-fluid flow, and we derive the free-surface conditions from the general interface conditions.

2.2 Governing Equations for Fluid Flow

2.2.1 Conservation Laws

Fluid flows are presumed to be governed by *conservation laws*. These conservation laws state that mass, momentum and energy are conserved during the motion of the fluid. To model a fluid flow, the state of the flow is described by a set of designated fluid-properties called the *state variables*, e.g., velocity, pressure, density, etc. The conserved quantities can be expressed in these state variables. The mathematical description of the conservation laws for the derived quantities is a system of partial differential equations for the state variables.

To present the governing equations for fluid flow, we consider a volume of fluid. The fluid occupies an open domain $\mathcal{V} \subset \mathbb{R}^d$ $(d = 2, 3)$. Positions in $\mathcal{V}$ are identified by spatial coordinates $(x_1, \ldots, x_d)$ relative to the horizontal Cartesian base vectors $\mathbf{e}_1, \ldots, \mathbf{e}_{d-1}$ and the vertical Cartesian base vector $\mathbf{e}_d$. The gravi-

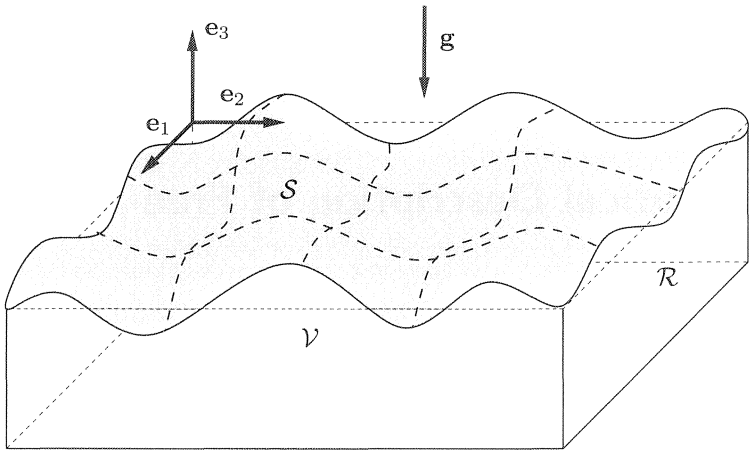

Figure 2.1: Schematic illustration of the free-surface flow problem.

tational acceleration, $\mathbf{g}$, is constant and vertically downward, i.e., $\mathbf{g} = -g\mathbf{e}_d$ for some constant $g \geq 0$. See Figure 2.1 for an illustration.

Suitable state variables for a viscous, compressible fluid are the velocity, the pressure, the density, the temperature and the internal energy of the fluid. Denoting time by $t \geq 0$, we identify the velocity by $\mathbf{v}(\mathbf{x}, t)$, the pressure by $p(\mathbf{x}, t)$, the density by $\rho(\mathbf{x}, t)$, the temperature by $T(\mathbf{x}, t)$ and the internal energy per unit mass by $e(\mathbf{x}, t)$. The total energy is defined by $E := \rho(e + |\mathbf{v}|^2/2)$. Conservation of mass, momentum and energy is then expressed by, respectively,

$$\frac{\partial}{\partial t}\rho + \operatorname{div}(\rho\mathbf{v}) = 0\,, \qquad \mathbf{x} \in \mathcal{V}, t > 0\,, \tag{2.1a}$$

$$\frac{\partial}{\partial t}\rho\mathbf{v} + \operatorname{div}(\rho\mathbf{v}\mathbf{v} + p\mathbb{I} - \boldsymbol{\tau}) - \rho\mathbf{g} = 0\,, \qquad \mathbf{x} \in \mathcal{V}, t > 0\,, \tag{2.1b}$$

$$\frac{\partial}{\partial t}E + \operatorname{div}\big((E+p)\mathbf{v} - \mathbf{v}\cdot\boldsymbol{\tau} - k\nabla T\big) - \rho\mathbf{v}\cdot\mathbf{g} = 0\,, \qquad \mathbf{x} \in \mathcal{V}, t > 0\,, \tag{2.1c}$$

with k the thermal conductivity of the fluid. The tensor $\boldsymbol{\tau}$ in (2.1b) is called the *viscous stress tensor*. In the absence of $\boldsymbol{\tau}$ and k, the equations (2.1) are called the *Euler equations*.

The velocity vector can be represented by d Cartesian components $v_j := \mathbf{v}\cdot\mathbf{e}_j$. Similarly, the viscous stress tensor has d^2 Cartesian components τ_{ij}. Hence, the unknowns in (2.1) are ρ, v_j $(j = 1, \ldots, d)$, p, T, e and τ_{ij} $(i, j = 1, \ldots, d)$, and their number is $d^2 + d + 4$. The momentum equations (2.1b) can be separated into d independent conditions. Hence, (2.1) specifies $d + 2$ relations. Closure of the system of equations therefore requires $d^2 + 2$ supplementary relations. These relations are provided by a *constitutive relation*, which relates the viscous stress

tensor to the state variables, and two additional *equations of state*, which give a mutual relation between the state variables; see also [77].

A common constitutive relation for the viscous stress tensor is (see, for instance, Ref. [6])

$$\boldsymbol{\tau} := \mu \left((\nabla \mathbf{v}) + (\nabla \mathbf{v})^T - \tfrac{2}{3} (\operatorname{div} \mathbf{v})\, \mathbf{I} \right), \tag{2.1d}$$

where μ is the dynamic viscosity of the fluid. A fluid with constitutive relation (2.1d) for the viscous stress tensor is called a *Newtonian fluid*. The momentum equations (2.1b) with $\boldsymbol{\tau}$ according to (2.1d) are called the *Navier–Stokes equations*.

The flows considered in the sequel have a constant temperature and internal energy. The considered fluid either satisfies a barotropic equation of state $p := p(\rho)$, or it is homogeneous and incompressible, i.e., ρ is constant and $\mathbf{v}$ is solenoidal. In both cases, conservation of mass and momentum implies conservation of energy, and (2.1c) is redundant.

2.2.2 Dimensionless Equations

It is often convenient to express the quantities that are used to describe the flow problem on scales that are relevant for the considered problem. For example, an appropriate reference length for flow around a ship hull is the length of the hull. For the considered fluid flows, three independent reference scales can be assigned, viz., a reference length L_0, a reference velocity V_0 and a reference density ρ_0. All other scales in the problem are then implicitly defined, e.g., the implied time scale is L_0/V_0.

Let L_0, V_0 and ρ_0 denote a suitable reference length, velocity and density, respectively. We introduce the dimensionless variables

$$\mathbf{x}' := \mathbf{x}/L_0, \quad t' := t\, V_0/L_0, \quad \mathbf{v}' := \mathbf{v}/V_0, \quad \rho' := \rho/\rho_0 \quad p' := (p - p_0)/\rho_0 V_0^2, \tag{2.2}$$

with p_0 a reference pressure, typically, the atmospheric pressure. The dimensionless form of the Navier–Stokes equations is obtained by inserting (2.2) into (2.1b), (2.1d). Upon omitting the primes, we obtain

$$\frac{\partial}{\partial t} \rho \mathbf{v} + \operatorname{div} \left(\rho \mathbf{v}\mathbf{v} + p\mathbf{I} - \boldsymbol{\tau} \right) + \rho \mathrm{Fr}^{-2} \mathbf{e}_d = 0, \qquad \mathbf{x} \in \mathcal{V}, t > 0\,, \tag{2.3a}$$

with $\boldsymbol{\tau}$ the dimensionless viscous stress tensor,

$$\boldsymbol{\tau} := \mathrm{Re}^{-1} \left((\nabla \mathbf{v}) + (\nabla \mathbf{v})^T - \tfrac{2}{3} (\operatorname{div} \mathbf{v})\, \mathbf{I} \right), \tag{2.3b}$$

and

$$\mathrm{Re} := \frac{\rho_0 V_0 L_0}{\mu}\,, \qquad \mathrm{Fr} := \frac{V_0}{\sqrt{g L_0}}\,. \tag{2.3c}$$

The dimensionless numbers Re and Fr are called the *Reynolds number* and the *Froude number*, respectively. The Reynolds number is the ratio of inertial and

viscous forces in the flow. The Froude number is the ratio of the reference velocity over the velocity of a particular gravity wave, viz., a sinusoidal wave with dimensionless wave-number one in a fluid of infinite depth. In the absence of free-surface stresses, such as surface tension, the parameters Re and Fr are the distinguishing parameters for a viscous flow subject to gravity.

2.2.3 Additional Conditions and Well-Posedness

To complete the description of a flow problem, the governing equations (2.1) must be provided with additional conditions. The additional conditions specify conditions which the state variables must satisfy at the boundaries of the considered space–time domain. In general, we can distinguish *initial conditions* and *boundary conditions*. The partial differential equations (2.1) and the additional conditions form an *initial boundary value problem*.

The properties of an initial boundary value problem depend critically on the additional conditions. In particular, the additional conditions determine whether a boundary value problem is well posed or ill posed. An initial boundary value problem is said to be well posed if it possesses the following properties:

Existence: a solution exists,

Uniqueness: the solution is unique,

Stability: the solution is stable,

and ill posed otherwise. The stability requirement implies that the solution can be bounded in terms of the right-hand side of the differential equations and of the additional conditions (in some appropriate sense).

Only in specific cases has it been established that initial boundary value problems from fluid dynamics are well posed. A detailed discussion of additional conditions and of existence, uniqueness and stability of initial boundary value problems is beyond the scope of our research. Relevant references on the subject of additional conditions and posedness include, e.g.: [70, 71] for homogeneous, incompressible fluids, [62] for non-homogeneous incompressible fluids, [41] for boundary conditions for hyperbolic systems with constant or variable coefficients, and [17] for absorbing boundary conditions on truncated spatial domains.

2.3 Interface Conditions

2.3.1 Two-Fluid Flow Interface Conditions

We consider a flow of two distinct contiguous fluids, separated by an interface. Equations (2.1) describe the behavior of the flow in each of the fluids. At the interface, the state variables must comply with interface conditions. These interface conditions provide a relation between the state variables of the contiguous fluids.

The interface conditions consist of kinematic and dynamic conditions. The kinematic conditions are related to the continuity of velocity of the fluids at the interface. The dynamic conditions express conservation of momentum at the interface. A detailed model for the behavior of fluid interfaces and the corresponding interface conditions are presented in [5, 58]. Without additional assumptions on the properties of the interface, the dynamic conditions depend in a complicated manner on the geometry of the interface. To simplify the dynamic interface conditions, we assume that the contributions of interface viscosity, interface tension and interface density to the dynamic conditions are negligible. These assumptions are valid in many practical applications.

To present the interface conditions, we consider an interface $\mathcal{S}$ between the two contiguous fluids. One fluid is designated the primary fluid and the other fluid the secondary fluid. Denoting the unit normal vector to $\mathcal{S}$ from the primary to the secondary fluid by $\mathbf{n}(\mathbf{x}, t)$, we define

$$\mathbf{x}^{\pm} := \lim_{\epsilon \downarrow 0} \mathbf{x} \pm \epsilon \mathbf{n} \,, \tag{2.4}$$

i.e., $\mathbf{x}^-$ and $\mathbf{x}^+$ are at the interface in the primary and secondary fluid, respectively. Under the aforementioned assumptions, the stresses exerted on the interface by the primary and secondary fluid must cancel:

$$-\mathbf{n} \cdot (p\mathbf{I} - \boldsymbol{\tau})\Big|_{\mathbf{x}^-}^{\mathbf{x}^+} = 0 \,. \tag{2.5}$$

Conditions (2.5) are called the *dynamic interface conditions*. In equation (2.5), we can distinguish d separate conditions. If $\mathbf{t}_j(\mathbf{x}, t)$ $(j = 1, \ldots, d-1)$ are orthogonal tangent vectors to $\mathcal{S}$, the inner product of (2.5) and $\mathbf{t}_j$ yields $d-1$ conditions:

$$\mathbf{t}_j \cdot \boldsymbol{\tau} \cdot \mathbf{n}\Big|_{\mathbf{x}^-}^{\mathbf{x}^+} = 0 \,, \qquad j = 1, \ldots, d-1. \tag{2.6a}$$

Conditions (2.6a) prescribe continuity of shear stresses across the interface. These conditions are called the tangential dynamic conditions. The inner product of (2.5) and $\mathbf{n}$ yields:

$$-(p - \boldsymbol{\tau} : \mathbf{nn})\Big|_{\mathbf{x}^-}^{\mathbf{x}^+} = 0 \,. \tag{2.6b}$$

This condition is called the normal dynamic condition.

The kinematic conditions for the interface prescribe that the flow velocity is continuous across the interface:

$$\mathbf{v}\Big|_{\mathbf{x}^-}^{\mathbf{x}^+} = 0 \,, \tag{2.7a}$$

and that the interface moves with the local flow velocity. The latter implies that if the interface position is written in parametric form as

$$\mathcal{S} := \{\mathbf{x} \in \mathbb{R}^d : \mathbf{x} = \mathbf{X}(\mathbf{y}, t)\}$$

Table 2.1: Appropriate number of interface conditions n, for different combinations of the contiguous fluids in a two-fluid flow in $\mathbb{R}^d$.

combination	n
viscous /viscous	$2d+1$
viscous /inviscid	$d+2$
inviscid/inviscid	3

with $\mathbf{y} \in \mathbb{R}^{d-1}$, then

$$\frac{\partial \mathbf{X}(\mathbf{y},t)}{\partial t} = \mathbf{v}(\mathbf{X}(\mathbf{y},t),t)\,. \tag{2.7b}$$

Note that the velocity at the interface is uniquely defined by virtue of (2.7a).

The interface conditions (2.6) and (2.7) are only valid if both fluids are viscous. If either of the fluids is inviscid, the kinematic conditions (2.7) must be modified. The continuity condition (2.7a) then only applies in the direction normal to the interface, i.e.,

$$\mathbf{n}\cdot\mathbf{v}\Big|_{\mathbf{x}^-}^{\mathbf{x}^+} = 0\,, \tag{2.8a}$$

and only the normal velocity of the interface is prescribed:

$$\mathbf{n}\cdot\frac{\partial \mathbf{X}}{\partial t} = \mathbf{n}\cdot\mathbf{v}\,. \tag{2.8b}$$

Moreover, the tangential dynamic conditions then imply that the shear stress of the viscous fluid must vanish at the interface.

If both fluids are inviscid, the dynamic conditions are modified as well. In that case, the tangential dynamic conditions (2.6a) are discarded and the normal dynamic condition reduces to:

$$-p\Big|_{\mathbf{x}^-}^{\mathbf{x}^+} = 0\,. \tag{2.9}$$

Condition (2.9) states that the pressure is continuous across the interface.

The above implies that the number of interface conditions depends on the properties of the contiguous fluids. Table 2.1 lists the appropriate number of interface conditions for different combinations of the contiguous fluids.

2.3.2 Free-Surface Conditions

A free surface can be regarded as a particular instance of an interface, in which the stresses exerted on the interface by one fluid are negligible on a reference scale that is appropriate for the other. This occurs if the difference in densities of the contiguous fluids is large.

In order to derive the free-surface conditions from the general interface conditions, we consider a flow of two adjacent fluids with different densities. Let ρ_0^- and

ρ_0^+ denote the reference densities for the primary and secondary fluid, respectively, and let V_0 be a suitable reference velocity for the flow. The derived reference stress $\rho_0^+ V_0^2$ is suitable for the secondary fluid if moderate constants $\underline{c}_j$ and $\overline{c}_j$ $(j = 1, 2)$ exist such that

$$\underline{c}_1 \leq \frac{\|p - p_0\|}{\rho_0^+ V_0^2} \leq \overline{c}_1 \,, \qquad \underline{c}_2 \leq \frac{\|\boldsymbol{\tau}\|}{\rho_0^+ V_0^2} \leq \overline{c}_2 \,, \tag{2.10}$$

with $\|\cdot\|$ the maximum norm of $\cdot$ in the secondary fluid for all $t > 0$. Equation (2.10) is expressed with respect to the reference stress $\rho_0^- V_0^2$, which is suitable for the primary fluid, by

$$\underline{c}_1\left(\frac{\rho_0^+}{\rho_0^-}\right) \leq \frac{\|p - p_0\|}{\rho_0^- V_0^2} \leq \overline{c}_1\left(\frac{\rho_0^+}{\rho_0^-}\right) , \qquad \underline{c}_2\left(\frac{\rho_0^+}{\rho_0^-}\right) \leq \frac{\|\boldsymbol{\tau}\|}{\rho_0^- V_0^2} \leq \overline{c}_2\left(\frac{\rho_0^+}{\rho_0^-}\right) . \tag{2.11}$$

This implies that if the density ratio ρ_0^+/ρ_0^- is small, the deviation from $p_0\mathbf{n}$ of the stress exerted on the interface by the secondary flow is insignificant for the primary flow. The primary flow is then independent of the secondary flow and, moreover, the motion of the interface depends exclusively on the primary flow. In this case, the interface is called a free surface (or free boundary) of the primary flow.

The free-surface conditions follow from the general interface conditions under the assumption that the secondary flow is inviscid and exerts a constant pressure on the interface. The dynamic free-surface conditions follow immediately from (2.5): in dimensionless form,

$$\mathbf{n} \cdot (p\mathbf{I} - \boldsymbol{\tau}) = 0 \,, \qquad \mathbf{x} \in \mathcal{S}, t > 0 \,, \tag{2.12}$$

with p and $\boldsymbol{\tau}$ the dimensionless pressure and viscous stress tensor,, respectively. The kinematic condition (2.8b) describes the motion of the free surface. Condition (2.8b) can be recast into a convenient form, if the free surface is represented as a level set:

$$S := \{\mathbf{x} \in \mathbb{R}^d : \psi(\mathbf{x}, t) = 0\} \,. \tag{2.13}$$

The kinematic free-surface condition can then be recast into

$$\frac{\partial \psi}{\partial t} + \mathbf{v} \cdot \boldsymbol{\nabla} \psi = 0 \,, \qquad \mathbf{x} \in \mathcal{S}, t > 0 \,. \tag{2.14}$$

In the absence of overturning waves, the free surface is often represented by a height function of the horizontal coordinates. If $\eta(x_1, \ldots, x_{d-1}, t)$ denotes the height of the surface with respect to some fixed reference surface, then the corresponding level set is $\psi(\mathbf{x}, t) = \eta(x_1, \ldots, x_{d-1}, t) - x_d$. The kinematic condition then assumes the familiar form:

$$\frac{\partial \eta}{\partial t} + \sum_{j=1}^{d-1} v_j \frac{\partial \eta}{\partial x_j} - v_d = 0 \,, \qquad \mathbf{x} \in \mathcal{S}, t > 0 \,. \tag{2.15}$$

Equations (2.8b), (2.14) and (2.15) are different formulations of the condition that the free surface moves in its normal direction with the normal component of the local flow velocity.

2.4 Problem Statement

We are concerned with the steady flow of water underlying air. The ratio of the density of air to the density of water is sufficiently small to treat the water–air interface as a free surface. Moreover, for our purposes, water can be treated as a homogeneous, incompressible, viscous fluid.

To formulate the free-surface flow problem, let $\mathcal{V}$ denote the volume occupied by the water, $\partial\mathcal{V}$ its boundary, $\mathcal{S}$ the free surface and $\mathcal{R} = \partial\mathcal{V} \setminus \mathcal{S}$ the rigid boundary; see Figure 2.1 on page 6. The steady free-surface flow problem is described by the aforementioned equations with the partial derivatives with respect to t omitted. Because the water is assumed to be homogeneous and incompressible, the density can be removed from the dimensionless governing equations. The steady free-surface flow problem is then stated as: Given the rigid boundary $\mathcal{R}$, find $\mathcal{S}$ and $\mathbf{v} : \overline{\mathcal{V}} \mapsto \mathbb{R}^d$ and $p : \overline{\mathcal{V}} \mapsto \mathbb{R}$ such that:

$$\operatorname{div}\left(\mathbf{v}\mathbf{v} + p\mathbf{I} - \boldsymbol{\tau}\right) = -\mathrm{Fr}^{-2}\mathbf{e}_d\,, \qquad \mathbf{x} \in \mathcal{V}\,, \tag{2.16a}$$

$$\operatorname{div}\mathbf{v} = 0\,, \qquad \mathbf{x} \in \mathcal{V}\,, \tag{2.16b}$$

with the viscous stress tensor $\boldsymbol{\tau}$ according to (2.3b), subject to the free-surface conditions

$$\mathbf{n}\cdot(p\mathbf{I} - \boldsymbol{\tau}) = 0\,, \qquad \mathbf{x} \in \mathcal{S}\,, \tag{2.17a}$$

$$\mathbf{n}\cdot\mathbf{v} = 0\,, \qquad \mathbf{x} \in \mathcal{S}\,, \tag{2.17b}$$

and the *rigid-boundary conditions* on $\mathcal{R}$.

The above problem statement contains the envisaged problem. However, to facilitate the investigation of numerical techniques, in the ensuing sections we will also consider closely related problems, e.g., the two-fluid compressible Euler equations or the steady free-surface potential flow equations.

Chapter 3

Analysis of Viscous Free-Surface Flow in Primitive Variables

3.1 Introduction

Flows that are partially bounded by a freely moving boundary occur in many practical applications, for instance, ship hydrodynamics, hydraulics and coating technology. Classically, free-surface flow problems have been examined by means of perturbation methods and Fourier techniques; see, e.g., Refs. [42, 46, 65]. These analyses are restricted to generic problems, such as perturbations of a uniform flow. However, these generic problems already contain important information on the general properties of free-surface flow problems. Presently, computational methods play an important role in the analysis of free-surface flow problems that occur in actual engineering applications.

The analysis of numerical methods for (initial) boundary value problems generally proceeds in the same manner as the classical analyses based on perturbation methods and Fourier techniques. The differential operators in the continuum problem are then replaced by their difference approximation. The familiar von Neumann stability analysis (see, for instance, Refs. [27, 53, 77]) is in fact an application of perturbation methods and Fourier techniques to difference equations. The analyses are important in the assessment of the stability of discretizations and of the convergence behavior of numerical solution methods.

It appears that an analysis of viscous free-surface flow problems in primitive variables, i.e., velocity and pressure, is not available. The classical analyses of viscous free-surface flows [42] and, in a more general context, stratified flows [28] adopt a vorticity-based formulation of the flow equations. Recent investigations of viscous free-surface flows (e.g., Ref. [16]) maintain this formulation. This outset has two disadvantages. Firstly, these analyses are generally inappropriate for the investigation of numerical methods, because most numerical methods for viscous free-surface flow problems treat the flow equations in primitive variables. Secondly,

the analyses are restricted to two spatial dimensions and, due to the properties of the vorticity formulation (see, e.g., Ref. [20]), cannot be straightforwardly extended to include the practically relevant case of three spatial dimensions.

In this chapter we present an analysis of the viscous free-surface flow equations in primitive variables. We consider the generic problem of perturbations in a uniform horizontal flow of finite depth in two- and three spatial dimensions. Only first-order perturbations are considered. Our primary interest is in the application of the analysis to the assessment of numerical methods for the viscous free-surface flow problem. However, this application is not currently presented. The presented analysis has *raison d'être* independently, as it yields important information on the properties of viscous free-surface flows in three spatial dimensions. Classical results in two spatial dimensions are included as a special case. The results concern the dispersive behavior of surface gravity waves, the asymptotic temporal behavior of wave groups, and the structure and properties of the free-surface boundary layer.

3.2 Statement of Objectives

We consider the dimensionless Navier–Stokes equations for an incompressible homogeneous fluid subject to gravity. The velocity being solenoidal, $\operatorname{div}\boldsymbol{\tau} = \mu\Delta\mathbf{v}$, with $\mu := 1/\mathrm{Re}$. Hence, we consider

$$\mathbf{v}_t + \operatorname{div}\mathbf{v}\mathbf{v} + \nabla p - \mu\Delta\mathbf{v} = -\mathrm{Fr}^{-2}\mathbf{e}_d\,, \qquad \mathbf{x}\in\mathcal{V}_\eta, t>0\,, \tag{3.1a}$$

$$\operatorname{div}\mathbf{v} = 0\,, \qquad \mathbf{x}\in\mathcal{V}_\eta, t>0\,. \tag{3.1b}$$

The considered spatial domain $\mathcal{V}_\eta$ is defined by

$$\mathcal{V}_\eta := \{\mathbf{x}\in\mathbb{R}^d : -\infty < x_1,\ldots,x_{d-1} < +\infty, -1 < x_d < \eta\}, \tag{3.2}$$

with $\eta := \eta(x_1,\ldots,x_{d-1},t)$. The domain $\mathcal{V}_\eta$ is bounded by the moving boundary $\mathcal{S}_\eta := \{x_d = \eta\}$ and the rigid boundary $\mathcal{R} := \{x_d = -1\}$.

At the boundary $\mathcal{R}$ we impose the free-slip boundary conditions:

$$\mathbf{e}_d\cdot\mathbf{v} = 0\,, \qquad \mathbf{e}_d\cdot\left((\nabla\mathbf{v}) + (\nabla\mathbf{v})^T\right)\cdot\mathbf{e}_j = 0\,, \qquad \mathbf{x}\in\mathcal{R}, t>0\,, \tag{3.3}$$

with $j = 1,\ldots,d-1$. At $\mathcal{S}_\eta$ the dynamic free-surface conditions are imposed:

$$p - 2\mu\,\mathbf{n}\cdot\nabla\mathbf{v}\cdot\mathbf{n} = 0\,, \qquad \mathbf{n}\cdot\left((\nabla\mathbf{v}) + (\nabla\mathbf{v})^T\right)\cdot\mathbf{t}_j = 0\,, \qquad \mathbf{x}\in\mathcal{S}_\eta, t>0\,, \tag{3.4}$$

with $\mathbf{n}$ the unit normal vector to $\mathcal{S}_\eta$ and $\mathbf{t}_j$, $j = 1,\ldots,d-1$, orthogonal unit tangential vectors to $\mathcal{S}_\eta$. Moreover, the vertical displacement η of the moving boundary $\mathcal{S}_\eta$ is related to the velocity of the underlying fluid flow by the kinematic condition

$$\eta_t + \mathbf{v}\cdot\nabla\eta - v_d = 0\,, \qquad \mathbf{x}\in\mathcal{S}_\eta, t>0\,. \tag{3.5}$$

The moving boundary $\mathcal{S}_\eta$ is then a free surface.

Equations (3.1)–(3.5) must be supplemented with suitable initial conditions

$$\mathbf{v}(\mathbf{x},0) = \mathbf{v}_0(\mathbf{x}) \,, \qquad p(\mathbf{x},0) = p_0(\mathbf{x}) \,, \qquad \mathbf{x} \in \overline{\mathcal{V}}_\eta \,, \tag{3.6a}$$

with $\overline{\mathcal{V}}_\eta$ the closure of $\mathcal{V}_\eta$, and

$$\eta(\mathbf{x},0) = \eta_0(\mathbf{x}) \,, \qquad \mathbf{x} \in \mathcal{S}_0 \,, \tag{3.6b}$$

with $\mathbf{v}_0$, p_0 and η_0 given.

Our objective it to determine asymptotic solutions of (3.1)–(3.6) in the limit as $\|\eta\| \to 0$, i.e., for small displacements of the free surface. Moreover, we investigate the properties of such solutions.

3.3 Infinitesimal Solutions

3.3.1 Generating Solution

If the initial displacement of the free surface is specified

$$\eta(\mathbf{x},0) = 0 \,, \qquad \mathbf{x} \in \mathcal{S}_0 \,, \tag{3.7a}$$

and the initial conditions (3.6a) are specified

$$\mathbf{v}(\mathbf{x},0) = \mathbf{v}^{(0)} \,, \qquad p(\mathbf{x},0) = -\mathrm{Fr}^{-2} x_d \,, \qquad \mathbf{x} \in \overline{\mathcal{V}}_0 \,, \tag{3.7b}$$

where $\mathbf{v}^{(0)} := (v_1^{(0)}, \ldots, v_{d-1}^{(0)}, 0)$, with $v_1^{(0)}, \ldots, v_{d-1}^{(0)}$ constant velocity components, and $\bar{\cdot}$ denotes closure, then the corresponding solution of (3.1)–(3.6) reads

$$\eta(\mathbf{x},t) = 0 \,, \qquad \mathbf{x} \in \mathcal{S}_0, t \geq 0 \,, \tag{3.8a}$$

and

$$\mathbf{v}(\mathbf{x},t) = \mathbf{v}^{(0)} \,, \qquad p(\mathbf{x},t) = -\mathrm{Fr}^{-2} x_d \,, \qquad \mathbf{x} \in \overline{\mathcal{V}}_0, t \geq 0 \,. \tag{3.8b}$$

The above solution corresponds to a uniform horizontal flow. A uniform horizontal flow is indeed a (steady) solution of the considered free-surface flow problem.

If, instead, the initial displacement of the free surface is specified

$$\eta(\mathbf{x},0) = \epsilon h_0(\mathbf{x}) \,, \qquad \mathbf{x} \in \mathcal{S}_0 \,, \tag{3.9a}$$

with h_0 independent of ϵ, and, accordingly,

$$\mathbf{v}(\mathbf{x},0) = \mathbf{v}_0(\mathbf{x};\epsilon) \,, \qquad p(\mathbf{x},0) = p_0(\mathbf{x};\epsilon) \,, \qquad \mathbf{x} \in \overline{\mathcal{V}}_\eta \,, \tag{3.9b}$$

where $\mathbf{v}_0(\mathbf{x};\epsilon) \to \mathbf{v}^{(0)}$ and $p_0(\mathbf{x};\epsilon) \to -\mathrm{Fr}^{-2} x_d$ as $\epsilon \to 0$, then the corresponding solution of (3.1)–(3.5) approaches (3.8) as $\epsilon \to 0$. In this context, the solution (3.8) is called a *generating solution*.

3.3.2 Infinitesimal Conditions

We consider the free-surface flow problem (3.1)–(3.5), supplemented with the initial conditions (3.9). Motivated by §3.3.1, we assume that as $\epsilon \to 0$ the corresponding perturbed solution can be expanded asymptotically as

$$\eta(\mathbf{x},t;\epsilon) = \sum_{l=1}^{n} \chi_l(\epsilon)\,\eta^{(l)}(\mathbf{x},t) + o(\chi_n)\,, \tag{3.10a}$$

$$v_j(\mathbf{x},t;\epsilon) = v_j^{(0)} + \sum_{l=1}^{n} \psi_l^j(\epsilon)\,v_j^{(l)}(\mathbf{x},t) + o(\psi_n^j)\,, \qquad j=1,\ldots,d\,, \tag{3.10b}$$

$$p(\mathbf{x},t;\epsilon) = -\mathrm{Fr}^{-2}x_d + \sum_{l=1}^{n} \phi_l(\epsilon)\,p^{(l)}(\mathbf{x},t) + o(\phi_n)\,, \tag{3.10c}$$

for all $n = 1,2,\ldots$, with respect to certain uniform asymptotic sequences $\{\psi_l^j(\epsilon)\}$, $j=1,\ldots,d$, $\{\phi_l(\epsilon)\}$ and $\{\chi_l(\epsilon)\}$, with $l=1,2,\ldots$. For a definition of asymptotic sequences and the Landau symbols, o and O, used below, see, e.g., Ref. [39].

The condition that (3.10a) complies with (3.9a) implies that χ_1 must be of $O(\epsilon)$. We choose $\chi_1 = \epsilon$. The functions $\psi_1^j(\epsilon)$ and $\phi_1(\epsilon)$ are required to be of $o(1)$ as $\epsilon \to 0$. We assume that the expansion (3.10) is uniformly valid in $(\mathbf{x},t)$ for $\mathbf{x} \in \mathcal{V}_\eta$ and $t \geq 0$. The representation (3.10) of the solution as an asymptotic series is referred to as a *formal solution*. We refer to the first term in the series expansion as the *infinitesimal perturbation* or the *first-order perturbation*.

Upon inserting (3.10) in (3.1), we obtain

$$\sum_{l=1}^{n}\left(\psi_l^j\left[\frac{\partial v_j^{(l)}}{\partial t} + \sum_{k=1}^{d-1} v_k^{(0)}\frac{\partial v_j^{(l)}}{\partial x_k} - \mu\sum_{k=1}^{d}\frac{\partial^2 v_j^{(l)}}{\partial x_k^2}\right] + \phi_l\,\frac{\partial p^{(l)}}{\partial x_j}\right) + \sum_{l=1}^{n}\sum_{m=1}^{n}\sum_{k=1}^{d}\left(\psi_l^j\psi_m^k v_k^{(m)}\frac{\partial v_j^{(l)}}{\partial x_k}\right) + o(\psi_n^j) + o(\phi_n) = 0\,, \tag{3.11a}$$

and

$$\sum_{j=1}^{d}\left(\sum_{l=1}^{n}\psi_l^j\frac{\partial v_j^{(l)}}{\partial x_j} + o(\psi_n^j)\right) = 0\,, \tag{3.11b}$$

for all $\mathbf{x} \in \mathcal{V}_\eta, t \geq 0$. Because terms of different order in ϵ must vanish separately as $\epsilon \to 0$, (3.11a) implies: (1) that $\psi_l^j = O(\phi_l)$ to maintain a meaningful relation between $\mathbf{v}$ and p; (2) that $\phi_l = O(\phi_1\phi_{l-1}) = O(\phi_1^l)$ to maintain a meaningful relation between successive terms in the expansion. Based on (1), we choose $\psi_l^j = \phi_l$.

The requirement that (3.10) satisfies (3.1)–(3.5) and (3.9) imposes certain conditions on the successive terms in the expansion. The *infinitesimal conditions*, i.e., the conditions which the first-order perturbation must satisfy, are obtained

by inserting the expansion (3.10) in (3.1)–(3.5) and (3.9), and collecting terms of order $O(\phi_1)$.

Collecting terms of order $O(\phi_1)$ in (3.11):

$$\mathbf{v}_t^{(1)} + \mathbf{v}^{(0)} \cdot \nabla \mathbf{v}^{(1)} + \nabla p^{(1)} - \mu \Delta \mathbf{v}^{(1)} = 0 \,, \qquad \mathbf{x} \in \mathcal{V}_\eta, t > 0 \,, \tag{3.12a}$$

$$\operatorname{div} \mathbf{v}^{(1)} = 0 \,, \qquad \mathbf{x} \in \mathcal{V}_\eta, t > 0 \,. \tag{3.12b}$$

Inserting (3.10) in (3.3) and collecting terms of $O(\phi_1)$, the boundary conditions at the rigid boundary $\mathcal{R}$ yield

$$v_d^{(1)} = 0 \,, \qquad \mathbf{x} \in \mathcal{R},\ t > 0 \,, \tag{3.13a}$$

$$\frac{\partial v_j^{(1)}}{\partial x_d} + \frac{\partial v_d^{(1)}}{\partial x_j} = 0 \,, \qquad \mathbf{x} \in \mathcal{R},\ t > 0,\ j = 1, \ldots, d-1 \,. \tag{3.13b}$$

To obtain the free-surface conditions for the infinitesimal perturbation, an asymptotic expansion of the unit tangential and normal vectors to $\mathcal{S}_\eta$ is required. If the tangential and normal vectors to the undisturbed free surface $\mathcal{S}_0$ are $\mathbf{e}_j$ and $\mathbf{e}_d$, respectively, then the unit tangential and normal vectors to $\mathcal{S}_\eta$ can be expanded as

$$\mathrm{t}_j(\mathbf{x} + \eta(\mathbf{x}, t)\, \mathbf{e}_d) = \mathbf{e}_j + \big(\mathbf{e}_j \cdot \nabla \eta(\mathbf{x}, t)\big)\, \mathbf{e}_d + O(\epsilon^2) \,, \tag{3.14a}$$

$$\mathrm{n}(\mathbf{x} + \eta(\mathbf{x}, t)\, \mathbf{e}_d) = \mathbf{e}_d - \sum_{j=1}^{d-1} \big(\mathbf{e}_j \cdot \nabla \eta(\mathbf{x}, t)\big)\, \mathbf{e}_j + O(\epsilon^2) \,, \tag{3.14b}$$

with $\mathbf{x} \in \mathcal{S}_0$. The remainder is $O(\epsilon^2)$ because $\eta = O(\epsilon)$.

Taylor expansion of $\mathbf{v}(\mathbf{x}, t)$ around $\mathbf{x} \in \mathcal{S}_0$ yields

$$\mathbf{v}(\mathbf{x} + \eta(\mathbf{x})\, \mathbf{e}_d, t) = \mathbf{v}(\mathbf{x}, t) + \eta(\mathbf{x}, t)\, \mathbf{e}_d \cdot \nabla \mathbf{v}(\mathbf{x}, t) + O(\epsilon^2) \,, \tag{3.15a}$$

$$\nabla \mathbf{v}(\mathbf{x} + \eta(\mathbf{x})\, \mathbf{e}_d, t) = \nabla \mathbf{v}(\mathbf{x}, t) + \eta(\mathbf{x}, t)\, \mathbf{e}_d \cdot \nabla \nabla \mathbf{v}(\mathbf{x}, t) + O(\epsilon^2) \,. \tag{3.15b}$$

Hence, by (3.10),

$$\mathbf{v}(\mathbf{x} + \eta(\mathbf{x})\, \mathbf{e}_d, t) = \mathbf{v}^{(0)} + \phi_1 \mathbf{v}^{(1)}(\mathbf{x}, t) + r(\epsilon) \,, \tag{3.16a}$$

$$\nabla \mathbf{v}(\mathbf{x} + \eta(\mathbf{x})\, \mathbf{e}_d, t) = \phi_1 \nabla \mathbf{v}^{(1)}(\mathbf{x}, t) + r(\epsilon) \,, \tag{3.16b}$$

with $\mathbf{x} \in \mathcal{S}_0$ and the remainder $r(\epsilon) = O(\epsilon^2) + O(\epsilon\phi_1) + O(\phi_1^2)$. Similarly, we obtain for the pressure

$$p(\mathbf{x} + \eta(\mathbf{x})\, \mathbf{e}_d, t) = \phi_1 p^{(1)}(\mathbf{x}, t) - \epsilon\, \mathrm{Fr}^{-2} \eta^{(1)}(\mathbf{x}, t) + \bar{r}(\epsilon) \,, \qquad \mathbf{x} \in \mathcal{S}_0 \,, \tag{3.17}$$

with $\bar{r}(\epsilon) = O(\phi_1^2) + O(\epsilon\phi_1) + O(\chi_2)$. Equation (3.17) yields a meaningful relation between p and η, provided $\phi_1 = O(\epsilon)$. We choose $\phi_1 = \epsilon$. From the remainder $\bar{r}$ we infer that a meaningful relation between successive terms in the approximation is only obtained if $\chi_l = O(\epsilon^l)$. Hence, the remainders r and $\bar{r}$ are both of $O(\epsilon^2)$.

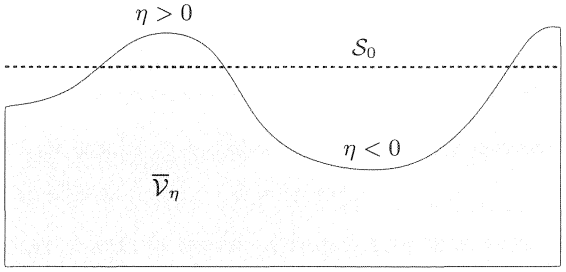

Figure 3.1: The spatial domain $\overline{\mathcal{V}}_\eta$ and the undisturbed free surface $\mathcal{S}_0$; $\mathcal{S}_0$ is not contained in $\overline{\mathcal{V}}_\eta$.

Inserting (3.10) and (3.14)–(3.17) in (3.4)–(3.5) and collecting terms of $O(\epsilon)$, we obtain the infinitesimal conditions

$$p^{(1)} - \mathrm{Fr}^{-2}\eta^{(1)} - 2\mu \frac{\partial v_d^{(1)}}{\partial x_d} = 0\,, \qquad \mathbf{x} \in \mathcal{S}_0, t > 0\,, \tag{3.18a}$$

$$\frac{\partial v_j^{(1)}}{\partial x_d} + \frac{\partial v_d^{(1)}}{\partial x_j} = 0\,, \qquad \mathbf{x} \in \mathcal{S}_0, t > 0\,, \tag{3.18b}$$

and

$$\frac{\partial \eta^{(1)}}{\partial t} + \sum_{j=1}^{d-1} v_j^{(0)} \frac{\partial \eta^{(1)}}{\partial x_j} - v_d^{(1)} = 0\,, \qquad \mathbf{x} \in \mathcal{S}_0, t > 0\,. \tag{3.18c}$$

Observe that (3.18) must be satisfied on the undisturbed free surface $\mathcal{S}_0$. However, $\mathbf{v}^{(1)}$ and $p^{(1)}$ are defined on the spatial domain $\overline{\mathcal{V}}_\eta$. Because $\mathcal{S}_0$ is not necessarily contained in $\overline{\mathcal{V}}_\eta$, it can occur that $\mathbf{v}^{(1)}$ and $p^{(1)}$ in (3.18) are not properly defined; see Figure 3.1. To avoid this, we assume that $\mathbf{v}^{(1)}$ and $p^{(1)}$ can be extended smoothly beyond the boundary $\mathcal{S}_\eta$ in such a manner that they are well defined in a neighborhood of $\mathcal{S}_\eta$ including $\mathcal{S}_0$. For $\mathbf{x} \in \mathcal{S}_0, \mathbf{x} \notin \overline{\mathcal{V}}_\eta$, we then define $\mathbf{v}^{(1)}$ and $p^{(1)}$ in (3.18) by their smooth extension from $\mathcal{S}_\eta$.

Ignoring terms of $O(\epsilon^2)$, the initial conditions (3.9) yield

$$\epsilon\eta^{(1)}(\mathbf{x}, 0) = \epsilon h_0(\mathbf{x})\,, \qquad \mathbf{x} \in \mathcal{S}_0\,, \tag{3.19a}$$

$$\mathbf{v}^{(1)}(\mathbf{x}, 0) = \mathbf{v}_0(\mathbf{x}; \epsilon) - \mathbf{v}^{(0)}\,, \qquad \mathbf{x} \in \mathcal{V}_\eta\,, \tag{3.19b}$$

$$p^{(1)}(\mathbf{x}, 0) = p_0(\mathbf{x}; \epsilon) + \mathrm{Fr}^{-2} x_d\,, \qquad \mathbf{x} \in \mathcal{V}_\eta\,. \tag{3.19c}$$

Equation (3.19) specifies the infinitesimal initial conditions.

3.3.3 Generic Modes

To determine the infinitesimal perturbation, i.e., the solution of (3.12)–(3.13) and (3.18)–(3.19), we first determine generic modes in compliance with (3.12). Subsequently, we use these generic modes to form the infinitesimal perturbation.

For convenient notation, let $\mathbf{q}(\mathbf{x},t) := \big(v_1^{(1)},\ldots,v_d^{(1)},p^{(1)}\big)(\mathbf{x},t)$ and $h(\mathbf{x},t) := \eta^{(1)}(\mathbf{x},t)$. To construct a Fourier representation of $\mathbf{q}(\mathbf{x},t)$, we first consider an isolated mode:

$$\mathbf{q}(\mathbf{x},t) := \hat{\mathbf{q}}(\mathbf{k},s,\omega)\exp\left(\mathrm{i}\mathbf{k}\cdot\mathbf{x}+sx_d+\mathrm{i}\omega t\right), \tag{3.20a}$$

$$h(\mathbf{x},t) := \hat{h}(\mathbf{k},\omega)\exp\left(\mathrm{i}\mathbf{k}\cdot\mathbf{x}+\mathrm{i}\omega t\right), \tag{3.20b}$$

with $\mathbf{k} := k_1\mathbf{e}_1+\cdots+k_{d-1}\mathbf{e}_{d-1}$, $k_j\in\mathbb{R}$ the horizontal *wave number*, $\omega\in\mathbb{C}$ the *radian frequency* and $s\in\mathbb{C}$. Note that the product $\mathbf{k}\cdot\mathbf{x}$ yields $k_1x_1+\ldots+k_{d-1}x_{d-1}$. Inserting (3.20a) into (3.12), we obtain

$$\hat{\mathbf{P}}(\mathbf{k},s,\omega)\cdot\hat{\mathbf{q}}(\mathbf{k},s,\omega)\exp\left(\mathrm{i}\mathbf{k}\cdot\mathbf{x}+sx_d+\mathrm{i}\omega t\right)=0, \tag{3.21}$$

with the *Fourier symbol* $\hat{\mathbf{P}}(\mathbf{k},s,\omega)$ according to

$$\hat{\mathbf{P}}(\mathbf{k},s,\omega) := \begin{pmatrix} \hat{H}(\mathbf{k},s,\omega) & 0 & \ldots & 0 & \mathrm{i}k_1 \\ 0 & \hat{H}(\mathbf{k},s,\omega) & \ldots & 0 & \mathrm{i}k_2 \\ \vdots & \vdots & \ddots & \vdots & \vdots \\ 0 & 0 & \ldots & \hat{H}(\mathbf{k},s,\omega) & s \\ \mathrm{i}k_1 & \mathrm{i}k_2 & \ldots & s & 0 \end{pmatrix}, \tag{3.22a}$$

where

$$\hat{H}(\mathbf{k},s,\omega) := \mathrm{i}\omega+\mathrm{i}\mathbf{v}^{(0)}\cdot\mathbf{k}+\mu\big(|\mathbf{k}|^2-s^2\big). \tag{3.22b}$$

Hence, (3.20a) complies with (3.12) if

$$\hat{\mathbf{q}}(\mathbf{k},s,\omega)\in\operatorname{kernel}\big(\hat{\mathbf{P}}(\mathbf{k},s,\omega)\big). \tag{3.23}$$

Equation (3.23) only allows nontrivial $\hat{\mathbf{q}}(\mathbf{k},s,\omega)$ if $\hat{\mathbf{P}}(\mathbf{k},s,\omega)$ is rank-deficient. This requires that $\mathbf{k}$, s and ω satisfy

$$\det(\hat{\mathbf{P}}(\mathbf{k},\omega)) = \big(|\mathbf{k}|^2-s^2\big)\big(\hat{H}(\mathbf{k},s,\omega)\big)^{d-1}=0. \tag{3.24}$$

For $d=2$, the kernels of $\hat{\mathbf{P}}(\mathbf{k},s,\omega)$ corresponding to the different roots of (3.24) are:

$$\operatorname{span}\left\{\begin{pmatrix}1\\0\\0\end{pmatrix},\begin{pmatrix}0\\1\\0\end{pmatrix},\begin{pmatrix}0\\0\\1\end{pmatrix}\right\}, \qquad \text{if } \mathbf{k},s,\omega=0, \tag{3.25a}$$

or otherwise

$$\operatorname{span}\left\{\begin{pmatrix} \mathrm{i}k_1 \\ (-1)^j|\mathbf{k}| \\ -\mathrm{i}\big(\omega+\mathbf{v}^{(0)}\cdot\mathbf{k}\big)\end{pmatrix}\right\}, \qquad \text{if } s=(-1)^j|\mathbf{k}| \ \ (j=1,2)\,, \tag{3.25b}$$

$$\operatorname{span}\left\{\begin{pmatrix} s \\ -\mathrm{i}k_1 \\ 0\end{pmatrix}\right\}, \qquad \text{if } \hat{H}(\mathbf{k},s,\omega)=0\,. \tag{3.25c}$$

For $d=3$,

$$\operatorname{span}\left\{\begin{pmatrix}1\\0\\0\\0\end{pmatrix},\begin{pmatrix}0\\1\\0\\0\end{pmatrix},\begin{pmatrix}0\\0\\1\\0\end{pmatrix},\begin{pmatrix}0\\0\\0\\1\end{pmatrix}\right\}, \qquad \text{if } \mathbf{k},s,\omega=0\,, \tag{3.26a}$$

or otherwise

$$\operatorname{span}\left\{\begin{pmatrix} \mathrm{i}k_1 \\ \mathrm{i}k_2 \\ (-1)^j|\mathbf{k}| \\ -\mathrm{i}\big(\omega+\mathbf{v}^{(0)}\cdot\mathbf{k}\big)\end{pmatrix}\right\}, \qquad \text{if } s=(-1)^j|\mathbf{k}| \ \ (j=1,2)\,, \tag{3.26b}$$

$$\operatorname{span}\left\{\begin{pmatrix} s \\ 0 \\ -\mathrm{i}k_1 \\ 0\end{pmatrix},\begin{pmatrix} 0 \\ s \\ -\mathrm{i}k_2 \\ 0\end{pmatrix}\right\}, \qquad \text{if } \hat{H}(\mathbf{k},s,\omega)=0\,. \tag{3.26c}$$

Note that (3.25a) and (3.26a) correspond to *constant modes*. Because (3.25b) and (3.26b) are independent of μ, the associated modes are called *inviscid modes*. In contrast, the modes corresponding to (3.25c) and (3.26c) are *viscous modes*.

In view of the linearity of (3.12), a solution of (3.12) can be represented as a linear combination of the modes (3.25) or (3.26). Hence, a *generic inviscid mode* can be defined by

$$\mathbf{q}^i(\mathbf{k},\omega,\mathbf{x},t)=\sum_{j=1}^{2}\theta_j^i(\mathbf{k},\omega)\,\hat{\mathbf{q}}_j^i(\mathbf{k},\omega)\exp\big(\mathrm{i}\mathbf{k}\cdot\mathbf{x}+(-1)^j|\mathbf{k}|x_d+\mathrm{i}\omega t\big)\,, \tag{3.27a}$$

with $\theta_j^i:\mathbb{R}^{d-1}\times\mathbb{C}\mapsto\mathbb{C}$ $(j=1,2)$, and

$$\hat{\mathbf{q}}_j^i(\mathbf{k},\omega)=\begin{pmatrix} \mathrm{i}k_1 \\ \vdots \\ \mathrm{i}k_{d-1} \\ (-1)^j|\mathbf{k}| \\ -\mathrm{i}\big(\omega+\mathbf{v}^{(0)}\cdot\mathbf{k}\big)\end{pmatrix}. \tag{3.27b}$$

A *generic viscous mode* is

$$\mathbf{q}^v(\mathbf{k},\omega,\mathbf{x},t) = \sum_{l=1}^{d-1}\sum_{j=1}^{2} \theta^v_{l,j}(\mathbf{k},\omega)\,\hat{\mathbf{q}}^v_{l,j}(\mathbf{k},\omega)\exp\left(\mathrm{i}\mathbf{k}\cdot\mathbf{x}+(-1)^j\sigma x_d+\mathrm{i}\omega t\right), \quad (3.28a)$$

with $\theta^v_{l,j} : \mathbb{R}^{d-1}\times\mathbb{C}\mapsto\mathbb{C}$ $(l=1,\ldots,d-1,\ j=1,2)$,

$$\sigma := \sigma(\mathbf{k},\omega) = \sqrt{|\mathbf{k}|^2+\mathrm{i}\big(\omega+\mathbf{v}^{(0)}\cdot\mathbf{k}\big)/\mu}\,, \quad (3.28b)$$

and

$$\hat{\mathbf{q}}^v_{1,j}(\mathbf{k},\omega) = \begin{pmatrix}(-1)^j\sigma\\ -\mathrm{i}k_1\\ 0\end{pmatrix}, \qquad \text{if } d=2\,, \quad (3.28c)$$

and

$$\hat{\mathbf{q}}^v_{1,j}(\mathbf{k},\omega) = \begin{pmatrix}(-1)^j\sigma\\ 0\\ -\mathrm{i}k_1\\ 0\end{pmatrix}, \qquad \hat{\mathbf{q}}^v_{2,j}(\mathbf{k},\omega) = \begin{pmatrix}0\\ (-1)^j\sigma\\ -\mathrm{i}k_2\\ 0\end{pmatrix}, \qquad \text{if } d=3\,. \quad (3.28d)$$

3.3.4 Surface Gravity Waves

A solution of (3.12)–(3.13) and (3.18) can be formed by linear combination of the generic modes (3.27)–(3.28). The case $d=2$ can be treated as a particular case of $d=3$, with $\theta^v_{2,j}$ and k_2 set to 0, and will therefore not be considered separately.

To enforce the boundary conditions (3.13), we choose

$$\theta^i_j(\mathbf{k},\omega) = \theta^i(\mathbf{k},\omega)\exp\left((-1)^j|\mathbf{k}|\right), \qquad \theta^v_{l,j}(\mathbf{k},\omega) = \theta^v_l(\mathbf{k},\omega)\exp\left((-1)^j\sigma\right), \quad (3.29)$$

with $\theta^i(\mathbf{k},\omega) : \mathbb{R}^{d-1}\times\mathbb{C}\mapsto\mathbb{C}$ and $\theta^v_l(\mathbf{k},\omega) : \mathbb{R}^{d-1}\times\mathbb{C}\mapsto\mathbb{C}$, where $j=1,2$ and $l=1,2$. Equations (3.27) and (3.28) then yield

$$\mathbf{q}^i(\mathbf{k},\omega,\mathbf{x},t) \;=\; \theta^i(\mathbf{k},\omega)\begin{pmatrix}\mathrm{i}k_1\cosh\left(|\mathbf{k}|(1+x_d)\right)\\ \mathrm{i}k_2\cosh\left(|\mathbf{k}|(1+x_d)\right)\\ |\mathbf{k}|\sinh\left(|\mathbf{k}|(1+x_d)\right)\\ -\Omega\cosh\left(|\mathbf{k}|(1+x_d)\right)\end{pmatrix}\exp\left(\mathrm{i}\mathbf{k}\cdot\mathbf{x}\;+\;\mathrm{i}\omega t\right), \quad (3.30a)$$

with

$$\Omega := \Omega(\mathbf{k},\omega) = \mathrm{i}(\omega+\mathbf{v}^0\cdot\mathbf{k})\,, \quad (3.30b)$$

and

$$\mathbf{q}^v(\mathbf{k},\omega,\mathbf{x},t) = \theta_1^v(\mathbf{k},\omega)\begin{pmatrix}\sigma\cosh\big(\sigma(1+x_d)\big)\\ 0\\ -\mathrm{i}k_1\sinh\big(\sigma(1+x_d)\big)\\ 0\end{pmatrix}\exp\big(\mathrm{i}\mathbf{k}\cdot\mathbf{x}+\mathrm{i}\omega t\big)$$
$$+\,\theta_2^v(\mathbf{k},\omega)\begin{pmatrix}0\\ \sigma\cosh\big(\sigma(1+x_d)\big)\\ -\mathrm{i}k_2\sinh\big(\sigma(1+x_d)\big)\\ 0\end{pmatrix}\exp\big(\mathrm{i}\mathbf{k}\cdot\mathbf{x}+\mathrm{i}\omega t\big)\,, \quad (3.30c)$$

respectively.

The sum of the above inviscid and viscous modes, $\mathbf{q}^i+\mathbf{q}^v$, and the infinitesimal surface displacement (3.20b) satisfy the conditions (3.18) if the following conditions hold:

$$\theta^i\Omega\cosh|\mathbf{k}| + \mathrm{Fr}^{-2}\hat{h} + 2\mu(\theta^i|\mathbf{k}|^2\cosh|\mathbf{k}| - \mathrm{i}\sigma\cosh\sigma\,(\theta_1^v k_1+\theta_2^v k_2)) = 0\,, \quad (3.31a)$$
$$\Omega\hat{h} - (\theta^i|\mathbf{k}|\sinh|\mathbf{k}| - \mathrm{i}\sinh\sigma\,(\theta_1^v k_1+\theta_2^v k_2)) = 0\,, \quad (3.31b)$$
$$\theta^i\,2\mathrm{i}k_1|\mathbf{k}|\sinh|\mathbf{k}| + \theta_1^v(\sigma^2+k_1^2)\sinh\sigma = 0\,, \quad (3.31c)$$
$$\theta^i\,2\mathrm{i}k_2|\mathbf{k}|\sinh|\mathbf{k}| + \theta_2^v(\sigma^2+k_2^2)\sinh\sigma = 0\,, \quad (3.31d)$$

Eliminating the ratios $\hat{h}/\theta^i$, θ_1^v/θ^i and θ_2^v/θ^i from these equations, we obtain

$$\Big(k_1^2(\sigma^2+k_2^2)+k_2^2(\sigma^2+k_1^2)\Big)\Big(4\mu\Omega\sigma|\mathbf{k}|(\tanh|\mathbf{k}|/\tanh\sigma)+2\mathrm{Fr}^{-2}|\mathbf{k}|\tanh|\mathbf{k}|\Big)$$
$$-\,(\sigma^2+k_1^2)(\sigma^2+k_2^2)\Big(\Omega(\Omega+2\mu|\mathbf{k}|^2)+\mathrm{Fr}^{-2}|\mathbf{k}|\tanh|\mathbf{k}|\Big) = 0\,. \quad (3.32)$$

Recall that σ is defined by (3.28b). Hence, (3.32) specifies a relation between the radian frequency ω and the wave number $\mathbf{k}$. Such a relation is called a *dispersion relation*. Elimination of σ^2 from (3.32) by means of the definition (3.28b) yields the following implicit relation for the dispersion relation:

$$\Omega\big(\Omega+\mu|\mathbf{k}|^2\big)\Big(\big(\Omega+2\mu|\mathbf{k}|^2\big)^2+\mathrm{Fr}^{-2}|\mathbf{k}|\tanh|\mathbf{k}|\Big)$$
$$-\,\mu^2\Big(4\Omega\sigma|\mathbf{k}|(\tanh|\mathbf{k}|/\tanh\sigma)\Big(|\mathbf{k}|^2(\Omega+\mu|\mathbf{k}|^2)+2\mu k_1^2k_2^2\Big)$$
$$+\,k_1^2k_2^2\Big(3\mathrm{Fr}^{-2}|\mathbf{k}|\tanh|\mathbf{k}|-\Omega(\Omega+2\mu|\mathbf{k}|^2)\Big)\Big) = 0\,. \quad (3.33)$$

It appears impossible to explicitly extract the dispersion relation $\omega(\mathbf{k})$ from equation (3.33). However, an asymptotic expansion of the dispersion relation in the limit $\mu\to 0$ can be constructed. As $\mu\to 0$, (3.33) possesses two distinct roots

$$\omega_j(\mathbf{k};\mu) = -\mathbf{v}^{(0)}\cdot\mathbf{k} + (-1)^j\Phi(\mathbf{k}) + \mathrm{i}2\mu|\mathbf{k}|^2 + o(\mu)\,, \quad (3.34a)$$

with $j = 1, 2$ and

$$\Phi(\mathbf{k}) = \sqrt{\mathrm{Fr}^{-2}|\mathbf{k}|\tanh|\mathbf{k}|}\,. \tag{3.34b}$$

To construct the expansion (3.34), it is important to note that

$$\frac{\sigma}{\tanh\sigma} = \frac{\sqrt{\mu|\mathbf{k}|^2+\Omega}}{\sqrt{\mu}}\,\frac{\exp\bigl(2\sqrt{|\mathbf{k}|^2+\Omega/\mu}\bigr)+1}{\exp\bigl(2\sqrt{|\mathbf{k}|^2+\Omega/\mu}\bigr)-1} = O\bigl(1/\sqrt{\mu}\bigr)\,, \tag{3.35}$$

as $\mu \to 0$. Hence, the remainder in (3.34) is indeed $o(\mu)$.

If (3.34) is inserted in (3.20a) and terms of $o(\mu)$ are ignored, it follows that an isolated Fourier mode behaves in $x_1, \ldots, x_{d-1}$ and t as:

$$\exp\bigl(-2\mu|\mathbf{k}|^2 t\bigr)\exp\bigl(\mathrm{i}\mathbf{k}\cdot\mathbf{x} - \mathrm{i}\bigl(\mathbf{v}^{(0)}\cdot\mathbf{k} - (-1)^j\Phi(\mathbf{k})\bigr)t\bigr)\,. \tag{3.36}$$

Equation (3.36) associates a traveling wave with each root of the dispersion relation. These waves are called *surface gravity waves*. The surface gravity waves move with the *phase velocity*

$$\mathbf{c}(\mathbf{k}) = |\mathbf{k}|^{-2}\bigl(\mathbf{v}^{(0)}\cdot\mathbf{k} - (-1)^j\Phi(\mathbf{k})\bigr)\,\mathbf{k}\,, \qquad j = 1, 2\,, \tag{3.37}$$

(see, e.g., Ref. [78]) and attenuate as $\exp(-2\mu|\mathbf{k}|^2 t)$.

3.3.5 Constant Perturbations

A solution of (3.12)–(3.13) and (3.18) can also be formed by linear combination of the constant modes (3.26a). One can infer that for $d = 3$ any such *constant perturbation* can be represented as

$$\begin{pmatrix} v_1^{(1)} \\ v_2^{(1)} \\ v_3^{(1)} \\ p^{(1)} \end{pmatrix}(\mathbf{x}, t) = \bar{\mathbf{w}}\,, \quad \text{with} \quad \bar{\mathbf{w}} := \begin{pmatrix} \bar{v}_1 \\ \bar{v}_2 \\ 0 \\ \bar{p} \end{pmatrix}\,, \tag{3.38a}$$

and

$$h(\mathbf{x}, t) = \mathrm{Fr}^2\bar{w}_4\,, \tag{3.38b}$$

for arbitrary constants $\bar{v}_1, \bar{v}_2$ and $\bar{p}$. The case $d = 2$ can again be treated as a particular case of $d = 3$, with $\bar{v}_2$ set to 0, and will not be considered separately.

3.3.6 Compatibility of Initial Conditions

The surface gravity waves express the infinitesimal perturbation corresponding to a disturbance in the initial conditions in the form of an isolated Fourier mode. A general infinitesimal perturbation can be represented as a linear combination of the constant mode and the Fourier integral of these surface gravity waves, provided

that the perturbation in the initial conditions complies with certain compatibility conditions.

To facilitate the description of the compatibility conditions, we note that the conditions (3.31c)–(3.31d) specify an interdependence between the inviscid mode (3.30a) and the viscous mode (3.30c). For each root $\omega_j(\mathbf{k})$ of the dispersion relation (3.33), we can condense the corresponding surface gravity wave into

$$\hat{\mathbf{w}}_j(\mathbf{k}, x_d) \exp\left(\mathrm{i}\mathbf{k}\cdot\mathbf{x} + \mathrm{i}\omega_j(\mathbf{k})t\right), \tag{3.39a}$$

where

$$\hat{\mathbf{w}}_j(\mathbf{k}, x_d) := \hat{\mathbf{w}}_j^i(\mathbf{k}, x_d) - \mu\hat{\mathbf{w}}_j^v(\mathbf{k}, x_d), \tag{3.39b}$$

with

$$\hat{\mathbf{w}}_j^i(\mathbf{k}, x_d) := \begin{pmatrix} \mathrm{i}k_1 \cosh\big(|\mathbf{k}|(1+x_d)\big) \\ \mathrm{i}k_2 \cosh\big(|\mathbf{k}|(1+x_d)\big) \\ |\mathbf{k}| \sinh\big(|\mathbf{k}|(1+x_d)\big) \\ -\Omega_j \cosh\big(|\mathbf{k}|(1+x_d)\big) \end{pmatrix}, \tag{3.39c}$$

and

$$\begin{aligned} \hat{\mathbf{w}}_j^v(\mathbf{k}, x_d) := {} & \frac{2\mathrm{i}k_1|\mathbf{k}|\sinh|\mathbf{k}|}{\mu|\mathbf{k}|^2 + \Omega_j + \mu k_1^2} \begin{pmatrix} \sigma_j \cosh\big(\sigma_j(1+x_d)\big)/\sinh\sigma_j \\ 0 \\ -\mathrm{i}k_1 \sinh\big(\sigma_j(1+x_d)\big)/\sinh\sigma_j \\ 0 \end{pmatrix} \\ & + \frac{2\mathrm{i}k_2|\mathbf{k}|\sinh|\mathbf{k}|}{\mu|\mathbf{k}|^2 + \Omega_j + \mu k_2^2} \begin{pmatrix} 0 \\ \sigma_j \cosh\big(\sigma_j(1+x_d)\big)/\sinh\sigma_j \\ -\mathrm{i}k_2 \sinh\big(\sigma_j(1+x_d)\big)/\sinh\sigma_j \\ 0 \end{pmatrix}, \end{aligned} \tag{3.39d}$$

with $\Omega_j := \Omega(\mathbf{k}, \omega_j(\mathbf{k}))$ and $\sigma_j := \sigma(\mathbf{k}, \omega_j(\mathbf{k}))$ according to (3.30b) and (3.28b), respectively.

Moreover, from the conditions (3.31) it follows that the surface displacement carried by the surface gravity wave (3.39) is

$$\hat{h}_j(\mathbf{k}) \exp\left(\mathrm{i}\mathbf{k}\cdot\mathbf{x} + \omega_j(\mathbf{k})t\right), \tag{3.40a}$$

with

$$\begin{aligned} \hat{h}_j(\mathbf{k}) := -\mathrm{Fr}^2 \Bigg[& \Omega_j \cosh|\mathbf{k}| + 2\mu|\mathbf{k}|^2 \cosh|\mathbf{k}| \\ & - \frac{4\mu^2\sigma_j|\mathbf{k}|\sinh|\mathbf{k}|}{\tanh\sigma_j} \left(\frac{k_1^2}{\mu|\mathbf{k}|^2 + \Omega_j + \mu k_1^2} + \frac{k_2^2}{\mu|\mathbf{k}|^2 + \Omega_j + \mu k_2^2} \right) \Bigg]. \end{aligned} \tag{3.40b}$$

To specify the compatibility condition for the initial conditions (3.9), we define

$$\mathbf{q}_0(\mathbf{x}) := \lim_{\epsilon \to 0} \frac{1}{\epsilon} \begin{pmatrix} \mathbf{v}_0(\mathbf{x};\epsilon) - \mathbf{v}^{(0)} \\ p_0(\mathbf{x};\epsilon) + \mathrm{Fr}^{-2} x_d \end{pmatrix} . \tag{3.41}$$

Let m denote the number of roots of the dispersion relation (3.33). The initial conditions (3.9) are called *compatible* with (3.1)–(3.5) to $O(\epsilon^2)$ as $\epsilon \to 0$, if $\theta_j : \mathbb{R}^{d-1} \mapsto \mathbb{C}$ exist such that

$$\mathbf{q}_0(\mathbf{x}) = \bar{\mathbf{w}} + \int_{-\infty}^{\infty} \sum_{j=1}^{m} \theta_j(\mathbf{k})\, \hat{\mathbf{w}}_j(\mathbf{k}, x_d) \exp\left(\mathrm{i}\mathbf{k}\cdot\mathbf{x}\right) \mathrm{d}\mathbf{k} + O(\epsilon) , \tag{3.42a}$$

$$h_0(\mathbf{x}) = \mathrm{Fr}^2 \bar{w}_4 + \int_{-\infty}^{\infty} \sum_{j=1}^{m} \theta_j(\mathbf{k})\, \hat{h}_j(\mathbf{k}) \exp\left(\mathrm{i}\mathbf{k}\cdot\mathbf{x}\right) \mathrm{d}\mathbf{k} + O(\epsilon) . \tag{3.42b}$$

with $\bar{\mathbf{w}} \in \mathbb{R}^{d+1}$ a constant vector in accordance with (3.38a). The compatibility conditions (3.42) imply that the infinitesimal initial conditions (3.19) can be satisfied to $O(\epsilon^2)$ by a linear combination of the constant modes (3.38) and a Fourier integral of the surface gravity waves.

Existence of the integrals in (3.42) implies certain restrictions on the initial conditions, in addition to the compatibility conditions; see, e.g., Ref. [73]. However, many of these restrictions can be relaxed if θ_j is understood in a generalized sense [45].

3.3.7 General Infinitesimal Perturbations

The infinitesimal perturbation corresponding to an arbitrary compatible initial condition can be represented as

$$\mathbf{q}(\mathbf{x}, t) = \bar{\mathbf{w}} + \sum_{j=1}^{m} \int_{-\infty}^{\infty} \theta_j(\mathbf{k})\, \hat{\mathbf{w}}_j(\mathbf{k}, x_d) \exp\left(\mathrm{i}\mathbf{k}\cdot\mathbf{x} + \mathrm{i}\omega_j(\mathbf{k})t\right) \mathrm{d}\mathbf{k} , \tag{3.43a}$$

$$h(\mathbf{x}, t) = \mathrm{Fr}^2 \bar{w}_4 + \sum_{j=1}^{m} \int_{-\infty}^{\infty} \theta_j(\mathbf{k})\, \hat{h}_j(\mathbf{k}) \exp\left(\mathrm{i}\mathbf{k}\cdot\mathbf{x} + \mathrm{i}\omega_j(\mathbf{k})t\right) \mathrm{d}\mathbf{k} , \tag{3.43b}$$

for appropriate $\bar{\mathbf{w}}$ and $\theta_j(\mathbf{k})$. If $\theta_j(\mathbf{k})\, \hat{\mathbf{w}}_j(\mathbf{k}, x_d)$ and $\theta_j(\mathbf{k})\, \hat{h}_j(\mathbf{k})$ are analytic functions of $\mathbf{k}$ for all considered x_d, then the integrals describe the behavior of *wave groups*, i.e., a group of contiguous (in Fourier space) surface gravity waves.

Denoting the Fourier transforms of $\mathbf{q}_0(\mathbf{x})$ and $h_0(\mathbf{x})$ from $x_1, \ldots, x_{d-1}$ to $\mathbf{k}$ by $\hat{\mathbf{w}}_0(\mathbf{k}, x_d)$ and $\hat{h}_0(\mathbf{k})$, respectively, the infinitesimal initial conditions imply the

following conditions on $\bar{\mathbf{w}}$ and $\theta_j(\mathbf{k})$:

$$\hat{\mathbf{w}}_0(\mathbf{k}, x_d) = \bar{\mathbf{w}}\,\delta(\mathbf{k}) + \sum_{j=1}^{m} \theta_j(\mathbf{k})\hat{\mathbf{w}}_j(\mathbf{k}, x_d)\,, \tag{3.44a}$$

$$\hat{h}_0(\mathbf{k}) = \mathrm{Fr}^2\bar{w}_4\,\delta(\mathbf{k}) + \sum_{j=1}^{m} \theta_j(\mathbf{k})\hat{h}_j(\mathbf{k})\,, \tag{3.44b}$$

with $\delta(\mathbf{k})$ the Dirac δ-function. If the conditions (3.44) uniquely determine $\bar{\mathbf{w}}$ and $\theta_j(\mathbf{k})$ for all $\mathbf{k}$ such that $\hat{\mathbf{w}}_j(\mathbf{k}, x_d) \neq 0$ or $\hat{k}_j(\mathbf{k}) \neq 0$, then the infinitesimal perturbation (3.43) is uniquely determined by (3.1)–(3.5) and the initial conditions (3.9). This is, of course, a prerequisite for well posedness of the problem defined by (3.1)–(3.5) and (3.9).

From (3.33) and (3.39)–(3.40) it follows that $\hat{\mathbf{w}}_j(\mathbf{k}, x_d) = 0$ and $\hat{h}_j(\mathbf{k}) = 0$ iff $\mathbf{k} = 0$. The conditions (3.44) with $\mathbf{k} = 0$ then uniquely determine $\bar{\mathbf{w}}$. For all $\mathbf{k} \neq 0$, the conditions (3.44) uniquely determine $\theta_j(\mathbf{k})$, provided that the pairs $(\hat{\mathbf{w}}_j(\mathbf{k}, x_d), \hat{h}_j(\mathbf{k}))$, $j = 1, \ldots, m$, are linearly independent for some $x_d \in [0, 1]$.

For sufficiently small μ, the infinitesimal perturbation is unique: From (3.34) and (3.39) it follows that the number of roots of the dispersion relation is $m = 2$ as $\mu \to 0$ and that the associated pairs $(\hat{\mathbf{w}}_j(\mathbf{k}, x_d), \hat{h}_j(\mathbf{k}))$, $j = 1, 2$, are linearly independent for all $\mathbf{k} \neq 0$.

3.4 Solution Behavior

In this section we summarize several characteristic features of surface gravity waves and of surface gravity wave groups.

3.4.1 Evolution of Local Disturbances

The dispersive behavior of the surface gravity waves implies that the velocity of the waves varies with the wave number. This is apparent from expression (3.37) for the phase velocity. Consequently, the Fourier modes that are present in an initially local disturbance in the flow appear later at different positions. This well-known phenomenon is also described in the classical references [42, 46].

To illustrate this behavior, we consider the evolution of the free-surface displacement for a stagnant inviscid free-surface flow in two spatial dimensions, i.e., $v_1^{(0)} = 0$, $\mu = 0$ and $d = 2$, in the case that the infinitesimal initial displacement of the free surface is given by

$$h_0(x) = \mathrm{e}^{-x^2}\,, \qquad -\infty < x < \infty\,. \tag{3.45}$$

The Fourier components of the initial displacement $h_0(x)$ are

$$\hat{h}_0(k) := \frac{1}{2\pi}\int_{-\infty}^{\infty} h_0(x)\,\mathrm{e}^{-\mathrm{i}kx}\,\mathrm{d}x = \frac{\mathrm{e}^{-k^2/4}}{2\sqrt{\pi}}\,. \tag{3.46}$$

The infinitesimal free-surface displacement is expressed by (3.43b). Considering the typical case $\theta_2(k) = 0$, we obtain that the infinitesimal free-surface displacement is given by the wave group

$$h(x,t) = \int_{-\infty}^{\infty} \frac{\mathrm{e}^{-k^2/4}}{2\sqrt{\pi}} \exp\left(\mathrm{i}kx + \mathrm{i}\sqrt{\mathrm{Fr}^{-2}|k|\tanh|k|}\, t\right) \mathrm{d}k \,. \tag{3.47}$$

Figure 3.2 plots the real part of $h(x,t)$ according to (3.47) for $\mathrm{Fr} = \frac{1}{2}$. The separation of the Fourier components with different wave numbers that occurs due to the dispersive behavior of the surface gravity waves is indeed apparent.

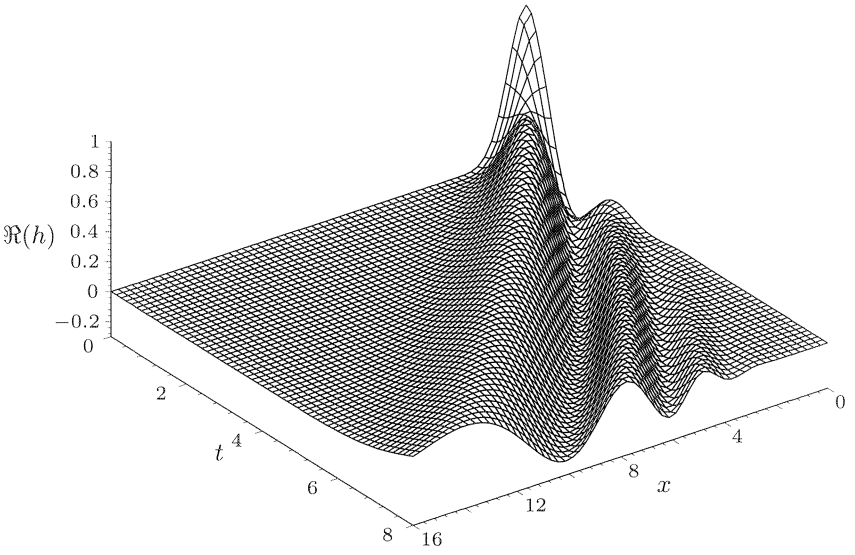

Figure 3.2: Evolution of a local disturbance in the free-surface position according to (3.47).

3.4.2 Steady Waves

Equations (3.39)–(3.40) imply that a surface gravity wave with wave number $\mathbf{k}$ is steady if the dispersion relation (3.33) has a root $\omega_j(\mathbf{k}) = 0$. For inviscid flows ($\mu = 0$), it follows from (3.34) that this occurs for $\mathbf{k}$ such that

$$\left(\mathbf{v}^{(0)} \cdot \mathbf{k}\right)^2 = \mathrm{Fr}^{-2}|\mathbf{k}|\tanh|\mathbf{k}| \,. \tag{3.48}$$

Without loss of generality, below we assume that the reference velocity is chosen such that $|\mathbf{v}^{(0)}| = 1$.

For $d = 2$, equation (3.48) yields a relation between the wave number and the Froude number:

$$|k|^{-1}\tanh|k| = \mathrm{Fr}^2 \,. \tag{3.49}$$

For subcritical flows, i.e., for $\mathrm{Fr} < 1$, equation (3.49) specifies a unique relation between the Froude number and the wave length $\lambda := 2\pi/k$. Figure 3.3 displays the relation between the wave length of the steady surface gravity wave and the Froude number, according to (3.49). For supercritical flows ($\mathrm{Fr} > 1$) a solution

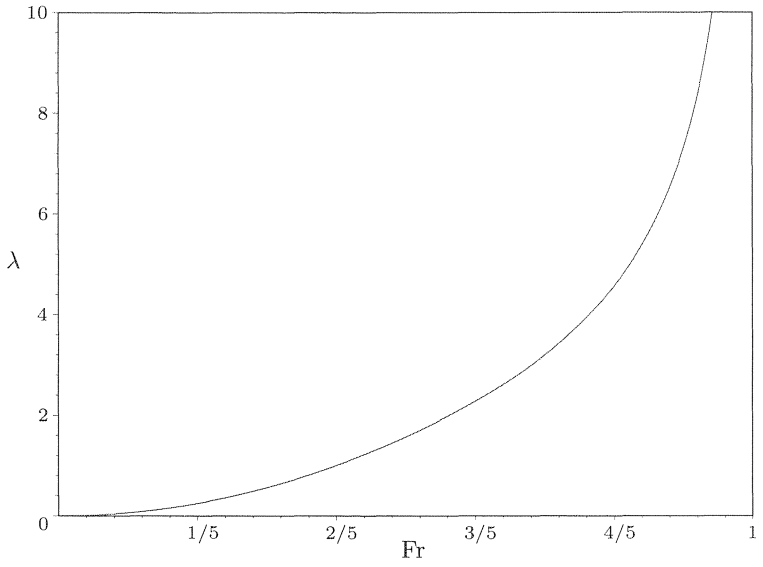

Figure 3.3: Relation between the wave length, λ, and the Froude number, Fr, for steady surface gravity waves in a channel of unit depth.

to (3.49) does not exists and, accordingly, a steady surface gravity wave does not occur.

To facilitate the derivation of the steady waves for $d = 3$, we assume, without loss of generality, that $\mathbf{v}^{(0)} = \mathbf{e}_1$, so that $\mathbf{v}^{(0)} \cdot \mathbf{k} = k_1$. Equation (3.48) then yields the following relation between k_1, k_2 and Fr:

$$\frac{k_1^2}{\sqrt{k_1^2 + k_2^2}\tanh\sqrt{k_1^2 + k_2^2}} = \mathrm{Fr}^{-2} \,. \tag{3.50}$$

Figure 3.4 on the next page displays curves in the (k_1, k_2)-plane on which the condition (3.50) is fulfilled for different values of Fr^{-2}. From Figure 3.4 it becomes apparent that for $d = 3$ the inviscid free-surface flow problem allows surface gravity waves with unbounded $|\mathbf{k}|$. From (3.36) it follows that these high wave number modes are effectively removed by viscosity.

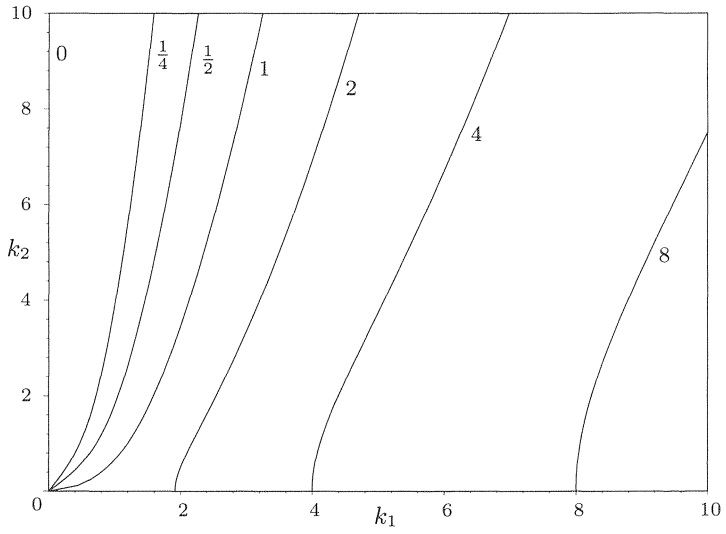

Figure 3.4: Wave-number curves of steady surface gravity waves in 3 dimensions for $\mathrm{Fr}^{-2} = 0, \frac{1}{4}, \frac{1}{2}, 1, 2, 4, 8$.

3.4.3 Asymptotic Temporal Behavior of Wave Groups

The asymptotic temporal behavior of a group of inviscid surface gravity waves is determined by the asymptotic properties of the inverse Fourier transforms in (3.43), with $\omega_j(\mathbf{k})$ by (3.34) and $\mu = 0$. The behavior of these integral transforms for $t \to \infty$ can be determined by means of the asymptotic expansion

$$\int_0^\infty \hat{f}(k) \exp\bigl(\mathrm{i}\xi(k)t\bigr)\,\mathrm{d}k = \left(\hat{f}(k_0)\sqrt{\frac{2\pi}{|\xi''(k_0)|t}}\exp\bigl(\mathrm{i}[\xi(k_0)t + \tfrac{1}{4}\pi\,\mathrm{sign}\,\xi''(k_0)]\bigr) + O\left(\frac{1}{t}\right)\right) + O(e^{-\beta t}), \quad (3.51)$$

with β a positive constant, $\hat{f}(k)$ an analytic function and k_0 a stationary point of $\xi(k)$, i.e., $\xi'(k_0) = 0$. In the absence of stationary points, the bracketed term vanishes and only the exponentially decaying term remains. The expansion (3.51) requires that $\xi(k)$ is smooth in the neighborhood of stationary points in the sense that the ratio $\xi'''(k_0)/|\xi''(k_0)|^{3/2}$ is small; see Ref. [42]. The method of stationary phase (sometimes called method of steepest descent) can be used to prove (3.51); see, e.g., Refs. [46, 79].

The inverse Fourier transforms in (3.43) can be evaluated for $t \to \infty$ by introducing a suitable coordinate transformation for $\mathbf{k}$ and applying (3.51) recursively with respect to the transformed coordinates. The following asymptotic behavior

of the inverse Fourier transforms (3.43) is then obtained:

$$(2\pi/t)^{(d-1)/2}\big(\det \mathbf{H}(\mathbf{k}_0)\big)^{-1/2} \exp\big(\mathrm{i}\xi(\mathbf{k}_0)t + \mathrm{i}\zeta\big) + O(e^{-\beta t}), \tag{3.52a}$$

as $t \to \infty$, where

$$\xi(\mathbf{k}) := \mathbf{k}\cdot\mathbf{x}/t + \omega_j(\mathbf{k})\,, \tag{3.52b}$$

$\mathbf{H}(\mathbf{k})$ denotes its Hessian and ζ is a multiple of $\pi/4$ depending on the properties of the Hessian; see also Ref. [78].

If $\mu = 0$ in (3.34), then for fixed $\mathbf{x}$ and $t \to \infty$, a stationary point $\mathbf{k}_0$ of $\xi(\mathbf{k})$ occurs when

$$\frac{\partial\Phi(\mathbf{k})}{\partial k_j} = \mathrm{Fr}^{-1}\frac{\tanh|\mathbf{k}| + |\mathbf{k}|(1-\tanh^2|\mathbf{k}|)}{2\sqrt{|\mathbf{k}|\tanh|\mathbf{k}|}}\frac{k_j}{|\mathbf{k}|} = v_j^{(0)}, \qquad j = 1,\ldots,d-1. \tag{3.53}$$

Without loss of generality, we assume that $\mathbf{v}^{(0)}$ is scaled such that $|\mathbf{v}^{(0)}| = 1$. A necessary and sufficient condition for a stationary point to exist is $\mathrm{Fr}^{-2}\Lambda(|\mathbf{k}|) = 1$, with

$$\Lambda(|\mathbf{k}|) := \frac{(\tanh|\mathbf{k}| + |\mathbf{k}|(1-\tanh^2|\mathbf{k}|))^2}{4\,|\mathbf{k}|\tanh|\mathbf{k}|}. \tag{3.54}$$

One can show that $\Lambda(|\mathbf{k}|)$ is a bijection from $\mathbb{R}_+$ to $(0,1]$. Therefore, a stationary point exists iff $\mathrm{Fr} \le 1$, i.e., for subcritical flows. This stationary point corresponds to a wave of which the group velocity (see, e.g., [46, 78]) equals the flow-velocity. Consequently, the energy associated with this wave remains at a fixed position and decays only due to dispersion.

By (3.52a), at subcritical Froude numbers the asymptotic temporal behavior of the wave groups in (3.43) in $\mathbb{R}^d$ is $O(t^{(1-d)/2})$ as $t \to \infty$. In particular, the wave groups attenuate as $1/\sqrt{t}$ in $\mathbb{R}^2$ and as $1/t$ in $\mathbb{R}^3$. At supercritical Froude numbers, a stationary point of $\xi(\mathbf{k})$ does not exist and the first term in (3.52a) disappears. The wave groups then vanish exponentially as $t \to \infty$.

3.4.4 Free-Surface Boundary Layer

A particular feature of viscous free-surface flows is the boundary layer that is present in the vicinity of the free surface. The boundary layer of a surface gravity wave (3.39) is contained in the viscous contribution (3.39d). From (3.39d) it follows that the typical structure of the free-surface boundary layer is

$$\frac{\cosh\big(\sigma_j(1+x_d)\big)}{\sinh\sigma_j}\,, \tag{3.55a}$$

and

$$\frac{\sinh\big(\sigma_j(1+x_d)\big)}{\sinh\sigma_j}\,, \tag{3.55b}$$

for the horizontal and vertical velocity components, respectively. The pressure does not exhibit a free surface boundary layer.

Figure 3.5 plots the modulus of (3.55a) versus the vertical coordinate for several values of μ. The modulus of (3.55b) behaves similarly. The setting of the remaining parameters is $\mathrm{Fr} = \sqrt{\tanh 1}$, $k_1 = 1$ and $k_2 = 0$. In the absence of viscosity, this setting corresponds to a steady surface gravity wave with $d = 2$; cf. (3.49). To create Fig. 3.5, for each value of μ we extracted the Ω closest to $-\mathrm{i}$ from (3.33) and, subsequently, we obtained the corresponding σ from (3.28b). The free-surface boundary layer structure is apparent in Figure 3.5.

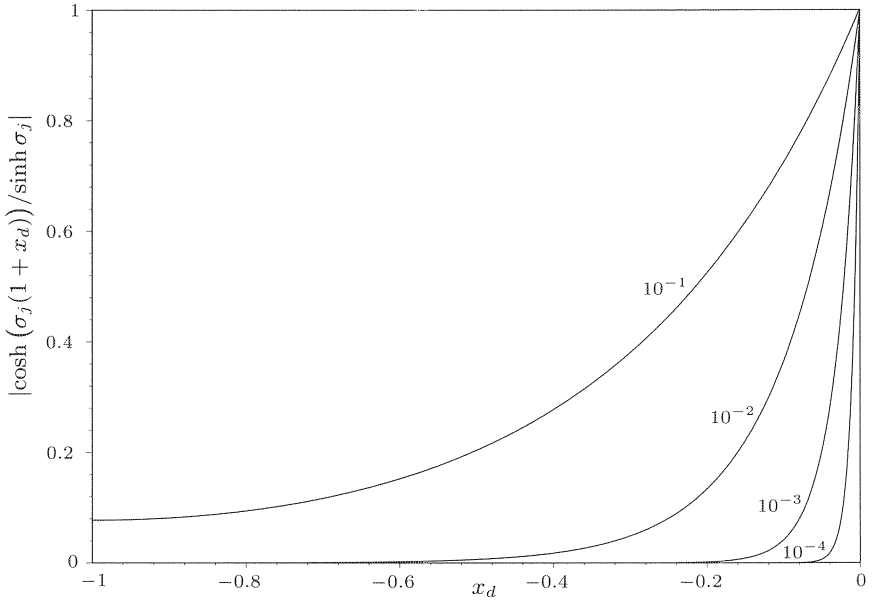

Figure 3.5: Structure of the free-surface boundary layer according to (3.55a) for $\mu = 10^{-1}, 10^{-2}, 10^{-3}, 10^{-4}$, with $\mathrm{Fr} = \sqrt{\tanh 1}$, $k_1 = 1$ and $k_2 = 0$.

The free-surface boundary layer is *weak* in the sense that the boundary layer vanishes as $\mu \to 0$. From (3.33) it follows that

$$\Omega_j = O(1)\,, \qquad \text{as } \mu \to 0\,. \tag{3.56}$$

The definition (3.28b) then implies

$$\sigma_j = O(1/\sqrt{\mu})\,, \qquad \text{as } \mu \to 0\,. \tag{3.57}$$

Hence, by (3.39), the viscous contribution to the horizontal velocity is $O(\sqrt{\mu})$ and the viscous contribution to the vertical velocity is only $O(\mu)$. This result is consistent with the statement in [6] that the velocity deviation through the free-surface

boundary layer is $O(1/\sqrt{\mathrm{Re}})$. The above implies that the free-surface boundary layer indeed vanishes as $\mu \to 0$. In contrast, the deviation of the horizontal and vertical velocities through the boundary layer near a rigid no-slip boundary is $O(1)$ and $O(\sqrt{\mu})$, respectively; see, e.g., Ref. [39]. Hence, the boundary layer near a rigid no-slip boundary persists as $\mu \to 0$.

Chapter 4

Efficient Numerical Solution of Steady Free-Surface Navier–Stokes Flows

4.1 Introduction

The numerical solution of flows that are partially bounded by a freely moving boundary is of great importance in ship hydrodynamics [3, 13, 18, 47], hydraulics, and many other practical applications, such as coating technology [54, 55]. In ship hydrodynamics, an important area of application is the prediction of the wave pattern that is generated by the ship at forward speed in still water. This wave generation is responsible for a substantial part of the ship's resistance and, therefore, it should be minimized by a proper hull form design. Computational methods play an important role in this design process. Most computational tools that are currently in use for solving gravity subjected free-surface flows around a surface-piercing body rely on a potential flow approximation. Present developments primarily concern the solution of the free-surface Navier–Stokes (or RANS) flow problem.

For time-dependent free-surface flows, generally there is no essential difference in the treatment of the free surface between numerical methods for potential flow or Navier–Stokes flow. Typically, the solution of the flow equations and the adaptation of the free boundary are separated. Each time step begins with computing the flow field with the dynamic conditions imposed at the free surface. Next, the free surface is adjusted through the kinematic condition, using the newly computed velocity field.

For *steady* free-surface flows, however, such a conformity of approaches for viscous and inviscid flow cannot be observed. For instance in ship hydrodynamics, whereas dedicated techniques have been developed for solving the free-surface potential flow problems (see, e.g., Ref. [52]), methods for Navier–Stokes flow usually continue the aforementioned transient process until a steady state is reached (see, e.g., Refs. [3, 13]). However, this time-integration method is often computation-

ally inefficient. In general, the convergence to steady state is retarded by slowly attenuating transient surface gravity waves. Moreover, the separate treatment of the flow equations and the kinematic condition yields a restriction on the allowable time-step. Due to the specific transient behavior of free-surface flows and the time-step restriction, the performance of the time-integration method deteriorates rapidly with decreasing mesh width. In practical computations, tens of thousands of time steps are often required, rendering the time-integration approach prohibitively expensive in actual design processes.

Several approaches have been suggested to improve the efficiency of time-integration methods, e.g., pseudo-time integration and quasi-steady methods; see Refs. [18, 75]. It appears that these approaches indeed improve the efficiency, but do not essentially improve the asymptotic convergence behavior of the time-integration method.

Alternative solution methods for steady free-surface Navier–Stokes flow exist, but they have not been widely applied in the field of ship hydrodynamics. In the field of coating technology successive approximation techniques are often employed, in particular, kinematic iteration and dynamic iteration [55]. Kinematic iteration imposes the dynamic conditions at the free surface and uses the kinematic condition to displace the boundary. Dynamic iteration imposes the kinematic and the tangential dynamic conditions at the free surface and uses the normal dynamic condition to adjust the boundary position. However, the convergence behavior of both iteration schemes depends sensitively on parameters in the problem; see, e.g., Refs. [12, 61]. A method that avoids the deficiencies of the aforementioned iterative methods, is Newton iteration of the full equation set [55]. The positions of the (free-surface) grid nodes are then added as additional unknowns and all equations, including the free-surface conditions, are solved simultaneously. An objection to this method is that simultaneous treatment of all equations is infeasible for problems with many unknowns, such as three-dimensional problems and problems requiring sharp resolution of boundary layers. Finally, the free-surface flow problem can be reformulated into an optimal shape design problem, which can then in principle be solved efficiently by the adjoint optimization method. A problem with this approach is its complexity: although much progress has been made in the formulation of adjoint equations for problems from fluid dynamics, including the Navier–Stokes equations [22], setting up the adjoint method remains involved. Moreover, efficiency is only obtained if proper preconditioning is applied [67, 69], and constructing the preconditioner for the free-surface Navier–Stokes flow problem is intricate.

The current work presents an iterative method for efficiently solving steady free-surface Navier–Stokes flow problems. Although our interest is the previously outlined ship hydrodynamics application, it is anticipated that the method is also applicable to other gravity dominated steady viscous free-surface flows at high Reynolds numbers, such as occur, for instance, in hydraulics. The proposed method is analogous to the method for solving steady free-surface potential flow problems presented in [52]. The method alternatingly solves the steady Navier–

Stokes equations with a so-called quasi free-surface condition imposed at the free surface, and adjusts the free surface using the computed solution. The quasi free-surface condition ensures that the disturbance induced by the subsequent displacement of the boundary is negligible. Each surface adjustment then yields an improved approximation to the actual free-boundary position.

The contents of this chapter are organized as follows: In Section 4.2 the equations governing incompressible, viscous free-surface flow are stated and the quasi free-surface condition is derived. Section 4.3 proves that the usual time-integration approach is generally unsuitable for solving steady free-surface flows. Section 4.4 outlines the iterative solution method and examines its convergence behavior. Numerical experiments and results for a two-dimensional test case are presented in Section 4.5. The application to actual ship wave computations is in progress and will be reported in a sequel. Section 4.6 contains concluding remarks.

4.2 Governing Equations

4.2.1 Incompressible Viscous Flow

An incompressible, viscous fluid flow, subject to a constant gravitational force is considered. Although only steady solutions are of interest, for the purpose of analysis the equations are considered in time-dependent form.

The fluid occupies an open, time-dependent domain $\mathcal{V}_\eta \subset \mathbb{R}^d$ $(d = 2, 3)$, which is enclosed by the free boundary, $\mathcal{S}_\eta$, and a fixed boundary, $\partial\mathcal{V}_\eta \setminus \mathcal{S}_\eta$. Positions in $\mathbb{R}^d$ are identified by their horizontal coordinates $(x_1, \ldots, x_{d-1})$ and a vertical coordinate y, with respect to the Cartesian base vectors $\mathbf{e}_1, \ldots, \mathbf{e}_{d-1}$ and $\mathbf{j}$, respectively. The origin is located in the undisturbed free surface $\mathcal{S}_0$, and the gravitational acceleration, $\mathbf{g}$, acts in the negative vertical direction. We consider free surfaces that can be represented by a so-called *height function*, i.e., $\mathcal{S}_\eta = \{(\mathbf{x}, \eta(\mathbf{x}, t))\}$. The height function η is assumed to be a smooth function of the horizontal coordinates and time. See Figure 4.1 on the following page for an illustration.

The distinguishing parameters of the viscous free-surface flow problem are the Froude number, $\mathrm{Fr} := U/\sqrt{g\ell}$, and the Reynolds number, $\mathrm{Re} := \rho U\ell/\mu$, with U an appropriate reference velocity, g the gravitational acceleration, ℓ a reference length and μ the dynamic viscosity of the fluid. The fluid density ρ is assumed to be constant. The state of the flow is then characterized by the (non-dimensionalized) fluid velocity $\mathbf{v}(\mathbf{x}, y, t)$ and pressure $p(\mathbf{x}, y, t)$. Incompressibility of the fluid implies that the velocity field is solenoidal:

$$\operatorname{div} \mathbf{v} = 0, \qquad (\mathbf{x}, y) \in \mathcal{V}_\eta, t > 0. \tag{4.1a}$$

Conservation of momentum in the fluid is described by the Navier–Stokes equations. The pressure is separated into a hydrodynamic component φ and a hydrostatic contribution as $p(\mathbf{x}, y, t) = \varphi(\mathbf{x}, y, t) - \mathrm{Fr}^{-2} y$. Because the gradient of the

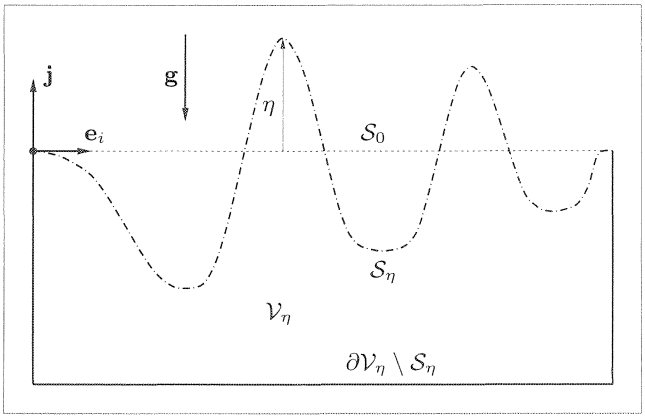

Figure 4.1: Schematic illustration of the free-surface flow problem.

hydrostatic pressure and the gravitational force cancel, the Navier–Stokes equations for a gravity subjected incompressible fluid read:

$$\frac{\partial \mathbf{v}}{\partial t} + \operatorname{div} \mathbf{v}\mathbf{v} + \nabla\varphi - \operatorname{div} \boldsymbol{\tau}(\mathbf{v}) = 0, \qquad (\mathbf{x}, y) \in \mathcal{V}_\eta, t > 0, \tag{4.1b}$$

where $\boldsymbol{\tau}(\mathbf{v})$ is the viscous stress tensor for an incompressible Newtonian fluid:

$$\boldsymbol{\tau}(\mathbf{v}) := \mathrm{Re}^{-1}\big((\nabla\mathbf{v}) + (\nabla\mathbf{v})^T\big). \tag{4.1c}$$

Our primary interest is in turbulent flows. We consider the Reynolds Averaged Navier–Stokes (RANS) equations, supplemented with a turbulence model that is based on eddy viscosity. For our purpose, the RANS equations are essentially the same as the Navier–Stokes equations, with the important difference that the RANS equations have steady solutions even at the envisaged high Reynolds numbers.

4.2.2 Free-Surface Conditions

Free-surface flows are essentially two-fluid flows, of which the properties of the contiguous bulk fluids are such that their mutual interaction at the interface can be ignored. For an elaborate discussion of two-fluid flows, see, e.g., Refs. [5, 58]. The free-surface conditions follow from the general interface conditions and the assumptions that both density and viscosity of the adjacent fluid vanish at the interface and, furthermore, that the interface is impermeable. Here it will moreover be assumed that interfacial stresses can be ignored, which is a valid assumption in the practical applications envisaged.

On the free surface, the fluid satisfies a kinematic condition and d dynamic conditions. Impermeability of the free surface is expressed by the kinematic condition

$$\frac{\partial \eta}{\partial t} + \mathbf{v} \cdot \nabla(\eta - y) = 0, \qquad (\mathbf{x}, y) \in \mathcal{S}_\eta, t > 0. \tag{4.2a}$$

Supposed that the viscous contribution to the normal stress at the free surface is negligible, continuity of stresses at the interface requires that the pressure vanishes at the free surface. This results in the normal dynamic condition

$$\varphi - \mathrm{Fr}^{-2}\eta = 0, \qquad (\mathbf{x}, y) \in \mathcal{S}_\eta, t > 0. \tag{4.2b}$$

The requirement that the tangential stress components vanish at the free surface is expressed by the $d-1$ tangential dynamic conditions

$$\mathbf{t}^i \cdot \boldsymbol{\tau}(\mathbf{v}) \cdot \mathbf{n} = 0, \qquad (\mathbf{x}, y) \in \mathcal{S}_\eta, t > 0. \tag{4.2c}$$

Here, $\mathbf{t}^i$ $(i = 1, \ldots, d-1)$ are orthogonal unit tangent vectors to $\mathcal{S}_\eta$ and $\mathbf{n}$ denotes the unit normal vector to $\mathcal{S}_\eta$.

One may note that the number of free-surface conditions for the viscous free-surface flow problem is $d+1$. The incompressible Navier–Stokes equations in $\mathbb{R}^d$ require d boundary conditions. Hence, the number of free-surface conditions is indeed one more than the number of required boundary conditions.

4.2.3 Quasi Free-Surface Condition

A fundamental problem in analyzing and computing free-surface flow problems, is the interdependence of the state variables $\mathbf{v}, p$ and their spatial domain of definition through the free-surface conditions. This problem can be avoided by deriving a condition that holds to good approximation on a fixed boundary in the neighborhood of the actual free boundary. We refer to such a condition as a *quasi free-surface condition*, because the qualitative solution behavior of the initial boundary value problem with this condition imposed is similar to that of the free-boundary problem, but the boundary does not actually move. A suitable quasi free-surface condition for the free-surface Navier–Stokes flow problem is derived below.

Let $\mathcal{S}_\eta$ denote the actual free surface, as defined before. In a similar manner, a nearby fixed boundary $\mathcal{S}_\theta := \{(\mathbf{x}, \theta(\mathbf{x}))\}$ is introduced, with $\theta(\mathbf{x})$ a smooth function on $\mathcal{S}_0$. We require that $\mathcal{S}_\theta$ is close to the actual free surface in such a manner that

$$\delta(\mathbf{x}, t) := \eta(\mathbf{x}, t) - \theta(\mathbf{x}) \,, \tag{4.3}$$

is small and sufficiently smooth. In particular, for all $t > 0$, δ must satisfy $\|\delta\|_{\mathcal{S}_\theta} + \|\nabla\delta\|_{\mathcal{S}_\theta} + \|\delta_t\|_{\mathcal{S}_\theta} \leq \epsilon$, for some $\epsilon \ll 1$. Here $\|\cdot\|_{\mathcal{S}_\theta}$ is a suitable norm on the approximate boundary. Assuming that p and $\mathbf{v}$ can be extended smoothly beyond the boundary $\mathcal{S}_\theta$, Taylor expansion in the neighborhood of $\mathcal{S}_\theta$ yields for p and $\mathbf{v}$

at the actual free surface,

$$p(\mathbf{x}, \eta(\mathbf{x},t), t) = p(\mathbf{x}, \theta(\mathbf{x}), t) + \delta(\mathbf{x},t)\, \mathbf{j}\cdot\nabla p(\mathbf{x}, \theta(\mathbf{x}), t) + O(\epsilon^2), \tag{4.4a}$$

$$\mathbf{v}(\mathbf{x}, \eta(\mathbf{x},t), t) = \mathbf{v}(\mathbf{x}, \theta(\mathbf{x}), t) + \delta(\mathbf{x},t)\, \mathbf{j}\cdot\nabla \mathbf{v}(\mathbf{x}, \theta(\mathbf{x}), t) + O(\epsilon^2), \tag{4.4b}$$

The normal dynamic condition (4.2b) demands that the left-hand side of (4.4a) vanishes. Hence, the elevation of the free surface can be expressed in terms of the pressure and its gradient at the approximate surface:

$$\eta(\mathbf{x},t) = \theta(\mathbf{x}) - \frac{p(\mathbf{x}, \theta(\mathbf{x}), t)}{\mathbf{j}\cdot\nabla p(\mathbf{x}, \theta(\mathbf{x}), t)} + O(\epsilon^2)\,. \tag{4.5}$$

To obtain an $O(\epsilon^2)$ accurate quasi free-surface condition, i.e., an $O(\epsilon^2)$ approximation of the conditions at $\mathcal{S}_\theta$, $\mathbf{v}$ and η in the kinematic condition (4.2a) can be replaced by (4.4b) and (4.5), respectively. The resulting condition is, however, intractable. Instead, two additional assumptions concerning $\mathbf{v}$ and p are introduced to obtain a convenient quasi free-surface condition. The first assumption is that the vertical derivative of the pressure is dominated by the hydrostatic component, $-\mathrm{Fr}^{-2}$. Generally, this assumption is valid for waves of moderate steepness. Specifically, we suppose that a constant $\sigma_p \ll 1$ exists such that for all $t > 0$,

$$\|1 + \mathrm{Fr}^2\, \mathbf{j}\cdot\nabla p\|_{\mathcal{S}_\theta} \leq \sigma_p\,. \tag{4.6}$$

The second assumption is that the vertical derivative of $\mathbf{v}$ is small, in such a manner that a constant $\sigma_{\mathbf{v}} \ll 1$ exists with the property that for all $t > 0$,

$$\|\mathbf{j}\cdot\nabla \mathbf{v}\|_{\mathcal{S}_\theta} \leq \sigma_{\mathbf{v}}\,. \tag{4.7}$$

Under this assumption, the velocity at the actual free boundary, $\mathbf{v}(\mathbf{x}, \eta(\mathbf{x},t), t)$, can be accurately approximated by the velocity at the fixed boundary, $\mathbf{v}(\mathbf{x}, \theta(\mathbf{x}), t)$. By (4.4b), the error in the approximation is only $O(\epsilon\sigma_{\mathbf{v}})$. In [6] it is shown that the velocity-deviation through the free-surface boundary layer is proportional to the surface curvature and $1/\sqrt{\mathrm{Re}}$. Moreover, $\sigma_{\mathbf{v}}$ in (4.7) increases with the wave steepness. Therefore, the assumption $\sigma_{\mathbf{v}} \ll 1$ is valid if the steepness and curvature of the free-surface waves are moderate and if Re is sufficiently large.

Under the above assumptions a convenient quasi free-surface condition can be derived. Substitution of the hydrostatic approximation of the pressure gradient in (4.5) yields

$$\eta(\mathbf{x},t) = \theta(\mathbf{x}) - \frac{p(\mathbf{x}, \theta(\mathbf{x}), t)}{-\mathrm{Fr}^{-2}(1 + O(\sigma_p))} = \theta(\mathbf{x}) + \mathrm{Fr}^2 p(\mathbf{x}, \theta(\mathbf{x}), t)(1 + O(\sigma_p))\,. \tag{4.8}$$

The dynamic condition (4.2b) and (4.4a) imply that $p = O(\epsilon)$ on $\mathcal{S}_\theta$. Hence, ignoring terms $O(\epsilon^2, \epsilon\sigma_p)$, the free-surface elevation is related to the hydrodynamic pressure at the approximate boundary by

$$\eta(\mathbf{x},t) = \theta(\mathbf{x}) + \mathrm{Fr}^2 p(\mathbf{x}, \theta(\mathbf{x}), t) = \mathrm{Fr}^2 \varphi(\mathbf{x}, \theta(\mathbf{x}), t)\,. \tag{4.9}$$

To transfer the kinematic condition (4.2a) to the approximate surface $\mathcal{S}_\theta$, η is replaced by (4.9) and $\mathbf{v}$ on $\mathcal{S}_\eta$ is replaced by $\mathbf{v}$ on $\mathcal{S}_\theta$. The error thus introduced is only $O(\epsilon^2, \epsilon\sigma_p, \epsilon\sigma_{\mathbf{v}})$. Special care is required in expressing the gradient of η, because (4.9) relates η to φ on the curvilinear surface $\mathcal{S}_\theta$:

$$\nabla\eta = \mathrm{Fr}^2 \frac{d\varphi}{d\mathbf{x}} = \mathrm{Fr}^2\Big(\frac{\partial\varphi}{\partial\mathbf{x}} + \frac{\partial\varphi}{\partial y}\frac{\partial\theta}{\partial\mathbf{x}}\Big) = \mathrm{Fr}^2\Big(\nabla\varphi + \frac{\partial\varphi}{\partial y}\Big(\frac{\partial\theta}{\partial\mathbf{x}} - \mathbf{j}\Big)\Big) \,. \tag{4.10}$$

It then follows that

$$\frac{\partial\eta}{\partial t} + \mathbf{v}\cdot\nabla(\eta - y) = \mathrm{Fr}^2\Big(\frac{\partial\varphi}{\partial t} + \mathbf{v}\cdot\nabla(\varphi - \mathrm{Fr}^{-2}y)\Big) + \mathrm{Fr}^2\frac{\partial\varphi}{\partial y}\mathbf{v}\cdot\Big(\frac{\partial\theta}{\partial\mathbf{x}} - \mathbf{j}\Big) + O(\epsilon^2, \epsilon\sigma_p, \epsilon\sigma_{\mathbf{v}}) = 0 \,. \tag{4.11}$$

Using the kinematic condition (4.2a) and definition (4.3), the second term on the right-hand side of (4.11) can be recast into

$$\mathrm{Fr}^2\frac{\partial\varphi}{\partial y}\mathbf{v}\cdot\nabla(\theta - y) = \mathrm{Fr}^2\frac{\partial\varphi}{\partial y}\mathbf{v}\cdot\nabla(\eta - \delta - y) = -\mathrm{Fr}^2\frac{\partial\varphi}{\partial y}(\mathbf{v}\cdot\nabla\delta + \delta_t) \tag{4.12}$$

By virtue of the smoothness of δ, the term in parenthesis is just $O(\epsilon)$ and (4.12) is only $O(\epsilon\sigma_p)$. The second term on the right-hand side of (4.11) can therefore be ignored. Hence, it follows that

$$\frac{\partial\varphi}{\partial t} + \mathbf{v}\cdot\nabla(\varphi - \mathrm{Fr}^{-2}y) = 0 \,, \tag{4.13}$$

approximates the conditions at the boundary $\mathcal{S}_\theta$ to $O(\epsilon^2, \epsilon\sigma_p, \epsilon\sigma_{\mathbf{v}})$. This implies that (4.13) is a quasi free-surface condition on any fixed boundary that is sufficiently close to the actual free surface, provided that (4.6) and (4.7) are fulfilled.

One may note that (4.13) is exactly satisfied at the actual free surface. Therefore, the quasi free-surface condition can replace either the kinematic condition (4.2a) or the normal dynamic condition in the formulation of the free-surface conditions in §4.2.2.

The importance of the quasi free-surface condition is that the quasi free-surface flow solution, i.e., the solution of the Navier–Stokes equations with (4.13) and (4.2c) imposed at a fixed boundary in the neighborhood of the actual free surface, is an accurate approximation to the actual free-surface flow solution. Because the tangential dynamic conditions are largely irrelevant to the shape of the free surface (see Ref. [6]), it is anticipated that the change in the solution due to imposing (4.2c) at $\mathcal{S}_\theta$ instead of $\mathcal{S}_\eta$ is negligible. In that case, if (4.13) holds at $\mathcal{S}_\theta$, then the free surface conditions (4.2b) and (4.2a) are satisfied to $O(\epsilon^2, \epsilon\sigma_p, \epsilon\sigma_{\mathbf{v}})$ at the boundary

$$\{(\mathbf{x}, \mathrm{Fr}^2\varphi(\mathbf{x}, \theta(\mathbf{x}, t)))\} \,. \tag{4.14}$$

Therefore, the solution of the quasi free-surface flow problem is an $O(\epsilon^2, \epsilon\sigma_p, \epsilon\sigma_{\mathbf{v}})$ approximation to the solution of the free-surface flow problem. Moreover, (4.14)

is an equally accurate approximation of the actual free-surface position. One may note that (4.14) just uses the normal dynamic condition to determine the position of the free surface.

4.3 Time Integration Methods

The most widely applied iterative method for solving gravity dominated steady free-surface Navier–Stokes flow is alternating time integration of the kinematic condition, and the Navier–Stokes equations subject to the dynamic conditions, until steady state is reached. This section examines the computational complexity of this time-integration method, i.e., the number of operations per grid point expended in the solution process.

The computational complexity of the time-integration method depends on the physical time that is required to reduce transient wave components in the initial estimate to the level of other errors in the numerical solution. The transient behavior of surface gravity waves therefore plays an essential part in the complexity analysis. This transient behavior is discussed in detail in Chapter 3. Sections 4.3.1 and 4.3.2 below summarize the main results. The implications on the computational complexity is examined in Section 4.3.3.

4.3.1 Surface Gravity Waves

We consider the specific case of a small amplitude disturbance of a uniform horizontal flow on a domain $\mathcal{V} \subset \mathbb{R}^d$ of infinite horizontal extent and unit vertical extent. The domain is bounded by the undisturbed free surface $\mathcal{S}_0 := \{(\mathbf{x}, 0)\}$ and a rigid impermeable free-slip bottom $\mathcal{B} := \{(\mathbf{x}, -1)\}$. The uniform flow velocity is $\mathbf{v}^{(0)} := (v_1^{(0)}, \ldots, v_{d-1}^{(0)}, 0)$, with $|v^{(0)}| = 1$. The above implies that the undisturbed fluid-depth and flow velocity are designated as reference length and velocity, respectively.

Suppose that a disturbance is generated in the flow, such that for all $t > 0$ the resulting surface elevation satisfies $\|\eta\|_{\mathcal{S}_0} + \|\nabla\eta\|_{\mathcal{S}_0} + \|\eta_t\|_{\mathcal{S}_0} \leq \epsilon$, for some positive ϵ. We assume that the corresponding perturbed free-surface flow solution can be written as

$$\begin{pmatrix} \mathbf{v} \\ \varphi \end{pmatrix} (\mathbf{x}, y, t; \epsilon) = \begin{pmatrix} \mathbf{v}^{(0)} \\ 0 \end{pmatrix} + \epsilon \begin{pmatrix} \mathbf{v}^{(1)} \\ \varphi^{(1)} \end{pmatrix} (\mathbf{x}, y, t) + O(\epsilon^2), \qquad \text{as } \epsilon \to 0\,. \tag{4.15}$$

From §4.2.3 it follows that the solution of the quasi free-surface flow problem on $\mathcal{V}$ is an $O(\epsilon^2, \epsilon\sigma_p, \epsilon\sigma_{\mathbf{v}})$ approximation of the actual free-surface flow, with σ_p and $\sigma_{\mathbf{v}}$ defined by (4.6) and (4.7), respectively. However, (4.15) implies that σ_p and $\sigma_{\mathbf{v}}$ are of $O(\epsilon)$. Hence, the quasi free-surface flow solution on $\mathcal{V}$ is an $O(\epsilon^2)$ approximation to the actual free-surface flow solution. Consequently, for sufficiently small and smooth perturbations the results on the behavior of the quasi free-surface flow solution apply immediately to the behavior of the actual free-surface flow solution.

Suppose that the disturbance can be written as a linear combination of horizontal Fourier modes $\exp\bigl(\mathrm{i}\mathbf{k}\cdot\mathbf{x}+\mathrm{i}\omega t\bigr)$, with $\mathbf{k}\in\mathbb{R}^{d-1}$ the wave number of the Fourier mode and ω its radian frequency. Because the perturbed quasi free-surface flow problem is linear to $O(\epsilon^2)$, it suffices to consider a single mode. If the following Fourier mode is inserted for the perturbations in (4.15),

$$\begin{pmatrix} v_1^{(1)} \\ \vdots \\ v_{d-1}^{(1)} \\ v_d^{(1)} \\ \varphi^{(1)} \end{pmatrix}(\mathbf{x},y,t) = \begin{pmatrix} \mathrm{i}k_1\cosh(|\mathbf{k}|\,(1+y)) \\ \vdots \\ \mathrm{i}k_{d-1}\cosh(|\mathbf{k}|\,(1+y)) \\ |\mathbf{k}|\sinh(|\mathbf{k}|\,(1+y)) \\ (-1)^j\,\mathrm{i}\Phi(\mathbf{k})\cosh(|\mathbf{k}|\,(1+y)) \end{pmatrix}\exp\bigl(\mathrm{i}\mathbf{k}\cdot\mathbf{x}+\mathrm{i}\omega_j(\mathbf{k})\,t\bigr)\,, \tag{4.16a}$$

where $\omega_j(\mathbf{k})$ is either of the two roots of the dispersion relation:

$$\omega_j(\mathbf{k}) := -\mathbf{v}^{(0)}\cdot\mathbf{k}-(-1)^j\Phi(\mathbf{k}), \qquad j=1,2, \tag{4.16b}$$

and

$$\Phi(\mathbf{k}) := \sqrt{\mathrm{Fr}^{-2}|\mathbf{k}|\tanh(|\mathbf{k}|)}\,, \tag{4.16c}$$

then the corresponding $\mathbf{v}$ and φ comply to $O(\epsilon^2)$ with the quasi free-surface flow problem, except the tangential dynamic conditions (4.2c), which yield

$$\mathbf{t}^i\cdot\boldsymbol{\tau}(\mathbf{v})\cdot\mathbf{n} = \mathrm{Re}^{-1}\,\epsilon\,2\,\mathrm{i}\,k_j\,|\mathbf{k}|\sinh(|\mathbf{k}|)\exp\bigl(\mathrm{i}\mathbf{k}\cdot\mathbf{x}+\mathrm{i}\omega_j(\mathbf{k})\,t\bigr)\,. \tag{4.17}$$

Because (4.17) is only $O(\epsilon|\mathbf{k}|^3/\mathrm{Re})$ as $|\mathbf{k}|\to 0$, the error is negligible for sufficiently small $\mathbf{k}$ and large Re. Hence, equation (4.16a) accurately describes the behavior of smooth free-surface waves in a uniform horizontal flow at sufficiently high Reynolds numbers. The perturbations (4.16a) are called *surface gravity waves*. For an elaborate discussion of surface gravity waves in potential flow see, e.g., Refs. [42, 46].

4.3.2 Asymptotic Temporal Behavior

The asymptotic temporal behavior of surface gravity waves is determined by the asymptotic properties of the Fourier integral of the modes (4.16a). The behavior of the integral transform for $t\to\infty$ can be determined by means of the asymptotic expansion

$$\int_0^\infty F(k)\exp\bigl(\mathrm{i}t\psi(k)\bigr)\,\mathrm{d}k = \left(F(k_0)\sqrt{\frac{2\pi}{t|\psi''(k_0)|}}\exp\bigl(\mathrm{i}[t\psi(k_0)+\tfrac{1}{4}\pi\,\mathrm{sign}\,\psi''(k_0)]\bigr)+O\left(\frac{1}{t}\right)\right)+O(e^{-\beta t}), \tag{4.18}$$

with β a positive constant, $F(k)$ an analytic function and k_0 a stationary point of $\psi(k)$, i.e., $\psi'(k_0) = 0$. In the absence of stationary points, the bracketed term vanishes and only the exponentially attenuating term remains. The expansion (4.18) requires that $\psi(k)$ is smooth near stationary points in the sense that the ratio $\psi'''(k_0)/|\psi''(k_0)|^{3/2}$ is small; see Ref. [42]. The method of stationary phase (sometimes called method of steepest descent) can be used to prove (4.18); see, e.g., Refs. [46, 79].

The Fourier integral of (4.16a) can be evaluated for $t \to \infty$ by introducing a suitable coordinate transformation for $\mathbf{k}$ and applying (4.18) recursively with respect to the transformed coordinates. Denoting by $\sigma(\mathbf{x}, y, t)$ a component in (4.16a) and by $\hat{\sigma}(\mathbf{k}, y)$ its Fourier transform, one obtains

$$\sigma(\mathbf{x}, y, t) = \hat{\sigma}(\mathbf{k}_0, y)\,(2\pi/t)^{(d-1)/2}\big(\det \mathbf{H}(\mathbf{k}_0)\big)^{-1/2} \exp\big(\mathrm{i}t\psi(\mathbf{k}_0) + \mathrm{i}\zeta\big) + O(e^{-\beta t}), \tag{4.19a}$$

as $t \to \infty$. In (4.19a) we have ignored $O(t^{d/2})$ contributions of the stationary points. The phase function $\psi(\mathbf{k})$ is defined as

$$\psi(\mathbf{k}) := \mathbf{k}\cdot\mathbf{x}/t + \omega_\alpha(\mathbf{k})\,, \tag{4.19b}$$

$\mathbf{H}(\mathbf{k})$ denotes its Hessian and ζ is a multiple of $\pi/4$ depending on the properties of the Hessian; see also [78]. By (4.16b) and (4.16c), for fixed $\mathbf{x}$ and $t \to \infty$, a stationary point $\mathbf{k}_0$ of $\psi(\mathbf{k})$ occurs when

$$\frac{\partial\Phi(\mathbf{k})}{\partial k_j} = \mathrm{Fr}^{-1}\frac{\tanh|\mathbf{k}| + |\mathbf{k}|(1-\tanh^2|\mathbf{k}|)}{2\sqrt{|\mathbf{k}|\tanh|\mathbf{k}|}}\frac{k_j}{|\mathbf{k}|} = v_j^{(0)}, \qquad j = 1, \ldots, d-1. \tag{4.20}$$

Assuming that $\mathbf{v}^{(0)}$ is scaled such that $|\mathbf{v}^{(0)}| = 1$, a sufficient and necessary condition for a stationary point to exist is $\mathrm{Fr}^{-2}\Lambda(|\mathbf{k}|) = 1$, with

$$\Lambda(|\mathbf{k}|) := \frac{(\tanh|\mathbf{k}| + |\mathbf{k}|(1-\tanh^2|\mathbf{k}|))^2}{4\,|\mathbf{k}|\tanh|\mathbf{k}|}. \tag{4.21}$$

One can show that $\Lambda(|\mathbf{k}|)$ is a bijection from $\mathbb{R}_+$ to $(0, 1]$. Therefore, a single stationary point exists iff $\mathrm{Fr} \le 1$, i.e., for subcritical flows. This stationary point corresponds to a wave of which the *group velocity* (see, e.g., Refs. [46, 78]) equals the flow-velocity. Consequently, the energy associated with this wave remains at a fixed position and decays only due to dispersion.

By (4.19a), at subcritical Froude numbers the asymptotic temporal behavior of the surface gravity waves (4.16) in $\mathbb{R}^d$ is $O(t^{(1-d)/2})$ as $t \to \infty$. In particular, surface gravity waves attenuate as $1/\sqrt{t}$ in $\mathbb{R}^2$ and as $1/t$ in $\mathbb{R}^3$. At supercritical Froude numbers, a stationary point of $\psi(\mathbf{k})$ does not exist and the first term in (4.19a) vanishes. The surface gravity waves then decay exponentially as $t \to \infty$.

4.3.3 Computational Complexity

If the objective is to solve a steady free-surface flow problem by the time-integration method, then the asymptotic temporal behavior of surface gravity waves can be used to estimate the asymptotic computational complexity of the method.

Spatial discretization of the incompressible Navier–Stokes equations with appropriate boundary conditions on fixed boundaries and the free-surface conditions on the free boundary yields a discrete operator $\mathbb{L}_h : \mathcal{A}_h \mapsto \mathcal{B}_h$, with $\mathcal{A}_h$ denoting the space of grid functions on a grid with characteristic mesh width h. The operator $\mathbb{L}_h$ is assumed to be stable and pth order consistent, i.e., the *discretization error*, ϵ_h, is $O(h^p)$ as $h \to 0$.

Numerical time integration of the spatially discretized free-surface flow problem yields a sequence $\mathbf{q}_h^n \in \mathcal{A}_h$, $n = 0, 1, 2, \ldots$. The grid-function $\mathbf{q}_h^0$ is a restriction of initial conditions to the grid. Assuming the time step in the time-integration method, τ, to be constant, $\mathbf{q}_h^n$ approximates the solution of the free-surface flow problem at time $t = n\tau$. Suppose that the discretized free-surface flow problem has a unique solution $\mathbf{q}_h^* \in \mathcal{A}_h$, and that the sequence $\mathbf{q}_h^n$ indeed approaches $\mathbf{q}_h^*$ as $n\tau \to \infty$. The evaluation error is defined by

$$\gamma^n := \|q_h^n - q_h^*\|. \tag{4.22}$$

If the aim is to approximate the solution of the steady free-surface flow problem, it is sufficient to reduce the evaluation error to the level of the discretization error. Further reduction does not yield an essential improvement in the approximation of the *continuum* solution anyway. By (4.19a), the asymptotic behavior of the evaluation error at subcritical Froude numbers is

$$\gamma^n = O((n\tau)^{(1-d)/2}), \qquad \text{as } n\tau \to \infty . \tag{4.23}$$

For an example of this convergence behavior in actual computations, see the numerical experiments on fine grids in [75]. From (4.23) it follows that $\gamma^n \leq \epsilon_h$ requires

$$n = O(h^{2p/(1-d)}\tau^{-1}), \qquad \text{as } h \to 0 . \tag{4.24}$$

Equation (4.24) implies an increase of the number of time-steps to reach steady state within the required tolerance. This is particularly manifest for high-order discretizations (large p) and low spatial dimension ($d = 2$).

An additional complication is that usually the allowable time-step decreases with h. Time integration of free-surface flow problems typically proceeds in two alternating steps:

(T1) Integrate the incompressible Navier–Stokes equations, subject to the dynamic conditions at the free surface and appropriate boundary conditions at fixed boundaries.

(T2) Integrate the kinematic condition to adjust the free-surface position, using the solution from (T1).

Due to this separate treatment and the hyperbolic character of the kinematic condition, stability of the numerical time-integration method requires that the time step complies with a CFL-condition, $\tau \propto h$.

Summarizing, equation (4.24) and the CFL-condition imply that the number of time steps required to reach $\gamma^n \leq \epsilon_h$ is $O(h^{-(1+2p/(d-1))})$. Assuming that the computational complexity of the time-integration method is proportional to the number of time steps, at subcritical Froude numbers the computational complexity is

$$W = O\big(h^{-(1+2p/(d-1))}\big), \qquad \text{as } h \to 0. \tag{4.25}$$

Equation (4.25) implies a severe increase in the computational expenses as h decreases. For example, in the typical case of a 2-nd order discretization of the three-dimensional problem, if the mesh-width is halved, the required computational work *per grid point* increases by a factor of 8.

4.4 Efficient Solution of Steady Free-Surface Flows

From Section 4.3 it is evident that the usual time-integration approach is inappropriate for solving steady free-surface flows at subcritical Froude numbers. In this section we present an efficient iterative solution method for gravity subjected steady free-surface flows. The method is outlined in Sect. 4.4.1. The convergence properties of the method and its computational complexity are examined in Sects. 4.4.2 and 4.4.3.

4.4.1 Iterative Solution Method

From the results in §4.2.3, it follows that an accurate approximation to the free-surface flow and to the free-surface position can be obtained by the following operations:

(I1) For a given initial boundary $\mathcal{S}$, solve $(\mathbf{v}, \varphi)$ from

$$\left.\begin{aligned} \operatorname{div} \mathbf{v}\mathbf{v} + \nabla\varphi - \operatorname{div} \boldsymbol{\tau}(\mathbf{v}) &= 0 \\ \operatorname{div} \mathbf{v} &= 0 \end{aligned}\right\}, \qquad (\mathbf{x}, y) \in \mathcal{V}, \tag{4.26a}$$

$$\mathbb{B}(\mathbf{v}, p) = \mathbf{b}(\mathbf{x}, y), \qquad (\mathbf{x}, y) \in \partial\mathcal{V} \setminus \mathcal{S}, \tag{4.26b}$$

$$\left.\begin{aligned} \mathbf{t}^i \cdot \boldsymbol{\tau}(\mathbf{v}) \cdot \mathbf{n} &= 0 \\ \mathbf{v} \cdot \nabla\varphi - \mathrm{Fr}^{-2}\mathbf{j} \cdot \mathbf{v} &= 0 \end{aligned}\right\}, \qquad (\mathbf{x}, y) \in \mathcal{S}\,, \tag{4.26c}$$

where (4.26b) represents boundary conditions on the fixed boundary.

(I2) Use the solution of (I1) to adjust the boundary $\mathcal{S}$ to

$$\big\{(\mathbf{x}, y + \mathrm{Fr}^2\varphi(\mathbf{x}, y)) : (\mathbf{x}, y) \in \mathcal{S}\big\}\,. \tag{4.27}$$

Note the appearance of the quasi free-surface condition in its steady form in (4.26c). The modified boundary approximates the actual free surface more accurately than

the initial boundary, provided that the conditions discussed in §4.2.3 are fulfilled. Hence, it is anticipated that the solution to the free-surface flow problem can be obtained by iterating the operations (I1) and (I2).

If $\mathcal{S}$ is the actual free surface, then the normal dynamic condition is satisfied, i.e., p vanishes on $\mathcal{S}$. In that case, $\mathbf{n} \parallel \nabla p$, and (4.26c) implies that the solution of (4.26) complies with the kinematic condition and the tangential dynamic conditions. Hence, operation (I1) then yields the free-surface flow. Moreover, the normal dynamic condition ensures that the surface adjustment in (I2) vanishes, so that the solution of the free-surface flow problem is indeed a fixed point of the iteration.

It is important to notice the absence of time-dependent terms in (I1) and (I2). Therefore, the slow decay of transient waves described in Section 4.3 is irrelevant to the convergence of the iterative process. The actual convergence properties of (I1)-(I2) are examined below.

4.4.2 Convergence

The convergence behavior of the iterative method (I1)-(I2) can be conveniently examined by rephrasing the free-surface flow problem as an optimal shape design problem. A general characteristic of free-boundary problems is that the number of free-boundary conditions is one more than the number of boundary conditions required by the governing boundary-value problem. A free-boundary problem can therefore be reformulated into the equivalent optimal shape design problem of finding the boundary that minimizes a norm of the residual of one of the free-surface conditions, subject to the boundary-value problem with the remaining free-surface conditions imposed.

To obtain an optimal shape design formulation of the steady free-surface flow problem, the *cost functional* E is defined by

$$E\big(\mathcal{S}, (\mathbf{v}, p)\big) := \int_{\mathcal{S}} |p(\mathbf{x}, y)| \, \mathrm{d}\mathcal{S} \,. \tag{4.28}$$

Assuming that (4.26) is well posed for all surfaces $\mathcal{S}$ in a space of admissible boundaries $\mathcal{O}$, and that $\mathcal{O}$ contains the actual free-surface, the free-surface flow problem is equivalent with the optimal shape design problem

$$\min_{\mathcal{S}\in\mathcal{O}} \big\{ E\big(\mathcal{S}, (\mathbf{v}, p)\big) : (\mathbf{v}, p) \text{ satisfies (4.26)} \big\} \,. \tag{4.29}$$

Notice that (4.29) is in fact a constrained optimization problem, with the boundary value problem (4.26) acting as a *constraint* on $(\mathbf{v}, p)$.

The optimal shape design formulation of the free-surface flow problem allows convenient assessment of the convergence properties of the iterative method (I1)-(I2). Each iteration adjusts the approximation to the free-surface position. Convergence of the iterative method is ensured if each surface adjustment yields a

reduction of the cost functional (4.28). Moreover, the reduction of the cost functional between successive iterations is a measure of the efficiency of the method.

To determine the effect of a surface adjustment, consider the boundary $\mathcal{S}$ and the modified boundary

$$\mathcal{S}_{\epsilon\alpha} := \{(\mathbf{x}, y) + \epsilon\alpha(\mathbf{x}, y)\,\mathbf{j} : (\mathbf{x}, y) \in \mathcal{S}\}\,, \tag{4.30}$$

for a suitably smooth function α independent of ϵ on $\mathcal{S}$. The modified boundary is the boundary of a domain $\mathcal{V}_{\epsilon\alpha}$, which approaches $\mathcal{V}$ as $\epsilon \to 0$. Following [51], $\mathcal{V}$ and $\mathcal{V}_{\epsilon\alpha}$ are embedded in a bounded set $\mathcal{E}$ and it is assumed that for all $\mathcal{V} \subset \mathcal{E}$ with $\mathcal{S} \in \mathcal{O}$, a solution of (4.26) can be extended smoothly beyond the boundary, so that $(\mathbf{v}, p)$ is well defined everywhere in $\mathcal{E}$.

The displacement of the boundary from $\mathcal{S}$ to $\mathcal{S}_{\epsilon\alpha}$ induces a disturbance in the solution of (4.26). Denoting by $(\mathbf{v}, p)_{\epsilon\alpha}$ the solution of (4.26) on $\mathcal{V}_{\epsilon\alpha}$, the *induced disturbance* is defined by

$$(\mathbf{v}, p)'_\alpha := \lim_{\epsilon \to 0} \tfrac{1}{\epsilon}\big((\mathbf{v}, p)_{\epsilon\alpha} - (\mathbf{v}, p)\big)\,. \tag{4.31}$$

Taylor expansion of the cost functional then yields

$$E\big(\mathcal{S}_{\epsilon\alpha}, (\mathbf{v}, p)_{\epsilon\alpha}\big) = \int_{\mathcal{S}} |p + \epsilon(\alpha\,\mathbf{j}\cdot\nabla p + p'_\alpha)|\,(1 + \epsilon\mu_\alpha)\,\mathrm{d}\mathcal{S} + O(\epsilon^2), \qquad \text{as } \epsilon \to 0. \tag{4.32}$$

In (4.32), the function $\mu_\alpha : \mathcal{S} \mapsto \mathbb{R}$ accounts for the change in the surface area from $\mathrm{d}\mathcal{S}$ to $\mathrm{d}\mathcal{S}_{\epsilon\alpha}$. Ignoring terms $O(\epsilon^2)$, the modified boundary $\mathcal{S}_{\epsilon\alpha}$ improves on $\mathcal{S}$ if a positive constant $\zeta < 1$ exists such that

$$\int_{\mathcal{S}} |p + \epsilon(\alpha\,\mathbf{j}\cdot\nabla p + p'_\alpha)|\,(1 + \epsilon\mu_\alpha)\,\mathrm{d}\mathcal{S} \le \zeta \int_{\mathcal{S}} |p|\,\mathrm{d}\mathcal{S}\,. \tag{4.33}$$

If (4.33) holds for some $\zeta < 1$, then the modification of the boundary from $\mathcal{S}$ to $\mathcal{S}_{\epsilon\alpha}$ yields a reduction of the cost functional. The smallest positive constant that satisfies (4.33) is called the *contraction number*. Clearly, a small contraction number implies a successful surface modification.

Operation (I2) in the iterative procedure gives a correction of the boundary position $\epsilon\alpha = \mathrm{Fr}^2 p$. In that case, the value of the cost functional corresponding to the modified surface is bounded by

$$E\big(\mathcal{S}_{\epsilon\alpha}, (\mathbf{v}, p)_{\epsilon\alpha}\big) \le \int_{\mathcal{S}} |p|\,|1 + \mathrm{Fr}^2\mathbf{j}\cdot\nabla p|\,(1 + \epsilon\mu_\alpha)\,\mathrm{d}\mathcal{S} + \int_{\mathcal{S}} |\epsilon p'_\alpha|\,\mathrm{d}\mathcal{S}\,. \tag{4.34}$$

Hence, the contraction number ζ of the iterative process (I1)-(I2) is bounded by

$$\zeta \le \sigma_p + \frac{\int_{\mathcal{S}} |\epsilon p'_\alpha|\,\mathrm{d}\mathcal{S}}{\int_{\mathcal{S}} |p|\,\mathrm{d}\mathcal{S}} + O(\epsilon)\,, \tag{4.35}$$

with σ_p defined by (4.6). From (4.35) it follows that if ϵ and σ_p are indeed small, then the induced disturbance determines the convergence behavior of the iterative method.

To establish convergence of (I1)-(I2), it remains to show that the induced disturbance p'_α is indeed small. Sec. 4.2.3 shows that the quasi free-surface condition (4.13) approximates the conditions at a fixed boundary in the neighborhood of the free surface to $O(\epsilon^2, \epsilon\sigma_p, \epsilon\sigma_{\mathbf{v}})$. Hence, displacing this condition from $\mathcal{S}$ to $\mathcal{S}_{\epsilon\alpha}$ yields no greater disturbance than that. In [6] it is shown that the tangential dynamic conditions are largely irrelevant to the shape of the free surface. Conversely, the induced disturbance due to enforcing the tangential dynamic conditions at $\mathcal{S}$ instead of $\mathcal{S}_{\epsilon\alpha}$ can be neglected. Therefore, the contraction number of the method (I1)-(I2) is estimated

$$\zeta = O(\epsilon, \sigma_p, \sigma_{\mathbf{v}}) \,. \tag{4.36}$$

4.4.3 Computational Complexity

Eq. (4.36) provides an upper bound for the contraction number of the method (I1)-(I2). One may note that if the approximate boundary is sufficiently close to the actual free surface (ϵ small), then (4.36) depends on properties of the continuum solution only. Therefore, if the free-surface flow problem is solved numerically, the behavior of the iterative method is asymptotically independent of the mesh width.

The iteration must be continued until the pressure defect at the free surface (4.28) has been reduced to the level of the spatial discretization error. Further reduction does not essentially improve the approximation of the *continuum* solution anyway. Each iteration reduces the pressure defect at the free-surface by a factor ζ. Therefore, the number of iterations n must satisfy

$$\zeta^n = O(h^p), \tag{4.37}$$

where p denotes the order of consistency of the spatial discretization. This implies that $n = O(p \log h / \log \zeta)$. Assuming that the computational complexity of the iterative method is proportional to the number of iterations, the following estimate of the computational complexity is obtained:

$$W = O(\log h) \,. \tag{4.38}$$

Hence, the efficiency of the method (I1)-(I2) decays only moderately as h decreases.

To eliminate the remaining weak h-dependence of the computational complexity, *nested iteration* can be used. Generally, an iterative solution method is used to solve the boundary value problem (4.26) in step (I1) of the algorithm. The nesting involves the use of the solution from the previous iteration as an initial estimate for the solution process. Because this initial estimate becomes increasingly accurate, the cost of performing (I1) reduces as the iteration progresses. In particular, assuming that the cost of solving (4.26) is proportional to the pressure defect at the free surface, the amount of work that is required to achieve (4.37) is

$$W = w + \zeta\, w + \zeta^2 w + \cdots + \zeta^n w \leq \frac{1}{1-\zeta} w \,, \tag{4.39}$$

with w the cost of solving (4.26) initially. Observe that the computational complexity (4.39) is indeed entirely independent of the mesh width.

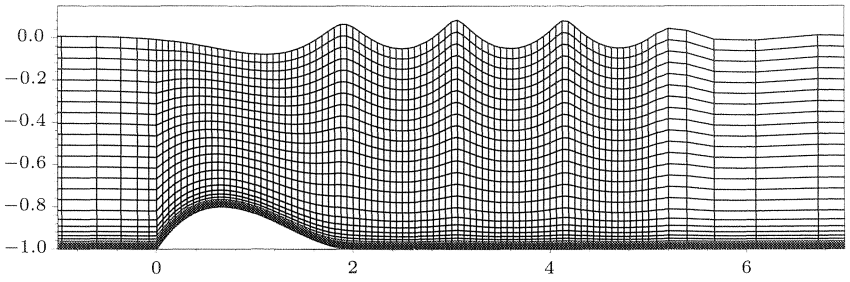

Figure 4.2: Example of a grid used in the numerical experiments. The grid is coarsened for illustration purposes.

4.5 Numerical Experiments and Results

The method is tested for subcritical flow over an obstacle in a channel of unit depth, at $\mathrm{Fr} = 0.43$ and $\mathrm{Re} = 1.5 \times 10^5$, with the undisturbed fluid depth and the undisturbed flow velocity at the free surface assigned as the reference length and velocity, respectively. The geometry of the obstacle is

$$y(x) = -1 + \frac{27}{4}\frac{H}{L^3}\, x\,(x-L)^2\,, \qquad 0 \le x \le L\,, \tag{4.40}$$

with H and L the (non-dimensionalized) height and length of the obstacle, respectively. Choosing $H = 0.2$ and $L = 2$, the setup is in agreement with [12]. At the bottom boundary no-slip boundary conditions are imposed. A boundary-layer velocity profile in accordance with the experiments from [12] is imposed at the inflow boundary.

The test case with $H = 0.2$ displays large amplitude waves that exhibit typical nonlinear effects, such as sharp wave crests and wave-length reduction. In addition, $H = 0.15$ is considered. This test case displays waves more in accordance with linear wave-theory, see, e.g., Refs. [42, 46].

The experiments are performed on grids with horizontal mesh widths $h = 2^{-5}, 2^{-6}$. The number of grid cells in the vertical direction is 70 and exponential grid stretching is applied to resolve the boundary layer at the bottom. Furthermore, the grid is coarsened towards the inflow and outflow boundaries to reduce reflections. A typical example of a grid used in the numerical experiments is presented in Figure 4.2. The RANS equations, closed with an eddy viscosity model due to Cebeci and Smith [14], and the boundary conditions are discretized and solved by the method described in [32]. After each evaluation, the grid is adapted using vertical stretching. An initial estimate of the solution on the adapted grid is subsequently generated by linear interpolation from the solution on the previous grid. Details of the discretization method and the setup of the numerical experiments can be found in [10].

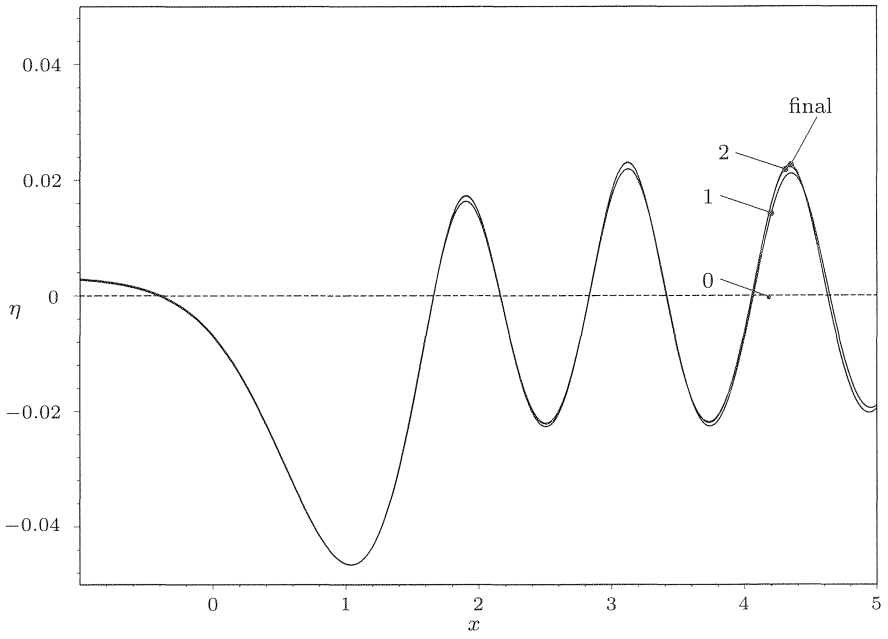

Figure 4.3: Wave profile obtained after successive iterations ($H = 0.15$).

Figure 4.3 and Figure 4.4 show the wave profiles obtained in successive iterations for $H = 0.15$ and $H = 0.2$, respectively. The initial estimate (0th iterate) is just the undisturbed free surface. One may note that the first iterate already displays a qualitatively correct wave profile. This confirms that the quasi free-surface flow solution is an accurate approximation to the actual free-surface flow solution. A converged solution is obtained in approximately 2 iterations for $H = 0.15$ and in approximately 10 iterations for $H = 0.2$. Due to the decreasing computational cost of each iteration (refer to §4.4.3), even for $H = 0.2$ the entire computation is just 2 to 3 times as expensive as the corresponding fixed domain problem with symmetry boundary conditions at the undisturbed surface.

Figure 4.5 on page 51 displays the pressure defect at the free surface after consecutive iterations. The results confirm convergence of the method. For $H = 0.15$, the average contraction number is $\zeta \approx 0.15$ and the convergence behavior is indeed independent of h. After several iterations the contraction number increases. However, this is entirely due to the fact that the quasi free-surface flow problem (4.26) is solved only by approximation. If the tolerance on the residual of (4.26) is reduced, i.e., if (4.26) is solved more accurately, then the original contraction number is recovered. For $H = 0.20$, the average contraction number is

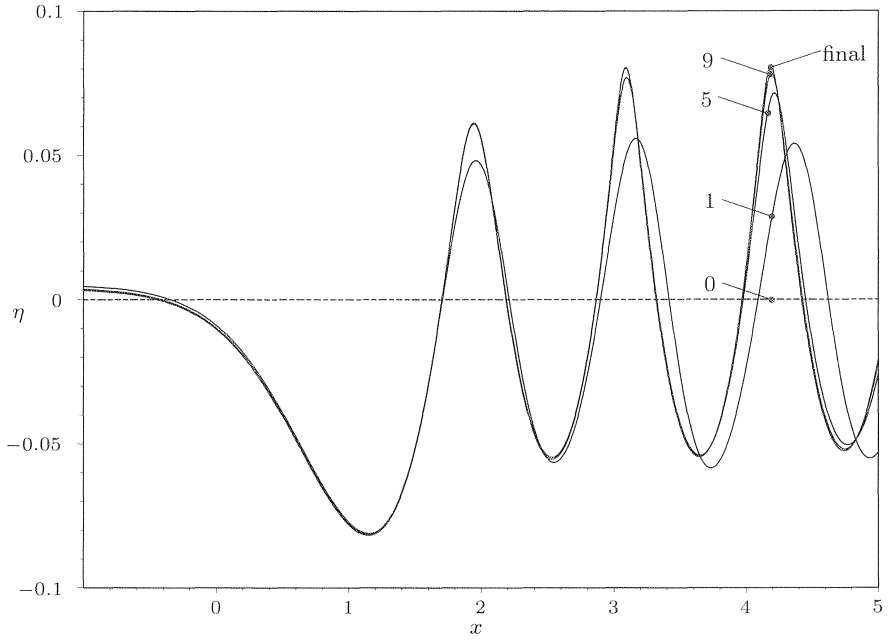

Figure 4.4: Wave profile obtained after successive iterations ($H = 0.2$).

$\zeta \approx 0.45$ for $h = 2^{-5}$ and $\zeta \approx 0.52$ for $h = 2^{-6}$. As a result of strong nonlinearity, the asymptotic mesh width independence of the convergence behavior is in this case not yet apparent.

A detailed investigation of the convergence behavior of time-integration methods for the test case with $H = 0.20$ is presented in [75]. Typically, the time-integration method requires approximately 10^4 surface adjustments to reduce the initial error by a factor of 10. The presented method achieves this in approximately 4 iterations, for a similar setting of the numerical experiment.

Figure 4.6 on page 52 compares the computed wave elevation with measurements from [12]. In [12], a non-dimensionalized amplitude $a = 4.5 \times 10^{-2} \pm 15\%$ and wave length $\lambda = 1.10 \pm 10\%$ are reported for the trailing wave. The trailing wave of the computed wave elevation on the grid with $h = 2^{-6}$ displays amplitude $a = 6.5 \times 10^{-2}$ and wave length $\lambda = 1.11$. Hence, the computed wave length agrees well with the measurements. The amplitude appears to be overestimated. However, the difference between the amplitude of the numerical results and of the experimental data is not unusual, see, e.g., Refs. [75, 76]. Observe also that the difference in the amplitude of the first wave and the second wave is correctly predicted.

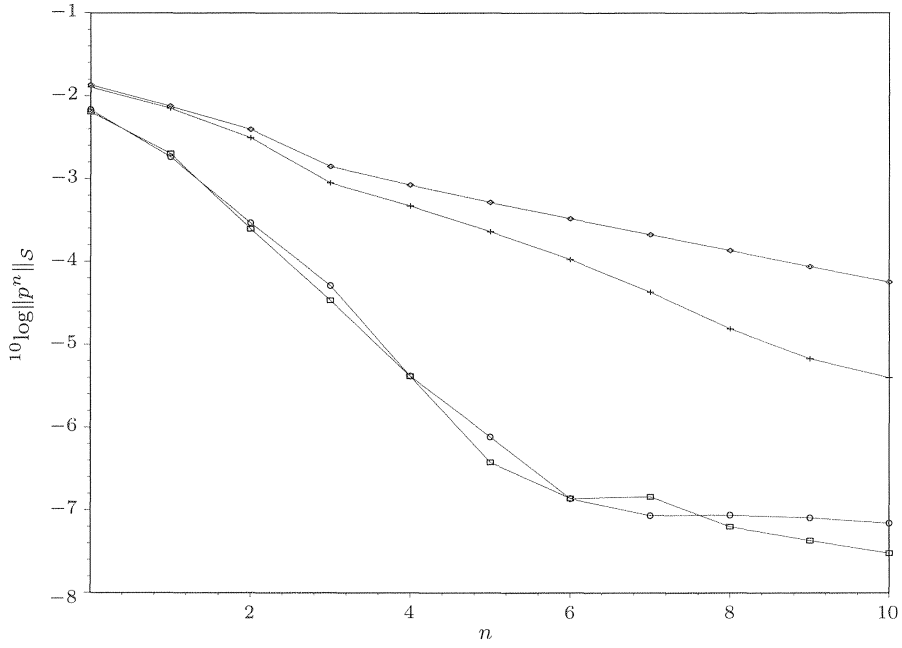

Figure 4.5: Pressure defect at the free surface versus the iteration number for $H = 0.15$, $h = 2^{-5}$ (□), $h = 2^{-6}$ (○) and $H = 0.20$, $h = 2^{-5}$ (+), $h = 2^{-6}$ (◇).

4.6 Conclusion

The usual time-integration method for solving steady free-surface Navier–Stokes flow problems was shown to be inefficient due to the specific transient behavior of surface gravity waves and a CFL-condition on the allowable time step.

Motivated by the demand for efficient computational methods in practical applications, we proposed a new iterative solution method. The method alternatingly solves the steady Navier–Stokes equations with a quasi free-surface condition imposed at the free surface, and adjusts the free surface using the computed solution and the normal dynamic condition.

Examination of the convergence properties of the iterative method revealed that the method uses the quasi free-surface condition to ensure that the disturbance induced by the displacement of the boundary is small. It was shown that the behavior of the method is asymptotically independent of the mesh width. The asymptotic computational complexity of the iterative method deteriorates only moderately with decreasing mesh width. Mesh width independence of the computational complexity can be achieved by means of nested iteration.

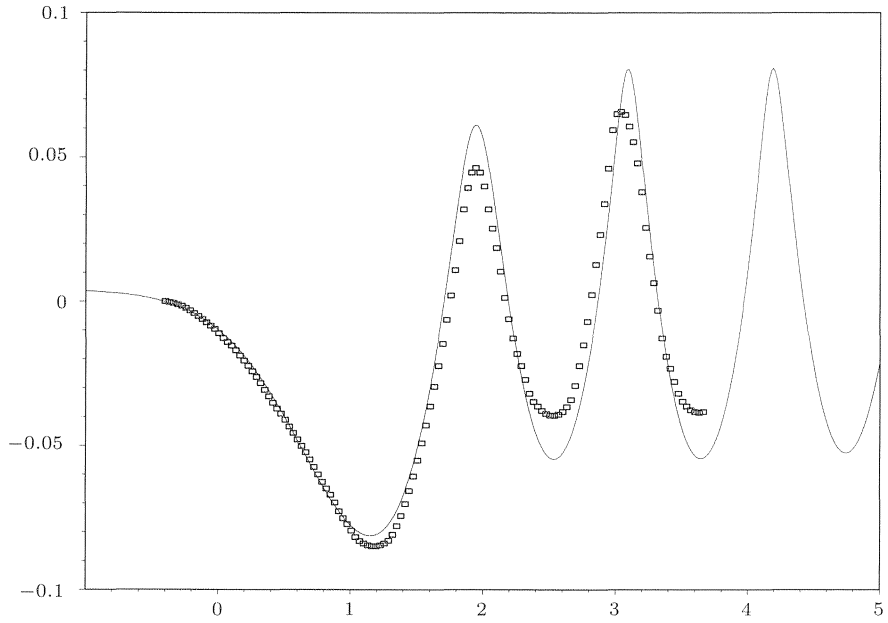

Figure 4.6: Computed wave elevation for $h = 2^{-6}$ (*solid line*) and measurements from [12] (*markers only*), for $H = 0.20$. The obstacle is located in the interval $x \in [0, 2]$.

Numerical results were presented for two-dimensional flow over an obstacle in a channel. For the presented test cases, a converged solution was obtained in at most 10 iterations. The numerical results agree well with measurements. The numerical experiments confirmed that the behavior of the method is asymptotically independent of the mesh width.

We believe that the proposed method will be useful in ship hydrodynamics, hydraulics and other fields of application in which the efficient computation of steady free-surface flows at high Reynolds number is required.

Chapter 5
Adjoint Shape Optimization for Steady Free-Surface Flows

5.1 Introduction

The numerical solution of flows that are partly bounded by a free boundary is of great importance in engineering applications, e.g., ship hydrodynamics [3, 13, 18], hydraulics and coating technology [54, 55]. A relevant class of free-surface flow problems are *steady* free-surface flows. An example of a steady free-surface flow is the wave pattern carried by a ship at forward speed in still water. The numerical techniques for free-surface potential flow are well developed; for an overview, see [74]. In particular, dedicated techniques have been developed for solving the steady free-surface potential-flow equations, e.g., Ref. [52]. In contrast, methods for the steady free-surface Navier–Stokes equations typically continue a transient process until a steady state is reached. This time-integration method is often computationally inefficient, due to the specific transient behavior of free-surface flows; see [11, 80]. Alternative solution methods for the steady free-surface Navier–Stokes equations exist. However, the performance of these methods usually depends sensitively on the parameters in the problem, or their applicability is too restricted; see, for instance, Refs. [55, 61]. In [11], an efficient iterative algorithm was presented. However, the implementation of the quasi free-surface condition that underlies the efficiency of this method can be involved. Hence, the investigation of numerical methods for the steady free-surface Navier–Stokes equations is warranted.

A general characteristic of free-boundary problems is that the number of free-boundary conditions is one more than the number of boundary conditions required by the governing boundary value problem. A free-boundary problem can therefore be reformulated into the equivalent shape optimization problem of finding the boundary that minimizes a norm of the residual of one free-boundary condition, subject to the boundary value problem with the other free-boundary conditions imposed.

Optimal shape design problems can in principle be solved efficiently by means of the adjoint method. In recent years, much progress has been made in the development of adjoint techniques for problems from fluid dynamics. Applications to the Navier–Stokes equations include flow control (see [21] and the references therein), a posteriori error estimation and adaptivity (for instance, [7, 8]) optimal design (e.g., Refs. [22, 25]) and domain decomposition (cf. Ref. [26]). The techniques that are required to solve the optimal shape design problem associated with steady free-surface flow are readily available.

The present work investigates the suitability of the adjoint shape optimization method for solving steady free-surface flow problems. Our primary interest is in the steady free-surface Navier–Stokes equations. However, because inviscid, irrotational flow adequately describes the prominent features of free-surface flow and to avoid the excessive complexity of the Navier–Stokes equations, we base our investigation on the free-surface potential-flow equations. It is anticipated that the adjoint shape optimization method is equally applicable to the free-surface Navier–Stokes equations, although the specifics of the method are much more involved in that case. Our investigation serves as an indication of the properties of the adjoint shape optimization method for steady free-surface flow problems.

The contents of this chapter are organized as follows: In Section 5.2 the equations governing steady free-surface potential flow and the associated design problem are stated. Section 5.3 formulates the adjoint equations and sets up the adjoint optimization method. Section 5.4 presents an analysis of the properties of the optimization problem and the behavior of the adjoint method, using Fourier techniques from [69]. Motivated by the results of the Fourier analysis, we describe a preconditioning for the optimization problem in Section 5.5. Numerical experiments and results are presented in Section 5.6. Section 5.7 contains concluding remarks.

5.2 Problem Statement

We consider an incompressible, inviscid fluid flow, subject to a constant gravitational force, acting in the negative vertical direction. The fluid occupies a domain $\mathcal{V} \subset \mathbb{R}^d$ $(d = 2, 3)$ which is bounded by a free boundary, $\mathcal{S}$, and a fixed boundary $\partial\mathcal{V} \setminus \mathcal{S}$. The fixed boundary can be subdivided in an inflow boundary, an outflow boundary and a rigid, impermeable boundary.

5.2.1 Governing Equations

The (non-dimensionalized) fluid velocity and pressure are identified by $\mathbf{v}(\mathbf{x})$ and $p(\mathbf{x})$, respectively. Assuming that the velocity-field is irrotational, a velocity potential $\phi(\mathbf{x})$ exists such that $\mathbf{v} = \nabla\phi$. Enforcing incompressibility then yields that the velocity potential is governed by Laplace's equation,

$$\Delta\phi = 0\,, \qquad \mathbf{x} \in \mathcal{V}\,. \tag{5.1}$$

Assuming that $|\nabla\phi| = 1$ at the inflow boundary, Bernoulli's equation relates the pressure to the velocity potential by

$$p(\mathbf{x}) := \tfrac{1}{2} - (\tfrac{1}{2}|\nabla\phi|^2 + \mathrm{Fr}^{-2}x_d)\,, \tag{5.2}$$

with x_d the vertical coordinate and Fr the Froude number, defined by $\mathrm{Fr} := V/\sqrt{gL}$ with V an appropriate reference velocity, g the gravitational acceleration and L a reference length.

The free-surface conditions prescribe that the free surface is impermeable and that the pressure vanishes at the free surface:

$$\mathbf{n}\cdot\nabla\phi = 0, \qquad \mathbf{x}\in\mathcal{S}, \tag{5.3a}$$

$$p = 0, \qquad \mathbf{x}\in\mathcal{S}, \tag{5.3b}$$

with $\mathbf{n}(\mathbf{x})$ the unit normal vector to $\mathcal{S}$. Conditions (5.3a) and (5.3b) are referred to as the kinematic condition and the dynamic condition, respectively. A single appropriate boundary condition must be specified at the fixed boundary. We assume that this condition is of the form

$$a\,\mathbf{n}\cdot\nabla\phi + b\,\phi = c\,, \qquad \mathbf{x}\in\partial\mathcal{V}\setminus\mathcal{S}, \tag{5.4}$$

for certain functions $a, b, c : \partial\mathcal{V}\setminus\mathcal{S} \mapsto \mathbb{R}$.

The steady free-surface flow problem under consideration is the problem of finding $\mathcal{S}$ and ϕ such that ϕ satisfies (5.1)–(5.4). However, this problem is not necessarily well posed. Firstly, solutions can be non-unique due to the occurrence of arbitrary non-physical upstream waves. To remove these waves, a radiation condition must be imposed; cf., for instance, [42, 46, 65]. In numerical computations, this radiation condition can be conveniently enforced by introducing artificial damping (see Section 5.6) or by selecting a suitable discretization (see, e.g., Ref. [52]). Secondly, a steady solution can be nonexistent, in the sense that the transient problem underlying (5.1)–(5.4) does not approach a steady state as time progresses ad infinitum; see, for instance, Ref. [80].

5.2.2 Optimal Shape Design Formulation

One may note that the number of free-surface conditions (5.3) is one more than the number of boundary conditions required by (5.1). The free-boundary problem can therefore be reformulated into the equivalent optimal shape design problem of finding the boundary that minimizes a norm of the residual of one of the free-surface conditions, subject to the boundary value problem with the remaining free-surface conditions imposed.

To obtain an optimal shape design formulation of the steady free-surface flow problem, the *cost functional* E is defined by

$$E(\mathcal{S},\phi) := \int_{\mathcal{S}} \tfrac{1}{2}p(\mathbf{x})^2\,\mathrm{d}\mathbf{x}\,, \tag{5.5}$$

and the *constraint* C is defined by the boundary value problem (5.1), (5.3a) and (5.4):

$$C(\mathcal{S},\phi) := \begin{cases} \Delta\phi = 0\,, & \mathbf{x} \in \mathcal{V}\,, \\ \mathbf{n}\cdot\nabla\phi = 0\,, & \mathbf{x} \in \mathcal{S}\,, \\ a\,\mathbf{n}\cdot\nabla\phi + b\,\phi = c\,, & \mathbf{x} \in \partial\mathcal{V}\setminus\mathcal{S}\,. \end{cases} \tag{5.6}$$

Note that the cost functional is a norm of the residual of the dynamic condition (5.3b) and that the kinematic condition (5.3a) appears in the constraint. The free-surface flow problem is equivalent to the optimal shape design problem

$$\min_{\mathcal{S}}\{E(\mathcal{S},\phi) : C(\mathcal{S},\phi)\}\,, \tag{5.7}$$

i.e., minimize (5.5) over all $\mathcal{S}$, subject to the constraint that ϕ satisfies (5.6). Because the boundary value problem (5.6) associates a unique ϕ with each free boundary $\mathcal{S}$, it is often convenient to use the notation $E(\mathcal{S})$ for $E(\mathcal{S},\phi)$ with ϕ from (5.6).

5.3 Adjoint Optimization Method

Shape-optimization problems can in principle be solved efficiently by means of the adjoint optimization method. The essential problem in treating shape optimization problems is that a displacement of the free boundary induces a disturbance in the solution of the boundary value problem and, consequently, it is attended with an induced change in the cost functional. Efficient solution of a shape optimization problem requires control over the induced change in the cost functional. The adjoint optimization method eliminates the induced change by means of the solution of a dual problem. Upon elimination of the induced change, the gradient of the cost functional with respect to the free-boundary position is obtained. Improvement of the free-boundary position is then straightforward. This section outlines the adjoint optimization method for solving (5.7).

5.3.1 Induced Disturbance

To formulate the adjoint optimization method for (5.7), the induced disturbance in the solution of the constraint and the corresponding change in the cost functional must first be identified. To this end, we consider a domain $\mathcal{V}$ with free boundary $\mathcal{S}$ and a modified domain $\mathcal{V}_{\epsilon\alpha}$ with free boundary

$$\mathcal{S}_{\epsilon\alpha} := \{\mathbf{x} + \epsilon\alpha(\mathbf{x})\,\mathbf{n}(\mathbf{x}) : \mathbf{x} \in \mathcal{S}\}, \tag{5.8}$$

where α is a smooth function on $\mathcal{S}$, independent of ϵ. Following [51], $\mathcal{V}$ and $\mathcal{V}_{\epsilon\alpha}$ are embedded in a bounded set $\mathcal{E}$ and it is assumed that a solution of the constraint can be extended smoothly beyond the boundary, so that it is well defined in $\mathcal{E}$.

Denoting by ϕ the solution of $C(\mathcal{S},\phi)$ and by $\phi_{\epsilon\alpha}$ the solution of $C(\mathcal{S}_{\epsilon\alpha},\phi_{\epsilon\alpha})$, we define the *induced disturbance* by the function $\phi'_\alpha : \mathcal{E} \mapsto \mathbb{R}$ with the property

$$\phi_{\epsilon\alpha} = \phi + \epsilon\phi'_\alpha + O(\epsilon^2)\,, \qquad \text{as } \epsilon \to 0\,, \tag{5.9}$$

i.e., $\epsilon\phi'_\alpha$ approximates to $O(\epsilon^2)$ the change in the solution of the constraint (5.6) due to the displacement of the free boundary from $\mathcal{S}$ to $\mathcal{S}_{\epsilon\alpha}$. The kinematic condition corresponding to the modified boundary yields:

$$\begin{aligned}&\big[\mathbf{n}_{\epsilon\alpha}\cdot\boldsymbol{\nabla}\phi_{\epsilon\alpha}\big]\big(\mathbf{x}+\epsilon\alpha(\mathbf{x})\mathbf{n}(\mathbf{x})\big) = \\ &\left[\left(\mathbf{n}-\epsilon\sum_{j=1}^{d-1}(\mathbf{t}_j\cdot\boldsymbol{\nabla}\alpha)\,\mathbf{t}_j+O(\epsilon^2)\right)\cdot\left(\boldsymbol{\nabla}\phi+\epsilon\boldsymbol{\nabla}\phi'_\alpha+\epsilon\alpha\mathbf{n}\cdot\boldsymbol{\nabla}\boldsymbol{\nabla}\phi+O(\epsilon^2)\right)\right](\mathbf{x}) = 0\,,\end{aligned} \tag{5.10}$$

for $\mathbf{x}\in\mathcal{S}$, with $\mathbf{n}_{\epsilon\alpha}$ the unit normal vector to $\mathcal{S}_{\epsilon\alpha}$ and $\mathbf{t}_j$ orthogonal tangent vectors to $\mathcal{S}$. Hence, inserting (5.9) in $C(\mathcal{S}_{\epsilon\alpha},\phi_{\epsilon\alpha})$ and collecting terms $O(\epsilon)$, it follows that the induced disturbance satisfies the boundary value problem:

$$\Delta\phi'_\alpha = 0\,, \qquad \mathbf{x}\in\mathcal{V}\,, \tag{5.11a}$$

$$\mathbf{n}\cdot\boldsymbol{\nabla}\phi'_\alpha = -\alpha\mathbf{n}\mathbf{n} : \boldsymbol{\nabla}\boldsymbol{\nabla}\phi + \sum_{j=1}^{d-1}(\mathbf{t}_j\cdot\boldsymbol{\nabla}\alpha)\,(\mathbf{t}_j\cdot\boldsymbol{\nabla}\phi)\,, \qquad \mathbf{x}\in\mathcal{S}\,, \tag{5.11b}$$

$$a\,\mathbf{n}\cdot\boldsymbol{\nabla}\phi'_\alpha + b\,\phi'_\alpha = 0\,, \qquad \mathbf{x}\in\partial\mathcal{V}\setminus\mathcal{S}\,. \tag{5.11c}$$

The operator $\mathbf{nn} : \boldsymbol{\nabla}\boldsymbol{\nabla}$ in (5.11b) represents the second order derivative in the normal direction.

To identify the induced change in the cost functional, the functional value corresponding to the modified boundary, $E(\mathcal{S}_{\epsilon\alpha})$, is expanded as

$$E(\mathcal{S}_{\epsilon\alpha}) := E(\mathcal{S}_{\epsilon\alpha},\phi_{\epsilon\alpha}) = E(\mathcal{S})+\epsilon\left(I'_\alpha(\mathcal{S})+J'_\alpha(\mathcal{S})\right)+O(\epsilon^2), \qquad \text{as } \epsilon\to 0, \tag{5.12a}$$

with

$$I'_\alpha(\mathcal{S}) := -\int_{\mathcal{S}} p\,\boldsymbol{\nabla}\phi\cdot\boldsymbol{\nabla}\phi'_\alpha \mathrm{d}\mathbf{x}\,, \tag{5.12b}$$

$$J'_\alpha(\mathcal{S}) := -\int_{\mathcal{S}} \alpha\left(\frac{p^2}{2R}+p\,\mathbf{n}\cdot\boldsymbol{\nabla}\tfrac{1}{2}|\boldsymbol{\nabla}\phi|^2+p\,\mathrm{Fr}^{-2}\mathbf{n}\cdot\mathbf{e}_d\right)\mathrm{d}\mathbf{x}\,, \tag{5.12c}$$

where $R(\mathbf{x})$ is the radius of curvature ($d=2$) or mean radius of curvature ($d=3$) and $\mathbf{e}_d$ is the vertical unit vector. The curvature-term in (5.12c) results from the change in the surface area from $\mathcal{S}$ to $\mathcal{S}_{\epsilon\alpha}$; see, e.g., Ref. [51]. Noting that only (5.12b) depends on ϕ'_α, the induced change in the cost functional is readily

identified as (5.12b). Integration by parts recasts (5.12b) into the convenient form:

$$I'_\alpha(\mathcal{S}) = \int_{\mathcal{S}} \phi'_\alpha \sum_{j=1}^{d-1} \mathbf{t}_j \cdot \boldsymbol{\nabla}(p\,\mathbf{t}_j \cdot \boldsymbol{\nabla}\phi)\,\mathrm{d}\mathbf{x}\,. \tag{5.13a}$$

Moreover, the second term in (5.12c) vanishes due to the kinematic condition (5.3a):

$$J'_\alpha(\mathcal{S}) = -\int_{\mathcal{S}} \alpha \left(\frac{p^2}{2R} + p\,\mathrm{Fr}^{-2}\mathbf{n}\cdot\mathbf{e}_d\right)\mathrm{d}\mathbf{x}\,. \tag{5.13b}$$

If $\alpha(\mathbf{x})$ is chosen such that $I'_\alpha + J'_\alpha < 0$, an adjustment of the free boundary from $\mathcal{S}$ to $\mathcal{S}_{\gamma\alpha}$, with γ a small positive number, results in a reduction of the cost functional and thus improves the approximation to the actual free-boundary position. Such a choice of α is called a *descent direction*.

5.3.2 Adjoint Operators and Duality

The inherent problem in determining a descent direction from (5.13), is the dependence of (5.13a) on ϕ'_α, which is connected to α through the boundary value problem (5.11). Equations (5.11) and (5.13) are useful to verify if a particular α is a descent direction. However, they are unsuitable to determine a descent direction.

The adjoint optimization method uses the equivalence of (5.11), (5.13a) to its dual problem to eliminate the induced change in the functional. To define the duality property, adjoint operators must be introduced. Let $(\cdot,\cdot)_{\mathcal{V}}$ and $(\cdot,\cdot)_{\partial\mathcal{V}}$ denote the L_2 integral inner products over the domain $\mathcal{V}$ and its boundary $\partial\mathcal{V}$, respectively. Consider the linear boundary value problem:

$$L_i(\phi) = l_i\,, \qquad \mathbf{x} \in \mathcal{V}\,, \tag{5.14a}$$

$$L_b(\phi) = l_b\,, \qquad \mathbf{x} \in \partial\mathcal{V}\,, \tag{5.14b}$$

and the functional

$$I = \big(f_i, F_i(\phi)\big)_{\mathcal{V}} + \big(f_b, F_b(\phi)\big)_{\partial\mathcal{V}}\,, \tag{5.15}$$

for certain interior operators L_i, F_i and boundary operators L_b, F_b. The adjoint operators L_i^*, F_i^* and adjoint boundary operators L_b^*, F_b^* are defined by the identity

$$\big(L_i^*(\lambda), F_i(\phi)\big)_{\mathcal{V}} + \big(L_b^*(\lambda), F_b(\phi)\big)_{\partial\mathcal{V}} = \big(F_i^*(\lambda), L_i(\phi)\big)_{\mathcal{V}} + \big(F_b^*(\lambda), L_b(\phi)\big)_{\partial\mathcal{V}}, \tag{5.16}$$

for all appropriate functions ϕ and λ. For example, if

$$L_i(\phi) = \Delta\phi\,, \quad L_b(\phi) = a\mathbf{n}\cdot\boldsymbol{\nabla}\phi + b\phi\,, \quad F_i(\phi) = \phi\,, \quad F_b(\phi) = \underline{a}\mathbf{n}\cdot\boldsymbol{\nabla}\phi + \underline{b}\phi\,, \tag{5.17a}$$

for certain functions $a, b, \underline{a}, \underline{b} : \partial\mathcal{V} \mapsto \mathbb{R}$ such that $b\underline{a} - a\underline{b} \neq 0$, then

$$L_i^*(\lambda) = L_i(\lambda)\,, \quad L_b^*(\lambda) = \frac{L_b(\lambda)}{b\underline{a} - a\underline{b}}\,, \quad F_i^*(\lambda) = F_i(\lambda)\,, \quad F_b^*(\lambda) = \frac{F_b(\lambda)}{b\underline{a} - a\underline{b}}\,. \tag{5.17b}$$

To prove that (5.17a) and (5.17b) indeed satisfy the identity (5.16):

$$\begin{aligned}
&\big(L_i^*(\lambda), F_i(\phi)\big)_{\mathcal{V}} + \big(L_b^*(\lambda), F_b(\phi)\big)_{\partial\mathcal{V}} \\
&\quad = \int_{\mathcal{V}} \phi\,\Delta\lambda\,\mathrm{d}\mathbf{x} + \oint_{\partial\mathcal{V}} \left(\frac{a\mathbf{n}\cdot\nabla\lambda + b\lambda}{b\underline{a} - a\underline{b}}\right)\left(\underline{a}\mathbf{n}\cdot\nabla\phi + \underline{b}\phi\right)\mathrm{d}\mathbf{x} \\
&\quad = \int_{\mathcal{V}} \lambda\,\Delta\phi\,\mathrm{d}\mathbf{x} + \oint_{\partial\mathcal{V}} (\phi\,\mathbf{n}\cdot\nabla\lambda - \lambda\,\mathbf{n}\cdot\nabla\phi)\,\mathrm{d}\mathbf{x} \\
&\qquad + \oint_{\partial\mathcal{V}} \left(\frac{a\mathbf{n}\cdot\nabla\lambda + b\lambda}{b\underline{a} - a\underline{b}}\right)\left(\underline{a}\mathbf{n}\cdot\nabla\phi + \underline{b}\phi\right)\mathrm{d}\mathbf{x} \\
&\quad = \int_{\mathcal{V}} \lambda\,\Delta\phi\,\mathrm{d}\mathbf{x} + \oint_{\partial\mathcal{V}} \left(\frac{\underline{a}\mathbf{n}\cdot\nabla\lambda + \underline{b}\lambda}{b\underline{a} - a\underline{b}}\right)\left(a\mathbf{n}\cdot\nabla\phi + b\phi\right)\mathrm{d}\mathbf{x} \\
&\quad = \big(F_i^*(\lambda), L_i(\phi)\big)_{\mathcal{V}} + \big(F_b^*(\lambda), L_b(\phi)\big)_{\partial\mathcal{V}}\,.
\end{aligned} \tag{5.18}$$

The identity (5.16) implies that (5.15) subject to (5.14) is equivalent to

$$I = \big(l_i, F_i^*(\lambda)\big)_{\mathcal{V}} + \big(l_b, F_b^*(\lambda)\big)_{\partial\mathcal{V}} \tag{5.19}$$

subject to

$$L_i^*(\lambda) = f_i\,, \qquad \mathbf{x} \in \mathcal{V}\,, \tag{5.20a}$$
$$L_b^*(\lambda) = f_b\,, \qquad \mathbf{x} \in \partial\mathcal{V}\,. \tag{5.20b}$$

To prove the equivalence:

$$\begin{aligned}
I &= \big(f_i, F_i(\phi)\big)_{\mathcal{V}} + \big(f_b, F_b(\phi)\big)_{\partial\mathcal{V}} = \big(L_i^*(\lambda), F_i(\phi)\big)_{\mathcal{V}} + \big(L_b^*(\lambda), F_b(\phi)\big)_{\partial\mathcal{V}} \\
&= \big(F_i^*(\lambda), L_i(\phi)\big)_{\mathcal{V}} + \big(F_b^*(\lambda), L_b(\phi)\big)_{\partial\mathcal{V}} = \big(F_i^*(\lambda), l_i\big)_{\mathcal{V}} + \big(F_b^*(\lambda), l_b\big)_{\partial\mathcal{V}}\,.
\end{aligned} \tag{5.21}$$

In this context, (5.14)–(5.15) is called the *primal* problem and (5.19)–(5.20) is called the *dual* problem. *Duality* is the equivalence of the primal and dual problem.

The adjoint optimization method uses duality to eliminate the induced change in the cost functional (5.13a). Observe that for given ϕ, the functional (5.13a) is the L_2 inner product of ϕ'_α with a given function and (5.11) acts as a constraint on ϕ'_α. Hence, (5.13a) subject to (5.11) is of the form (5.14)–(5.15). To obtain the dual problem for (5.11)–(5.13a), we note that (5.11) implies

$$\begin{aligned}
\int_{\mathcal{V}} \lambda\Delta\phi'_\alpha\mathrm{d}\mathbf{x} + \int_{\mathcal{S}} \psi\,\mathbf{n}\cdot\nabla\phi'_\alpha\,\mathrm{d}\mathbf{x} + \int_{\mathcal{S}} \psi\left(\alpha\,\mathbf{n}\mathbf{n} : \nabla\nabla\phi - \sum_{j=1}^{d-1}(\mathbf{t}_j\cdot\nabla\alpha)\,(\mathbf{t}_j\cdot\nabla\phi)\right)\mathrm{d}\mathbf{x} \\
+ \int_{\partial\mathcal{V}\setminus\mathcal{S}} \psi\left(a\,\mathbf{n}\cdot\nabla\phi'_\alpha + b\,\phi'_\alpha\right)\mathrm{d}\mathbf{x} = 0\,,
\end{aligned} \tag{5.22}$$

for all admissible functions $\lambda : \mathcal{V} \mapsto \mathbb{R}$ and $\psi : \partial\mathcal{V} \mapsto \mathbb{R}$. Integrating by parts, (5.22) can be recast into

$$\int_{\mathcal{V}} \phi'_\alpha \Delta\lambda \,\mathrm{d}\mathbf{x} - \int_{\mathcal{S}} \phi'_\alpha \mathbf{n}\cdot\nabla\lambda \,\mathrm{d}\mathbf{x} + \int_{\mathcal{S}} \alpha \left(\psi\, \mathbf{nn} : \nabla\nabla\phi + \sum_{j=1}^{d-1} \mathbf{t}_j \cdot \nabla(\psi\, \mathbf{t}_j \cdot \nabla\phi) \right) \mathrm{d}\mathbf{x}$$
$$+ \int_{\mathcal{S}} (\lambda + \psi)\, \mathbf{n}\cdot\nabla\phi'_\alpha \,\mathrm{d}\mathbf{x} + \int_{\partial\mathcal{V}\setminus\mathcal{S}} (b\,\psi - \mathbf{n}\cdot\nabla\lambda)\, \phi'_\alpha + (a\,\psi + \lambda)\, \mathbf{n}\cdot\nabla\phi'_\alpha \,\mathrm{d}\mathbf{x} = 0. \tag{5.23}$$

Hence, if ψ in (5.23) is set to

$$\psi(\mathbf{x}) = \begin{cases} -\lambda(\mathbf{x}), & \mathbf{x} \in \mathcal{S}, \\ -\lambda(\mathbf{x})/a(\mathbf{x}), & \mathbf{x} \in \partial\mathcal{V} \setminus \mathcal{S},\ a(\mathbf{x}) \neq 0\,, \\ \mathbf{n}\cdot\nabla\lambda(\mathbf{x})/b(\mathbf{x}), & \mathbf{x} \in \partial\mathcal{V} \setminus \mathcal{S},\ \text{otherwise}, \end{cases}$$

and if λ satisfies the dual problem

$$\Delta\lambda = 0\,, \qquad \mathbf{x} \in \mathcal{V}\,, \tag{5.24a}$$
$$\mathbf{n}\cdot\nabla\lambda = \sum_{j=1}^{d-1} \mathbf{t}_j \cdot \nabla(p\, \mathbf{t}_j \cdot \nabla\phi)\,, \qquad \mathbf{x} \in \mathcal{S}\,, \tag{5.24b}$$
$$a\,\mathbf{n}\cdot\nabla\lambda + b\,\lambda = 0\,, \qquad \mathbf{x} \in \partial\mathcal{V} \setminus \mathcal{S}\,, \tag{5.24c}$$

then

$$I'_\alpha(\mathcal{S}) = -\int_{\mathcal{S}} \alpha \left(\lambda\, \mathbf{nn} : \nabla\nabla\phi + \sum_{j=1}^{d-1} \mathbf{t}_j \cdot \nabla(\lambda\, \mathbf{t}_j \cdot \nabla\phi) \right) \mathrm{d}\mathbf{x}\,. \tag{5.25}$$

One may note that (5.25) expresses the induced change in the functional independent of the induced disturbance in the solution.

5.3.3 Optimization Method

Due to the absence of the induced disturbance in (5.25), a descent direction for α can be determined from (5.13b) and (5.25) in a straightforward manner. For this purpose, we define the gradient of E with respect to $\mathcal{S}$ by the function $grad\, E(\mathcal{S}) : \mathcal{S} \mapsto \mathbb{R}$ with the property:

$$\int_{\mathcal{S}} \alpha(\mathbf{x})\, grad\, E(\mathcal{S})(\mathbf{x}) \,\mathrm{d}\mathbf{x} = \lim_{\epsilon \to 0} \tfrac{1}{\epsilon}[E(\mathcal{S}_{\epsilon\alpha}) - E(\mathcal{S})]\,, \tag{5.26}$$

for all suitable α. By (5.12), (5.13) and (5.25), the gradient is readily identified as:

$$grad\, E(\mathcal{S}) = -\lambda\, \mathbf{nn} : \nabla\nabla\phi - \sum_{j=1}^{d-1} \mathbf{t}_j \cdot \nabla(\lambda\, \mathbf{t}_j \cdot \nabla\phi) - \frac{p^2}{2R} - p\,\mathrm{Fr}^{-2}\mathbf{n}\cdot\mathbf{e}_d\,. \tag{5.27}$$

From (5.26) it follows that if $\alpha = -grad\, E(\mathcal{S})$ and γ is set to a small positive number, then

$$E(\mathcal{S}_{\gamma\alpha}) - E(\mathcal{S}) = -\gamma \int_{\mathcal{S}} \left(grad\, E(\mathcal{S})\right)^2 \mathrm{d}\mathbf{x} + O(\gamma^2) \leq 0 + O(\gamma^2)\,. \tag{5.28}$$

Therefore, $\alpha = -grad\, E(\mathcal{S})$ is a descent direction and $\mathcal{S}_{\gamma\alpha}$ improves on $\mathcal{S}$. The free-surface flow problem can thus be solved by repeating the following operations:

(A1) For given $\mathcal{S}$, solve the primal problem (5.6) for ϕ.

(A2) Solve the dual problem (5.24) for λ.

(A3) Determine $\alpha = -grad\, E(\mathcal{S})$ from (5.27).

(A4) Choose the step size $\gamma > 0$ and adjust $\mathcal{S}$ to $\mathcal{S}_{\gamma\alpha}$.

The iterative process (A1)–(A4) is called the *adjoint optimization method*. The actual free boundary $\mathcal{S}^*$ is obtained if $grad\, E(\mathcal{S}^*) = 0$.

The condition $grad\, E(\mathcal{S}^*) = 0$ only ensures that a *local* minimum is attained. If the cost functional is non-convex, then multiple local minima can occur. The actual solution to the steady free-surface flow problem is then determined by the *global* minimum. The dynamic condition (5.3b) implies that the cost functional vanishes for the actual solution. Hence, the correct minimum is identifiable. If the cost functional is indeed non-convex, then it is important that the adjoint optimization method is provided with an initial approximation that is sufficiently close to the actual solution. For instance, a prolongated coarse-grid approximation to the solution can serve for this purpose.

5.4 Fourier Analysis of the Optimization Problem

The behavior of the cost functional in the neighborhood of a minimum is characterized by the *Hessian*, i.e., the second derivative of the cost functional with respect to the free boundary. As a result, the properties of the optimization problem and the convergence behavior of the adjoint optimization method depend on the characteristics of the Hessian. In this section we use Fourier analysis to examine the properties of the Hessian and we consider the implications for the solution behavior and the posedness of the optimal shape design problem and the convergence behavior of the adjoint method.

5.4.1 Hessian of the Functional

The behavior of the cost functional in the neighborhood of a minimum is characterized by its *Hessian*, which is defined by the function $grad^2 E(\mathcal{S}) : \mathcal{S} \times \mathcal{S} \mapsto \mathbb{R}$ with the property:

$$\int_{\mathcal{S}} \alpha(\mathbf{y})\, grad^2 E(\mathcal{S})(\mathbf{x}, \mathbf{y})\, \mathrm{d}\mathbf{y} = \lim_{\epsilon \to 0} \tfrac{1}{\epsilon} [grad\, E(\mathcal{S}_{\epsilon\alpha})(\mathbf{x}) - grad\, E(\mathcal{S})(\mathbf{x})]\,, \tag{5.29}$$

for all suitable α. To show that the properties of the optimization problem are essentially contained in the Hessian, we consider the following expansion of the cost functional:

$$E(\mathcal{S}_{\epsilon\alpha}) = E(\mathcal{S}) + \epsilon \int_{\mathcal{S}} \alpha(\mathbf{x})\, grad\, E(\mathcal{S})(\mathbf{x})\, \mathrm{d}\mathbf{x} + \frac{\epsilon^2}{2} \int_{\mathcal{S}} \int_{\mathcal{S}} \alpha(\mathbf{x})\, \alpha(\mathbf{y})\, grad^2 E(\mathcal{S})(\mathbf{x}, \mathbf{y})\, \mathrm{d}\mathbf{y}\, \mathrm{d}\mathbf{x} + O(\epsilon^3)\,, \qquad \text{as } \epsilon \to 0. \quad (5.30)$$

Clearly, in order to have a minimum, the gradient must vanish, so that indeed the Hessian determines the behavior of the cost functional in the neighborhood of a minimum.

To demonstrate that the Hessian determines the convergence behavior of the adjoint optimization method, we consider a perturbation $\mathcal{S}^*_{\epsilon\alpha}$ of the optimal boundary $\mathcal{S}^*$. Because $grad\, E(\mathcal{S}^*) = 0$, it follows from (5.29) that for sufficiently small ϵ,

$$grad\, E(\mathcal{S}^*_{\epsilon\alpha})(\mathbf{x}) = \epsilon \int_{\mathcal{S}} \alpha(\mathbf{y})\, grad^2 E(\mathcal{S}^*)(\mathbf{x}, \mathbf{y})\, \mathrm{d}\mathbf{y} + O(\epsilon^2)\,. \quad (5.31)$$

This implies that in the neighborhood of the optimum, the Hessian relates the gradient to the disturbance in the free-boundary position. Because the adjoint method uses the gradient to adjust the free boundary, the Hessian determines the change in the error in the boundary position. Hence, the Hessian indeed determines the convergence behavior of the adjoint optimization method.

5.4.2 Fourier Analysis of the Hessian

The properties of the Hessian can be conveniently examined by means of the Fourier analysis for optimization problems presented in [69]. We perform the analysis for the generic case of a domain $\mathcal{V}^* := \{\mathbf{x} \in \mathbb{R}^d : -1 < x_d < 0\}$ with free boundary $\mathcal{S}^* := \{\mathbf{x} \in \mathbb{R}^d : x_d = 0\}$ and fixed boundary $\partial\mathcal{V}^* \setminus \mathcal{S}^* = \{\mathbf{x} \in \mathbb{R}^d : x_d = -1\}$. Recall that x_d is the vertical coordinate. Assuming that the fixed boundary is impermeable, a in (5.6) is set to 1 and b and c are set to 0. The uniform horizontal flow potential $\phi^* = \mathbf{U}\cdot\mathbf{x}$, with $\mathbf{U}$ a constant vector in $\{\mathbf{U} \in \mathbb{R}^d : \|\mathbf{U}\| = 1, U_d = 0\}$, then satisfies the boundary value problem (5.6). The corresponding solution of the dual problem (5.24) is $\lambda^* = 0$ and the gradient (5.27) vanishes, so that $\mathcal{S}^*$ is the optimal boundary. Indeed, the uniform horizontal flow is a solution of the steady free-surface flow problem.

Next, consider the perturbed boundary $\mathcal{S}^*_{\epsilon\alpha}$. The solutions of the perturbed primal and dual problem are expanded as

$$\phi^*_{\epsilon\alpha} = \mathbf{U}\cdot\mathbf{x} + \epsilon\phi'_\alpha(\mathbf{x}) + O(\epsilon^2)\,, \quad (5.32a)$$

$$\lambda^*_{\epsilon\alpha} = 0 + \epsilon\lambda'_\alpha(\mathbf{x}) + O(\epsilon^2)\,. \quad (5.32b)$$

If (5.32a) and (5.32b) are inserted in (5.6) and (5.24), respectively, and the normal vector to $\mathcal{S}^*_{\epsilon\alpha}$ is expanded in the same manner as in (5.10), then collection of terms of $O(\epsilon)$ reveals that the induced disturbances are governed by:

$$\begin{aligned} \Delta\phi'_\alpha &= 0\,, && \mathbf{x} \in \mathcal{V}^*\,, && (5.33a)\\ \mathbf{e}_d \cdot \nabla\phi'_\alpha &= 0\,, && \mathbf{x} \in \partial\mathcal{V}^* \setminus \mathcal{S}^*\,, && (5.33b)\\ \mathbf{e}_d \cdot \nabla\phi'_\alpha &= \mathbb{U} \cdot \nabla\alpha\,, && \mathbf{x} \in \mathcal{S}^*, && (5.33c) \end{aligned}$$

and

$$\begin{aligned} \Delta\lambda'_\alpha &= 0\,, && \mathbf{x} \in \mathcal{V}^*\,, && (5.34a)\\ \mathbf{e}_d \cdot \nabla\lambda'_\alpha &= 0\,, && \mathbf{x} \in \partial\mathcal{V}^* \setminus \mathcal{S}^*\,, && (5.34b)\\ \mathbf{e}_d \cdot \nabla\lambda'_\alpha &= -\mathbb{U} \cdot \nabla(\mathbb{U} \cdot \nabla\phi'_\alpha + \mathrm{Fr}^{-2}\alpha)\,, && \mathbf{x} \in \mathcal{S}^*\,. && (5.34c) \end{aligned}$$

Moreover, upon inserting (5.32) in (5.27), one obtains that the gradient corresponding to the perturbed boundary $\mathcal{S}^*_{\epsilon\alpha}$ reads

$$grad\, E(\mathcal{S}^*_{\epsilon\alpha}) = \epsilon \left(\mathrm{Fr}^{-2}(\mathbb{U} \cdot \nabla\phi'_\alpha + \mathrm{Fr}^{-2}\alpha) - \mathbb{U} \cdot \nabla\lambda'_\alpha \right) + O(\epsilon^2)\,. \tag{5.35}$$

Note that for any perturbation α, the induced disturbances follow from (5.33) and (5.34). The gradient corresponding to the perturbed boundary can then be obtained from (5.35). Because $grad\, E(\mathcal{S}^*) = 0$, important information about the Hessian can subsequently be extracted from (5.29).

The analysis proceeds by assuming α, ϕ'_α and λ'_α to be a linear combination of horizontal Fourier modes. Because (5.33) through (5.35) are linear in α, ϕ'_α and λ'_α, it suffices to consider a single mode. Denoting by $\mathbf{k} = k_1\mathbf{e}_1 + \cdots + k_{d-1}\mathbf{e}_{d-1}$ the horizontal wave number, α is set to

$$\alpha(\mathbf{x}) := \hat{\alpha}(\mathbf{k}) \exp(\mathrm{i}\mathbf{k} \cdot \mathbf{x})\,, \tag{5.36}$$

with $\mathrm{i} = \sqrt{-1}$. The induced disturbances ϕ'_α and λ'_α comply with (5.33) and (5.34), respectively, if

$$\begin{aligned} \phi'_\alpha &= \hat{\phi}(\mathbf{k}) \exp(\mathrm{i}\mathbf{k} \cdot \mathbf{x}) \cosh\left(|\mathbf{k}|\,(x_d + 1)\right)\,, && (5.37a)\\ \lambda'_\alpha &= \hat{\lambda}(\mathbf{k}) \exp(\mathrm{i}\mathbf{k} \cdot \mathbf{x}) \cosh\left(|\mathbf{k}|\,(x_d + 1)\right)\,, && (5.37b) \end{aligned}$$

and

$$\begin{aligned} |\mathbf{k}| \sinh|\mathbf{k}|\, \hat{\phi}(\mathbf{k}) &= \mathrm{i}\mathbf{k} \cdot \mathbb{U}\, \hat{\alpha}(\mathbf{k})\,, && (5.38a)\\ |\mathbf{k}| \sinh|\mathbf{k}|\, \hat{\lambda}(\mathbf{k}) &= -\mathrm{i}\mathbf{k} \cdot \mathbb{U}\Big(\mathrm{i}\mathbf{k} \cdot \mathbb{U} \cosh|\mathbf{k}|\, \hat{\phi}(\mathbf{k}) + \mathrm{Fr}^{-2}\, \hat{\alpha}(\mathbf{k})\Big)\,. && (5.38b) \end{aligned}$$

Recalling that $grad\, E(\mathcal{S}^*) = 0$, by (5.35) through (5.38), the change in the gradient satisfies

$$\lim_{\epsilon \to 0} \tfrac{1}{\epsilon}[grad\, E(\mathcal{S}^*_{\epsilon\alpha}) - grad\, E(\mathcal{S}^*)] = \hat{H}(\mathbf{k})\, \hat{\alpha}(\mathbf{k}) \exp(\mathrm{i}\mathbf{k} \cdot \mathbf{x})\,, \tag{5.39}$$

with

$$\hat{H}(\mathbf{k}) := \left(\mathrm{Fr}^{-2} - \frac{(\mathbf{k}\cdot\mathbf{U})^2}{|\mathbf{k}| \tanh |\mathbf{k}|} \right)^2 . \tag{5.40}$$

The object $\hat{H}(\mathbf{k})$ is referred to as the *Fourier symbol* of the Hessian.

5.4.3 Properties of the Optimization Problem

The Fourier symbol of the Hessian contains important information about the posedness and the solution behavior of the optimization problem. To illustrate this, we consider the Fourier transform of the perturbation $\alpha(\mathbf{x})$ and its inverse

$$\hat{\alpha}(\mathbf{k}) := (2\pi)^{1-d} \int_{\mathcal{S}^*} \alpha(\mathbf{x}) \exp(-\mathrm{i}\mathbf{k}\cdot\mathbf{x}) \, \mathrm{d}\mathbf{x} , \qquad \alpha(\mathbf{x}) = \int_{-\infty}^{\infty} \hat{\alpha}(\mathbf{k}) \exp(\mathrm{i}\mathbf{k}\cdot\mathbf{x}) \, \mathrm{d}\mathbf{k} . \tag{5.41}$$

From (5.29) and (5.39) it then follows that

$$\int_{\mathcal{S}^*} \alpha(\mathbf{y}) \, grad^2 E(\mathcal{S}^*)(\mathbf{x},\mathbf{y}) \, \mathrm{d}\mathbf{y} = \int_{-\infty}^{\infty} \hat{H}(\mathbf{k}) \, \hat{\alpha}(\mathbf{k}) \exp(\mathrm{i}\mathbf{k}\cdot\mathbf{x}) \, \mathrm{d}\mathbf{k} . \tag{5.42}$$

Hence, by (5.30), if terms of $O(\epsilon^3)$ are ignored, the change in the cost functional due to the perturbation of the free boundary reads:

$$\begin{aligned}
E(\mathcal{S}^*_{\epsilon\alpha}) - E(\mathcal{S}^*) &= \frac{\epsilon^2}{2} \int_{\mathcal{S}} \alpha(\mathbf{x}) \int_{\mathcal{S}} \alpha(\mathbf{y}) \, grad^2 E(\mathcal{S}^*)(\mathbf{x},\mathbf{y}) \, \mathrm{d}\mathbf{y} \, \mathrm{d}\mathbf{x} \\
&= \frac{\epsilon^2}{2} \int_{\mathcal{S}} \alpha(\mathbf{x}) \int_{-\infty}^{\infty} \hat{H}(\mathbf{k}) \, \hat{\alpha}(\mathbf{k}) \exp(\mathrm{i}\mathbf{k}\cdot\mathbf{x}) \, \mathrm{d}\mathbf{k} \, \mathrm{d}\mathbf{x} \\
&= \frac{\epsilon^2}{2} \int_{-\infty}^{\infty} \hat{H}(\mathbf{k}) \, \hat{\alpha}(\mathbf{k}) \int_{\mathcal{S}} \alpha(\mathbf{x}) \exp(\mathrm{i}\mathbf{k}\cdot\mathbf{x}) \, \mathrm{d}\mathbf{x} \, \mathrm{d}\mathbf{k} \\
&= \frac{\epsilon^2}{2} (2\pi)^{d-1} \int_{-\infty}^{\infty} \hat{H}(\mathbf{k}) \, \hat{\alpha}(\mathbf{k}) \, \overline{\hat{\alpha}(\mathbf{k})} \, \mathrm{d}\mathbf{k} \\
&= \frac{\epsilon^2}{2} (2\pi)^{d-1} \int_{-\infty}^{\infty} \hat{H}(\mathbf{k}) \, |\hat{\alpha}(\mathbf{k})|^2 \, \mathrm{d}\mathbf{k} ,
\end{aligned} \tag{5.43}$$

with $\overline{\hat{\alpha}(\mathbf{k})}$ the complex conjugate of $\hat{\alpha}(\mathbf{k})$. Equation (5.43) implies that $\hat{H}(\mathbf{k})$ expresses the ability of the optimization problem to distinguish a boundary $\mathcal{S}^*$ from a perturbed boundary $\mathcal{S}^*_{\epsilon\alpha}$, with $\alpha(\mathbf{x})$ a Fourier mode with wave number $\mathbf{k}$.

To illustrate the behavior of the Fourier symbol $\hat{H}(\mathbf{k})$, we consider (5.40) for $\mathbf{k} \in \mathbb{R}^2$ (i.e., $d = 3$). Without loss of generality, we assume that $\mathbf{U} = \mathbf{e}_1$, so that $\mathbf{k}\cdot\mathbf{U} = k_1$. Figure 5.1 on the next page then displays contours of $\mathrm{Fr}^{-2} \pm \sqrt{\hat{H}(\mathbf{k})}$, e.g., if $\mathrm{Fr} = 1/2$, then $\mathrm{Fr}^{-2} \pm \sqrt{\hat{H}(\mathbf{k})} = 4$ is the contour for which $\hat{H}(\mathbf{k}) = 0$ and $\mathrm{Fr}^{-2} \pm \sqrt{\hat{H}(\mathbf{k})} \in \{0, 8\}$ are the contours for which $\hat{H}(\mathbf{k}) = 16$.

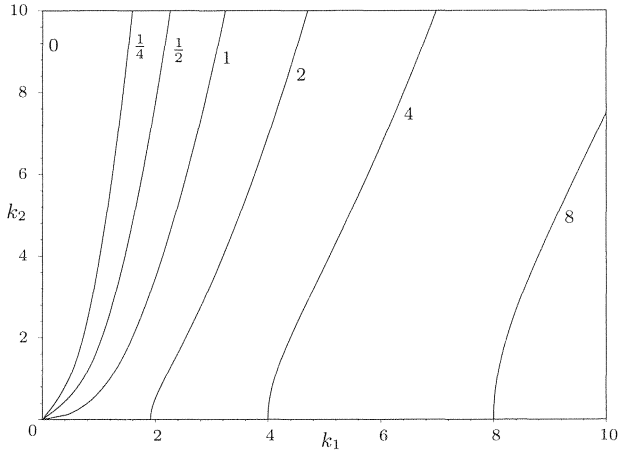

Figure 5.1: Contours of $\mathrm{Fr}^{-2} \pm \sqrt{\hat{H}(\mathbf{k})}$.

The solution behavior of the shape optimization problem is determined by the *critical modes*, i.e., the wave numbers for which $\hat{H}(\mathbf{k})$ vanishes. These critical modes yield a change in the cost functional of just $O(\epsilon^3)$, instead of $O(\epsilon^2)$. Hence, a small perturbation of the uniform free-surface flow is composed of a linear combination of the critical modes. It is important to observe that to each Froude number corresponds a curve of critical wave numbers. The critical modes are associated with steady surface gravity waves; see, e.g., Refs. [42, 46]. Note that for $d = 2$ ($k_2 = 0$) and $\mathrm{Fr} < 1$, the condition $\hat{H}(k) = 0$ yields a unique relation between the wave number of the surface gravity wave and the Froude number. For $d = 2$ and $\mathrm{Fr} \geq 1$, critical modes are absent and steady surface gravity waves do not occur.

The Fourier symbol of the Hessian also gives information about the posedness of the optimization problem. The optimization problem is said to be well posed if it has a unique solution that is stable to perturbations in the auxiliary data. Uniqueness is ensured if $\hat{H}(\mathbf{k}) > 0$ for all $\mathbf{k}$. From the above considerations, it is clear that uniqueness cannot be ensured. However, this does not necessarily imply that the optimization problem is ill posed. It merely implies that the behavior of critical modes is not described by the above theory. Linear stability of the optimization problem generally demands that

$$\hat{H}(\mathbf{k}) = O\big(|\mathbf{k}|^{\theta}\big), \qquad \text{as } |\mathbf{k}| \to \infty, \tag{5.44}$$

for some $\theta \geq 0$; see [69]. This requirement expresses that the optimization problem clearly notices high wave number perturbations of the free boundary. Unfortunately, if $\mathbf{k} \in \mathbb{R}^2$, the contours on which $\hat{H}(\mathbf{k}) = 0$ contain waves with $|\mathbf{k}| \to \infty$. Hence, the linear theory is insufficient to establish the stability of the 3 dimensional free-surface flow problem. However, such waves do not occur for $d = 2$ and, therefore, linear stability of the two-dimensional optimization problem is ensured.

5.4.4 Stability of the Adjoint Method

To examine the stability of the adjoint method, we consider a perturbation $\mathcal{S}^*_{\epsilon\alpha}$ of the optimal free boundary $\mathcal{S}^*$. One iteration of the adjoint optimization method yields a new approximation $\mathcal{S}^*_{\epsilon\underline{\alpha}}$, with

$$\epsilon\underline{\alpha}(\mathbf{x}) = \epsilon\alpha(\mathbf{x}) - \gamma\, grad\, E(\mathcal{S}^*_{\epsilon\alpha})(\mathbf{x})\,, \tag{5.45}$$

for some step-size $\gamma > 0$. Hence, by (5.31), $\underline{\alpha}$ and α are related in the following manner:

$$\underline{\alpha}(\mathbf{x}) = \alpha(\mathbf{x}) - \gamma \int_{\mathcal{S}} \alpha(\mathbf{y})\, grad^2 E(\mathcal{S}^*)(\mathbf{x},\mathbf{y})\, \mathrm{d}\mathbf{y}\,. \tag{5.46}$$

The *contraction number* ζ of the adjoint method is defined by the reduction of the error in the free-boundary position between successive iterations, i.e.,

$$\zeta := \sup_{\alpha} \frac{\left\| \alpha(\mathbf{x}) - \gamma \int_{\mathcal{S}^*} \alpha(\mathbf{y})\, grad^2 E(\mathcal{S}^*)(\mathbf{x},\mathbf{y})\, \mathrm{d}\mathbf{y} \right\|}{\|\alpha(\mathbf{x})\|}\,, \tag{5.47}$$

where the supremum is taken over all admissible functions $\alpha(\mathbf{x})$. Because $\|\underline{\alpha}\| \leq \zeta\|\alpha\|$, stability of the adjoint method is ensured if $\zeta \leq 1$.

If the L_2 norm is implied in (5.47), we can use (5.42) and Parseval's identity to recast (5.47) into:

$$\zeta = \sup_{\hat{\alpha}} \left(\frac{\int_{-\infty}^{\infty} \left(1 - \gamma \hat{H}(\mathbf{k})\right)^2 |\hat{\alpha}(\mathbf{k})|^2\, \mathrm{d}\mathbf{k}}{\int_{-\infty}^{\infty} |\hat{\alpha}(\mathbf{k})|^2\, \mathrm{d}\mathbf{k}} \right)^{1/2}\,. \tag{5.48}$$

If the problem (5.7) is solved numerically, then the infinite domain is usually truncated and $\alpha(\mathbf{x})$ is represented on a grid. In that case, if $\boldsymbol{\ell} = (\ell_1, \ldots, \ell_{d-1})$ is the horizontal length of the truncated domain and $\mathbf{h} = (h_1, \ldots, h_{d-1})$ is the horizontal mesh width of the applied grid, then we only have to consider isolated wave numbers in the set

$$\mathcal{W}_{\mathbf{h}} := \{\mathbf{k} : k_j = n\pi/\ell_j, n = \pm 1, \pm 2, \ldots, |k_j| \leq \pi/h_j\}\,; \tag{5.49}$$

see Figure 5.2 on the facing page for an illustration. It follows from (5.48) that ζ is then given by

$$\zeta = \sup_{\mathbf{k}\in\mathcal{W}_{\mathbf{h}}} |1 - \gamma \hat{H}(\mathbf{k})|\,. \tag{5.50}$$

Stability of the adjoint optimization method is ensured if the right hand side of (5.50) is at most 1. This can be accomplished by choosing the step size γ according to

$$\gamma = c \left(\sup_{\mathbf{k}\in\mathcal{W}_{\mathbf{h}}} \hat{H}(\mathbf{k}) \right)^{-1}\,, \tag{5.51}$$

for some constant $c \in]0, 2[$.

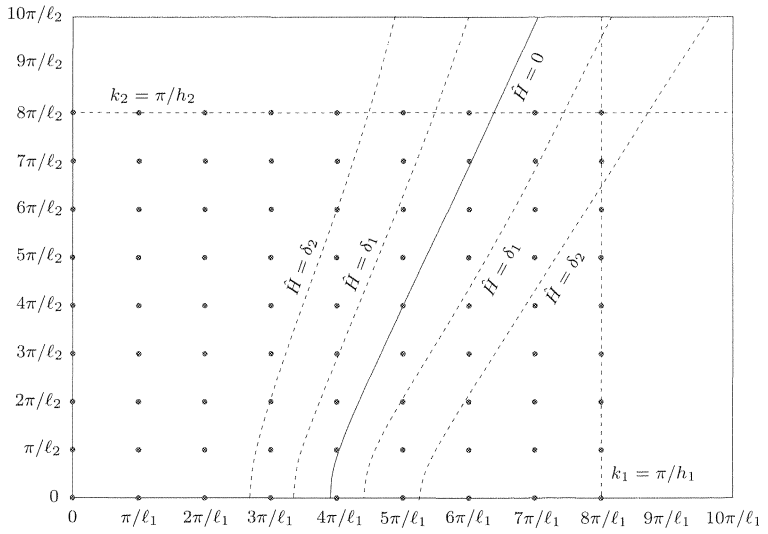

Figure 5.2: The set of wave numbers $\mathcal{W}_\mathbf{h}$ (dots) and $\hat{H}(\mathbf{k}) = 0$, $\hat{H}(\mathbf{k}) = \delta_{1,2}$.

The supremum of $\hat{H}$ in $\mathcal{W}_\mathbf{h}$ is for well posed problems determined by the highest wave number components in $\mathcal{W}_\mathbf{h}$; refer to (5.44). From (5.49) it follows that the highest wave number in $\mathcal{W}_\mathbf{h}$ is $O(1/|\mathbf{h}|)$. Hence, in general, the step size diminishes as $\gamma = O(|\mathbf{h}|^\theta)$ as $|\mathbf{h}| \to 0$. In particular, for the Fourier symbol (5.40), if the grid is refined in such a manner that $\mathbf{h} = |\mathbf{h}|\mathbf{c}$ as $|\mathbf{h}| \to 0$, with $\mathbf{c}$ a constant vector, then the supremum of $\hat{H}(\mathbf{k})$ in $\mathcal{W}_\mathbf{h}$ is $O(|\mathbf{h}|^{-2})$. The step size must then comply with

$$\gamma = O(|\mathbf{h}|^2)\,, \qquad \text{as } |\mathbf{h}| \to 0\,, \tag{5.52}$$

to maintain stability of the oscillatory modes, i.e., the modes with large $|\mathbf{k}|$. This implies that the step size in the adjoint optimization method must be reduced as the spatial grid is refined to maintain stability of the high wave number modes.

5.4.5 Convergence of the Adjoint Method

The convergence behavior of an iterative method is usually characterized by its contraction number. However, this characterization is inappropriate for problems with critical modes ($\hat{H}(\mathbf{k}) = 0$) and dispersive behavior, such as the considered free-surface flow problem. The contraction number is based on the behavior of isolated waves, whereas for dispersive problems the behavior of *wave groups* is relevant; see, e.g., Refs. [46, 78]. This distinction is essential if critical modes occur. As a result of the critical modes, the contraction number indicates that convergence lacks. However, due to the dispersive properties of the problem, this indication is too pessimistic.

To determine the convergence behavior of the adjoint optimization method (A1)–(A4), we reconsider the perturbation $\mathcal{S}^*_{\epsilon\alpha}$ of the optimal free boundary $\mathcal{S}^*$. The Fourier components of the perturbation can be separated into a contribution $\hat{\rho}(\mathbf{k})$ of the modes in the neighborhood of the critical modes and a remainder:

$$\hat{\alpha}(\mathbf{k}) = \hat{\rho}(\mathbf{k}) + \big(\hat{\alpha}(\mathbf{k}) - \hat{\rho}(\mathbf{k})\big)\,, \tag{5.53a}$$

where $\hat{\rho}(\mathbf{k}) := \hat{w}(\mathbf{k})\,\hat{\alpha}(\mathbf{k})$,

$$\hat{w}(\mathbf{k}) := \begin{cases} 1 & \text{if } \hat{H}(\mathbf{k}) \le \delta_1, \\ 0 & \text{if } \hat{H}(\mathbf{k}) \ge \delta_2, \end{cases} \tag{5.53b}$$

and $\delta_{1,2}$ are constants such that $\delta_2 > \delta_1 > 0$; see the illustration in Figure 5.2 on the page before. The transition of $\hat{w}(\mathbf{k})$ from 1 to 0 can be constructed in any suitable manner and is largely arbitrary. However, below, $\hat{\rho}(\mathbf{k})$ is required to be an analytic function.

Denoting by $\epsilon\alpha_n(\mathbf{x})$ the disturbance in the free-boundary position after n iterations of the adjoint method, we obtain from (5.42) and (5.46):

$$\hat{\alpha}_n(\mathbf{k}) = \Big(1 - \gamma\hat{H}(\mathbf{k})\Big)^n\,\hat{\alpha}(\mathbf{k})\,. \tag{5.54}$$

Hence, it follows from (5.53) that

$$\alpha_n(\mathbf{x}) = \int_{-\infty}^{\infty} \Big(1 - \gamma\hat{H}(\mathbf{k})\Big)^n\,\hat{\rho}(\mathbf{k})\exp\left(\mathrm{i}\mathbf{k}\cdot\mathbf{x}\right)\mathrm{d}\mathbf{k} + O\big(|1-\gamma\delta_1|^n\big)\,. \tag{5.55}$$

Because $|1 - \gamma\delta_1| < 1$, the remainder vanishes exponentially as $n \to \infty$. This implies that the asymptotic behavior of $\alpha_n(\mathbf{x})$ for large n is determined by the Fourier components in the neighborhood of the critical modes.

From (5.55) it follows that if $\hat{\rho}_n(\mathbf{k})$ is defined recursively by

$$\hat{\rho}_0(\mathbf{k}) = \hat{\rho}(\mathbf{k})\,, \tag{5.56a}$$

$$\hat{\rho}_n(\mathbf{k}) = \Big(1 - \gamma\hat{H}(\mathbf{k})\Big)\,\hat{\rho}_{n-1}(\mathbf{k}), \qquad n = 1, 2, \ldots, \tag{5.56b}$$

then $\alpha_n(\mathbf{x}) \sim \rho_n(\mathbf{x})$ as $n \to \infty$. Equation (5.56b) can be recast into:

$$\frac{\hat{\rho}_{n+1}(\mathbf{k}) - \hat{\rho}_n(\mathbf{k})}{\gamma} + \hat{H}(\mathbf{k})\,\hat{\rho}_n(\mathbf{k}) = 0\,. \tag{5.57}$$

Note that for sufficiently small γ, the first term can be conceived as a difference approximation to the derivative of $\hat{\rho}_n(\mathbf{k})$ with respect to *pseudo time* $n\gamma$. We assume that $\hat{\rho}_n(\mathbf{k}) \sim \exp\left(\tau n\gamma\right)\hat{\rho}_0(\mathbf{k})$ as $n \to \infty$. Equation (5.57) then implies

$$\left(\exp\left(\tau\gamma\right) - 1\right)/\gamma + \hat{H}(\mathbf{k}) = 0\,. \tag{5.58}$$

Taylor expansion of $\exp(\tau\gamma)$ yields

$$\tau = -\hat{H}(\mathbf{k}) \,, \tag{5.59}$$

provided that $O(\tau^2)$ terms are negligible. By (5.53b), $\hat{H}(\mathbf{k}) \leq \delta_2$. Hence, if δ_2 is chosen sufficiently small, the $O(\tau^2)$ terms in the Taylor expansion can indeed be ignored. Equation (5.59) relates the pseudo time behavior of a disturbance in the free-boundary position to its spatial behavior. Therefore, it appears appropriate to refer to (5.59) as the *pseudo dispersion relation* of the adjoint method.

From (5.55) to (5.59) it follows that as $n\gamma \to \infty$,

$$\alpha_n(\mathbf{x}) \sim \int_{-\infty}^{\infty} \hat{\rho}(\mathbf{k}) \exp\left(\mathrm{i}\Omega(\mathbf{k})\, n\gamma\right) \mathrm{d}\mathbf{k} \,, \tag{5.60}$$

with

$$\Omega(\mathbf{k}) := \mathrm{i}\hat{H}(\mathbf{k}) + \frac{\mathbf{k}\cdot\mathbf{x}}{n\gamma} \,. \tag{5.61}$$

The integral in (5.60) vanishes exponentially as $n\gamma \to \infty$, except near critical stationary points of $\hat{H}(\mathbf{k})$, i.e., the wave numbers $\mathbf{k}_0$ such that

$$\hat{H}(\mathbf{k}_0) = 0 \,, \qquad \frac{\partial \hat{H}}{\partial k_j}(\mathbf{k}_0) = 0 \,. \tag{5.62}$$

Each critical stationary point yields a contribution

$$\hat{\rho}(\mathbf{k}_0)\left(\frac{2\pi}{n\gamma}\right)^{(d-1)/2}\left(\det\left|\frac{\partial^2 \hat{H}}{\partial k_i \partial k_j}(\mathbf{k}_0)\right|\right)^{-1/2} \exp\left(\mathrm{i}\mathbf{k}_0\cdot\mathbf{x} + \mathrm{i}\xi\right) + O\Big((n\gamma)^{-d/2}\Big), \tag{5.63}$$

with ξ a multiple of $\pi/4$, depending on the properties of $\partial^2\hat{H}/\partial k_i \partial k_j$. The above can be proved by the method of stationary phase; see, e.g., Refs. [78, 79].

Due to the quadratic form of (5.40), any critical point is a stationary point as well. Hence, if we define the *evaluation error* e_n by the L_2 norm of the error in the boundary position, i.e., $\mathsf{e}_n := \|\epsilon\alpha_n\|$, then we anticipate that the adjoint method yields the following asymptotic convergence behavior:

$$\mathsf{e}_n = O\big(\zeta^{n\gamma}\big) \qquad \text{if } \forall \mathbf{k} : \hat{H}(\mathbf{k}) > 0 \,, \tag{5.64a}$$

$$\mathsf{e}_n = O\Big((n\gamma)^{(1-d)/2}\Big) \qquad \text{if } \exists \mathbf{k} : \hat{H}(\mathbf{k}) = 0 \,, \tag{5.64b}$$

as $n \to \infty$, for some constant ζ in $]0, 1[$. The implications of (5.64) for the convergence behavior of the adjoint method are summarized in Table 5.1 on the following page.

5.5 Preconditioning

The asymptotic error behavior (5.64) and the stability condition (5.52) imply that the performance of the adjoint optimization method deteriorates with decreasing mesh width. This deficiency of the method can be repaired by means of preconditioning. This section outlines the preconditioning operation.

Table 5.1: Convergence behavior of the adjoint method: asymptotic behavior of the evaluation error e_n for sub- and supercritical flow in 2D and 3D, with n the iteration counter, γ the step size and ζ a constant in $]0,1[$.

	$d=2$	$d=3$
subcritical	$O\big(1/\sqrt{n\gamma}\big)$	$O\big(1/(n\gamma)\big)$
supercritical	$O\big(\zeta^{n\gamma}\big)$	$O\big(1/(n\gamma)\big)$

5.5.1 Reconsideration of Objectives

To introduce the preconditioning operation, we consider the gradient of the cost functional at a perturbation $\mathcal{S}^*_{\epsilon\alpha}$ of the optimal boundary $\mathcal{S}^*$. By (5.39), the Fourier components of the gradient read:

$$\widehat{grad\, E(\mathcal{S}^*_{\epsilon\alpha})}(\mathbf{k}) = \epsilon\, \hat{H}(\mathbf{k})\, \hat{\alpha}(\mathbf{k})\,. \tag{5.65}$$

Equation (5.65) implies that for problems that are stable according to (5.44) with θ strictly positive, the gradient primarily contains highly oscillatory modes (large $|\mathbf{k}|$). Consequently, the adjoint optimization method effectively reduces the cost functional by removing the highly oscillatory disturbances in the boundary position. However, smooth error components are inadequately resolved.

In general, one is interested in obtaining the free-boundary position rather than minimizing the cost functional. If the objective is indeed to obtain the free boundary, then the gradient is unsuitable for adjusting the boundary position.

5.5.2 General Outline

The aim of preconditioning is to restore the relation between the boundary adjustment and the error in the boundary position. An accurate approximation to the error in the free-boundary position can be recovered from the gradient by solving

$$P\,\beta = grad\, E(\mathcal{S}^*_{\epsilon\alpha})\,, \tag{5.66}$$

where P is any convenient operator of which the Fourier symbol satisfies

$$\hat{H}(\mathbf{k}) \le \hat{P}(\mathbf{k})\,, \qquad \text{for all } \mathbf{k}\,, \tag{5.67a}$$

$$\lim_{|\mathbf{k}|\to\infty} \hat{H}(\mathbf{k})/\hat{P}(\mathbf{k}) = C\,, \qquad \text{for some } C \in]\,0,1\,]\,. \tag{5.67b}$$

The operator P simulates the relation between the gradient and the disturbance in the boundary position. The Fourier components $\hat{\beta}(\mathbf{k})$ are related to the components of the disturbance by:

$$\hat{\beta}(\mathbf{k}) = \big(\hat{H}(\mathbf{k})/\hat{P}(\mathbf{k})\big)\,\hat{\alpha}(\mathbf{k})\,. \tag{5.68}$$

Therefore, $\beta(\mathbf{x})$ is an accurate approximation to $\alpha(\mathbf{x})$ if $\hat{H}(\mathbf{k})/\hat{P}(\mathbf{k}) \approx 1$.

If the adjoint method uses $\beta(\mathbf{x})$ instead of the gradient to displace the free boundary, then the corresponding stability condition reads:

$$|1 - \gamma\, \hat{H}(\mathbf{k})/\hat{P}(\mathbf{k})| \leq 1\,. \tag{5.69}$$

Requirement (5.67a) ensures that $\hat{H}/\hat{P} \leq 1$ for all $\mathbf{k}$, so that the step size γ in the preconditioned method can be set to 1. Consequently, if the problem is solved numerically, the convergence behavior of the preconditioned method is independent of the mesh width of the applied grid. Condition (5.67b) makes certain that all Fourier components that are present in the boundary disturbance are also present in the correction, so that the error indeed vanishes as the iteration progresses.

It is important that the numerical methods for solving (5.66) do not reintroduce the mesh-width dependence. In general, preconditioners P can be constructed for which efficient solution methods, e.g., multigrid methods [9, 68], are available.

5.5.3 A Preconditioner for 2D Free-Surface Flows

The construction of the preconditioner from its symbol relies on the theory of pseudo-differential operators; see also [67]. In this section we set up a preconditioner for the 2D steady free-surface flow problem. It is anticipated that a preconditioner for 3D free-surface flows can be constructed similarly.

In two dimensions, the free-boundary is one dimensional and the considered wave number is $k \in \mathbb{R}$. Without loss of generality, we assume that the velocity is scaled such that $U = 1$ in (5.40). To derive the preconditioner, we first consider the asymptotic behavior of (5.40) for large k:

$$\hat{H}(k) \sim k^2\,, \qquad \text{as } k \to \infty\,. \tag{5.70}$$

The Fourier symbol $-k^2$ corresponds to a Laplace operator. An operator which has the desired behavior for high wave-number components is:

$$P_H\, \beta := (\mathrm{Fr}^{-2} - 1)^2 \beta - \frac{\partial^2 \beta}{\partial t^2}\,, \tag{5.71}$$

where $\partial/\partial t$ denotes the tangential derivative along the free boundary. The Fourier symbol of (5.71) is

$$\hat{P}_H(k) = (\mathrm{Fr}^{-2} - 1)^2 + k^2\,. \tag{5.72}$$

Indeed, $\hat{P}_H(k) \sim k^2$ as $k \to \infty$. Figure 5.3 on the next page compares the Fourier symbols $\hat{P}_H$ and $\hat{H}$. The behavior of $\hat{P}_H$ closely resembles that of $\hat{H}$ at high wave-numbers. Hence, P_H accurately recovers highly oscillatory errors in the boundary position. Moreover, P_H eliminates the mesh-width dependence of the step size.

The Fourier symbols $\hat{P}_H$ and $\hat{H}$ differ markedly at low wave numbers if $\mathrm{Fr} < 1$. For $\mathrm{Fr} < 1$, the low wave-number behavior of $\hat{H}$ is accurately approximated by:

$$\hat{P}_L(k) = \left(1 - (2 - 2\mu)(k/k_0)^2 + (1 - \mu)(k/k_0)^4\right)\left(\mathrm{Fr}^{-2} - 1\right)^2\,, \tag{5.73}$$

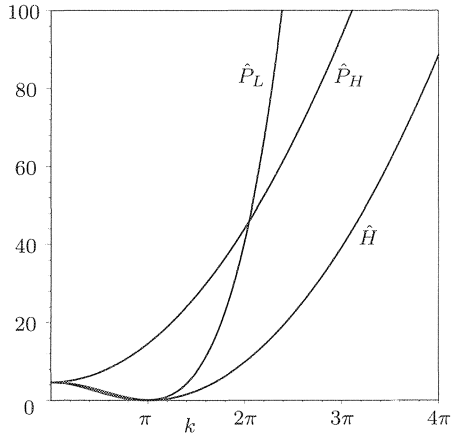

Figure 5.3: Fourier symbols $\hat{P}_L(k)$, $\hat{P}_H(k)$ and $\hat{H}(k)$ for $\mathrm{Fr} = \sqrt{\tanh(\pi)/\pi}$

with k_0 the critical wave number critical mode of (5.40) and μ a small positive constant; see Figure 5.3. The symbol $\hat{P}_L(k)$ corresponds to the differential operator

$$P_L\,\beta := \left(\mathrm{Fr}^{-2} - 1\right)^2 \left(\beta + \frac{2-2\mu}{k_0^2}\frac{\partial^2\beta}{\partial t^2} + \frac{1-\mu}{k_0^4}\frac{\partial^4\beta}{\partial t^4}\right). \tag{5.74}$$

The constant μ ensures that the polynomial $\hat{P}_L(k)$ has no real roots. This is a prerequisite for stability of the preconditioner. Unfortunately, it also implies that the preconditioner leaves the root of $\hat{H}$ undisturbed, i.e., $\hat{H}(k)/\hat{P}_L(k) = 0$ for critical modes. Hence, the asymptotic convergence behavior (5.64b) is not essentially improved.

Summarizing, for supercritical flows an effective correction of the free boundary can be obtained from (5.66) and (5.71). The mesh-width dependence of the convergence behavior is then eliminated. For subcritical flows, the correction is a combination of a high wave number correction β_H from (5.66), (5.71) and a low wave number correction β_L from (5.66), (5.74), e.g., $(\beta_L+\beta_H)/2$. The mesh-width dependence of the convergence behavior is then removed. However, the asymptotic convergence behavior is not improved, because the preconditioning does not remove the critical modes.

5.6 Numerical Experiments

The preconditioned adjoint optimization method is tested for 2 dimensional sub- and supercritical flow over an obstacle in a channel of unit depth at $\mathrm{Fr} = 0.43$ and $\mathrm{Fr} = 2.05$. The geometry of the obstacle is

$$y(x) = -1 + \frac{27}{4}\frac{H}{L^3}x(x-L)^2\,, \qquad 0 \le x \le L\,, \tag{5.75}$$

with H and L the (non-dimensionalized) height and length of the obstacle, respectively. We choose $H = 0.2$, $L = 2$ for the subcritical test case and $H = 0.44$ and $L = 4.4$ for the supercritical test case, in accordance with the experimental setup from [12]. In addition, we consider the subcritical test case with $H = 0.1$, $L = 2$ and the supercritical test case with $H = 0.22$ and $L = 4.4$.

The boundary value problems (5.7) and (5.24) are discretized with bilinear finite elements. The differential operators in the gradient (5.27) are discretized with central differences. The resulting discrete optimization problem is unstable and displays odd/even oscillations. These are simply removed by smoothing the gradient with the biharmonic operator. For subcritical flows (Fr < 1), a radiation condition must be imposed to avoid nonphysical upstream waves; cf. §5.2.1. The upstream waves are eliminated by smoothing the gradient upstream of the obstacle with the Laplace operator, and by applying the low wave number preconditioner P_L only downstream.

The numerical experiments are performed on grids with horizontal mesh width $h \in \{L/36, L/72\}$ and vertical mesh width $1/24$. For the supercritical test case, the correction is computed using (5.66) and (5.71). For the subcritical test case, the upstream correction is determined in the same manner and the downstream correction is taken as $(\beta_L + \beta_H)/2$, with β_H from (5.66), (5.71) and β_L from (5.66), (5.74). The constant μ in (5.74) is set to 0.025. In all cases the step size $\gamma = 1$ is employed.

For the supercritical test case, Fig. 5.4 on the following page plots the L_2 norm of the correction after n iterations, $\|\beta_n\|$, versus the iteration counter. The correction behaves as $\|\beta_n\| = O(\zeta^n)$, for some constant $\zeta \in]0, 1[$. The norm of the evaluation error after n iterations can be bounded by

$$\mathsf{e}_n \leq \sum_{j=n}^{\infty} \|\beta_j\| \,. \tag{5.76}$$

It follows from (5.76) that the evaluation error converges as $O(\zeta^n)$ as well. This is in accordance with the entry in Table 5.1 on page 70. From Fig. 5.4 we obtain $\zeta \approx 0.35$ for $H = 0.22$ and $\zeta \approx 0.5$ for $H = 0.44$. One may note that the convergence behavior is indeed independent of the mesh width. Fig. 5.5 on page 75 compares the computed surface elevation with measurements from [12] for the supercritical test case. The computed result agrees well with the measurements.

For the subcritical test case, $\|\beta_n\|$ is plotted versus n in Fig. 5.6 on page 75. Note that Fig. 5.6 is a log-log plot. In this case, $\|\beta_n\|$ behaves as $O(n^{-\sigma})$, with $\sigma \approx 1.5$ for $H = 0.1$ and $\sigma \approx 1.2$ for $H = 0.2$. It follows from (5.76) that the convergence behavior of the evaluation error is approximately $O(n^{-0.5})$ for $H = 0.1$ and $O(n^{-0.2})$ for $H = 0.2$. Hence, the test case with $H = 0.1$ confirms the entry in Table 5.1 on page 70. The deteriorated converge behavior for $H = 0.2$ can be attributed to apparent nonlinear behavior. One may note that the convergence behavior is virtually independent of the mesh width. Fig. 5.7 on page 76 compares the computed surface elevation with measurements from [12] for the subcritical

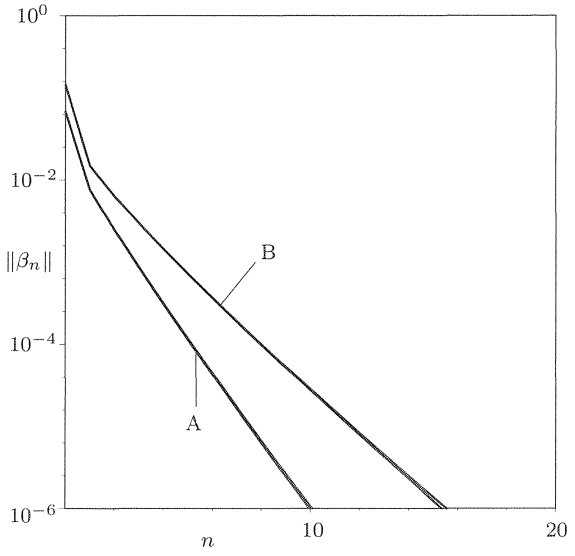

Figure 5.4: Supercritical test case: norm of the correction versus the iteration counter for $H = 0.22$ (A) and $H = 0.44$ (B) ($h = L/36$ and $h = L/72$ coincide).

test case. The surface elevation displays typical nonlinear effects, such as sharp wave crests and wave length reduction. The amplitude of the computed result is overestimated. However, the overestimation of the amplitude of the trailing wave is not unusual; see, for instance, [11, 75, 76]. The wave length of the computed result is in good agreement with the measurements.

5.7 Conclusions and Discussion

We investigated the suitability of the adjoint optimal shape design method for solving steady free-surface flows. To this end, the free-surface potential flow problem was reformulated into an equivalent optimal shape design problem. We then presented the adjoint optimization method for solving the design problem. We determined the asymptotic convergence behavior of the adjoint method for sub- and supercritical flows in 2D and 3D. Moreover, we showed that preconditioning is imperative to avoid mesh-width dependence of the convergence behavior and we presented a suitable preconditioner for the free-surface flow problem.

Numerical results were presented for two-dimensional flow over an obstacle in a channel. The observed convergence behavior is in agreement with the asymptotic estimates, i.e., the evaluation error behaves as $O(\zeta^n)$ for the supercritical test case and as $O(n^{-1/2})$ for the subcritical test case. Moreover, the numerical results

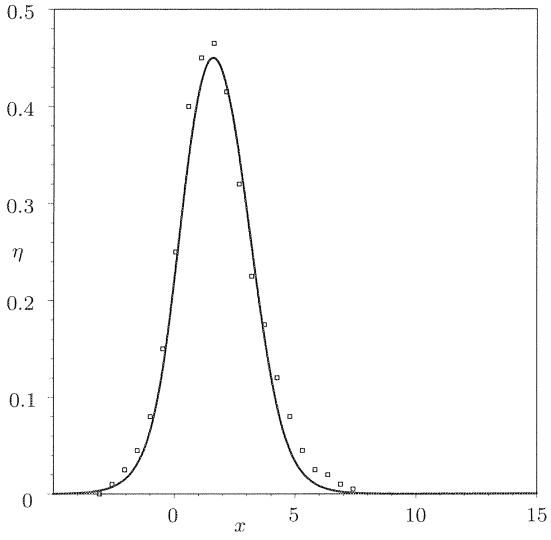

Figure 5.5: Supercritical test case: computed surface elevation with $H = 0.44$ and $h = L/72$ (*solid line*) and measurements from [12] (*markers only*)

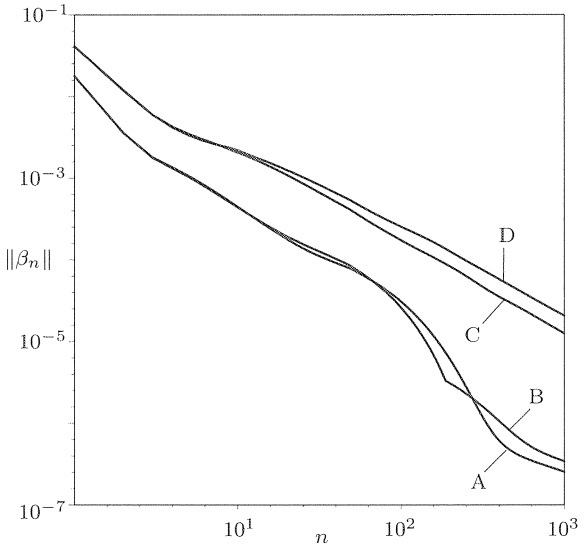

Figure 5.6: Subcritical test case: norm of the correction versus the iteration counter for $H = 0.1$, $h = L/36$ (A), $h = L/72$ (B) and $H = 0.2$, $h = L/36$ (C), $h = L/72$ (D)

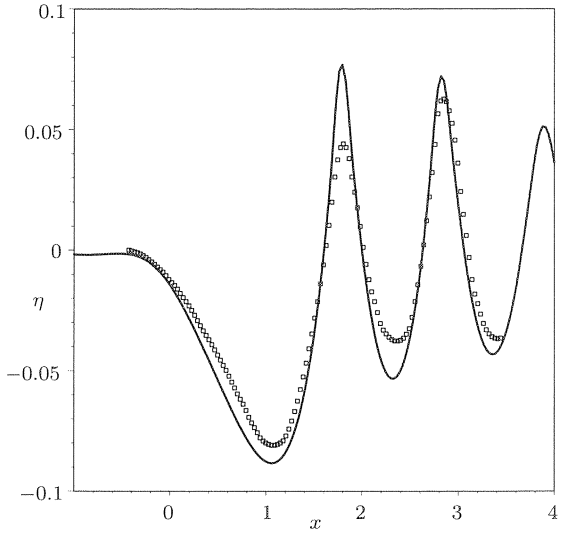

Figure 5.7: Subcritical test case: computed surface elevation with $H = 0.2$ and $h = L/72$ (*solid line*) and measurements from [12] (*markers only*)

confirm that the convergence behavior of the preconditioned adjoint method is independent of the mesh width. For both test cases the computed results agree well with measurements.

The convergence behavior of the adjoint shape optimization method for steady free surface flows is for two-dimensional problems similar to that of time-integration methods (see also [11]): the error converges as $O(\zeta^n)$ for supercritical flows and as $O(n^{-1/2})$ for subcritical flows. For three-dimensional problems, the anticipated convergence behavior of the adjoint method is $O(n^{-1})$ for sub- and supercritical flows. The convergence behavior of time-integration methods is $O(n^{-1})$ for subcritical flows and $O(\zeta^n)$ for supercritical flows. The convergence behavior of the preconditioned adjoint method is independent of the mesh width, whereas the convergence behavior of the usual time-integration method deteriorates with decreasing mesh width, due to a CFL-restriction on the admissible time step. Therefore, the preconditioned adjoint method is expected to be more efficient than time-integration methods, except in the case of 3D supercritical flow. However, for 3D flows and 2D subcritical flows, the convergence behavior of the adjoint method is less efficient than the mesh-width independent $O(\zeta^n)$ behavior of the method presented in [11].

The $O(n^{-1/2})$ (2D, subcritical) and $O(n^{-1})$ (3D) convergence behavior of the adjoint method is caused by the critical modes. It is therefore anticipated that a combination of the adjoint method and a solution method that effectively eliminates these critical modes yields $O(\zeta^n)$ convergence behavior.

Chapter 6
Interface Capturing

6.1 Introduction

Free-surface flows form a particular class of *two-fluid flows*, in which the stresses exerted on the interface by one fluid are negligible on a reference scale that is appropriate for the other. If the objective is the numerical solution of a free-surface flow problem, then it can be attractive to adhere to the two-fluid-flow formulation. In the absence of viscosity, two-fluid flows can be described by a system of hyperbolic conservation laws, and can be treated as such. This approach is referred to as *interface capturing*. For examples of interface capturing see, for instance, Refs. [15, 38, 48].

A common objection to conservative interface capturing is the occurrence of so-called *pressure oscillations*. These pressure oscillations expose the loss of certain invariance properties of the continuum problem under discretization. Several correctives have been proposed to avoid pressure oscillations, e.g., (locally) non-conservative discretization methods [1, 36, 37, 56], correction methods [35] and the ghost-fluid method [19]. For an overview of these correctives, and of their merits and deficiencies, see Ref. [2] and, for homentropic flows, Ref. [40]. A characteristic of these methods is that at the interface the conservative formulation is abandoned. Hence, these methods are generally non-conservative. Recently, enhancements of the ghost-fluid method have been proposed, which retain conservation; see Refs. [23, 49]. However, the interface treatment of these methods is not trivial and further investigation is warranted.

It is commonly assumed that the loss of the aforementioned invariance properties is inherent to any conservative formulation; see, e.g., Refs. [2, 57]. However, since the invariance properties are intrinsic to the continuum equations, irrespective of their form, we conjecture that it is possible to devise conservative numerical schemes that inherit the necessary invariance properties.

The interface-capturing approach requires that the employed numerical techniques remain robust and accurate in the presence of discontinuities. If one adheres to the conservative form of the equations, then Godunov-type schemes [24] are particularly useful in these circumstances. Such schemes can be suitably combined with finite volume methods and with discontinuous Galerkin finite element methods. For finite volume methods, the schemes can be implemented with higher-order limited interpolation methods, to achieve accuracy and secure monotonicity preservation in regions where large gradients occur (see, e.g., Refs. [64, 66]). For discontinuous Galerkin methods, accuracy and monotonicity preservation can be obtained by appropriate *hp*-adaptivity (see, e.g., Refs. [29, 33]) and stabilization.

The present chapter considers the interface-capturing approach to solving two-fluid flow problems. We investigate the pressure oscillations that are commonly incurred by discrete approximations of two-fluid flow problems, and we present a *non-oscillatory, conservative* Godunov-type method for barotropic fluids. Moreover, we set up a modified Osher-type flux-difference splitting scheme for the approximate solution of the two-fluid Riemann problems. The novelty of our method is its pressure invariance in combination with a formulation of the two-fluid flow problem as a system of hyperbolic conservation laws. It is generally accepted that methods based on such a formulation necessarily exhibit pressure oscillations; our results refute this.

The contents of this chapter are organized as follows: Section 6.2 presents the governing equations for two-fluid flows. In Section 6.3 we examine the pressure-oscillation phenomenon and we propose a non-oscillatory conservative formulation. Section 6.4 presents the modified Osher scheme for barotropic two-fluids. Numerical experiments and results are reported in Section 6.5. Section 6.6 contains concluding remarks.

6.2 Two-Fluid Flows

The basic notion underlying the interface-capturing method, is that a flow of two contiguous, inviscid compressible fluids can be construed as a flow of a single medium sustaining a discontinuity at the interface. In this section we derive the two-fluid Euler equations from the Euler equations for the separate fluids and the interface conditions.

6.2.1 Conservation Laws

We consider flows of two contiguous inviscid compressible fluids. For convenience, we arbitrarily designate one of the fluids as the primary fluid and the other as the secondary fluid. For our purposes, it suffices to consider a single spatial dimension. We refer to the corresponding spatial coordinate as x and to the temporal coordinate as t. The fluids occupy an open bounded space/time domain $\Omega \subset \{(x,t) \in \mathbb{R}^2\}$, which is the union of the disjoint open sets Ω_p and Ω_s, containing the primary and secondary fluid, respectively, and the *interface* $\Gamma := \overline{\Omega_\mathrm{p}} \cap \overline{\Omega_\mathrm{s}}$

(the overbar denoting closure); see Figure 6.1.

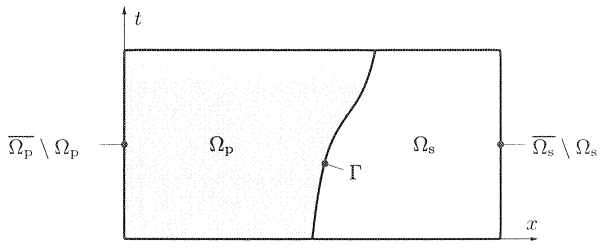

Figure 6.1: The space/time domain $\Omega := \Omega_p \cup \Omega_s \cup \Gamma$.

In both fluids the flow is characterized by the state variables $\rho : \Omega \mapsto \mathbb{R}_+$ and $v : \Omega \mapsto \mathbb{R}$, representing density and velocity, respectively. To facilitate the presentation of the governing equations, we introduce the notation:

$$\mathbf{q} := \begin{pmatrix} \rho \\ \rho v \end{pmatrix}, \quad \text{and} \quad \mathbf{f}(\mathbf{q}) := \begin{pmatrix} q_2 \\ q_2^2/q_1 + p \end{pmatrix}, \tag{6.1}$$

where p refers to the pressure. Eq. (6.1) must be furnished with equations of state for the primary and secondary fluid. Under the assumption that the fluids are barotropic (see, e.g., Ref. [77]), these equations of state have the form $p := p_p(\rho)$ and $p := p_s(\rho)$. In a proper functional setting, conservation of mass and momentum in the fluids is expressed by the variational statement

$$\int_\Omega \mathbf{w}_t \cdot \mathbf{q} + \mathbf{w}_x \cdot \mathbf{f}(\mathbf{q}) \, dx \, dt = 0, \qquad \forall \mathbf{w} \in \left[C_0^\infty(\Omega_p \cup \Omega_s)\right]^2, \tag{6.2}$$

where $C_0^\infty(G)$ denotes the space of functions that have continuous partial derivatives of all orders $k = 0, 1, 2, \ldots$ and that have compact support in G.

Eq. (6.2) combines the weak formulation of the Euler equations for the primary and secondary fluid. Because Ω_p and Ω_s are disjoint (Ω_p and Ω_s are contiguous at the interface, but the sets are open and therefore do not overlap), it holds that $\left[C_0^\infty(\Omega_p \cup \Omega_s)\right]^2 = \left[C_0^\infty(\Omega_p)\right]^2 \oplus \left[C_0^\infty(\Omega_s)\right]^2$. This implies that the variational statement (6.2) ensures conservation of mass and momentum in each of the fluids separately.

6.2.2 Interface Conditions

To present the interface conditions for the two-fluid flow, we define

$$(x,t)^\pm := \lim_{\epsilon \downarrow 0} (x \pm \epsilon, t), \qquad (x,t) \in \Gamma, \tag{6.3}$$

i.e., $(x,t)^-$ and $(x,t)^+$ are at the interface in the primary and secondary fluid, respectively. The interface conditions for the two-fluid flow prescribe that the velocity and pressure are continuous across the interface. In particular,

$$v\Big|_{(x,t)^-}^{(x,t)^+} = 0\,, \qquad (x,t) \in \Gamma\,, \tag{6.4a}$$

$$p\Big|_{(x,t)^-}^{(x,t)^+} = 0\,, \qquad (x,t) \in \Gamma\,. \tag{6.4b}$$

Eq. (6.4b) is referred to as the dynamic condition. Furthermore, the interface motion must comply with a kinematic condition. To express this kinematic condition, we identify the interface by a level set:

$$\Gamma := \{(x,t) \in \Omega : \theta(x,t) = 0\}\,,$$

with $\theta \in C^\infty(\Omega)$ a suitably chosen function. We assume that $\theta(\Omega_\mathrm{p}) > 0$ and $\theta(\Omega_\mathrm{s}) < 0$. The kinematic interface condition is stated:

$$\theta_t + v\,\theta_x = 0\,, \qquad (x,t) \in \Omega\,. \tag{6.4c}$$

Eq. (6.4c) implies that the interface moves with the local flow velocity and thus ensures immiscibility. Recall that the velocity at the interface is uniquely defined by virtue of (6.4a).

6.2.3 Two-Fluid Euler Equations

To formulate the two-fluid Euler equations, it is important to note that the interface conditions (6.4) imply that the Rankine-Hugoniot condition for discontinuities in hyperbolic systems (see, for instance, Ref. [63]) is satisfied at the interface:

$$s\big(\mathbf{q}(x,t)^+ - \mathbf{q}(x,t)^-\big) = \mathbf{f}\big(\mathbf{q}(x,t)^+\big) - \mathbf{f}\big(\mathbf{q}(x,t)^-\big)\,, \qquad (x,t) \in \Gamma\,, \tag{6.5}$$

with s the shock speed. In particular, for the interface, $s = v(x,t)$ for $(x,t) \in \Gamma$. The variational statement (6.2) subject to (6.5) is equivalent to

$$\int_\Omega \mathbf{w}_t \cdot \mathbf{q} + \mathbf{w}_x \cdot \mathbf{f}(\mathbf{q})\,\mathrm{d}x\,\mathrm{d}t = 0\,, \qquad \forall \mathbf{w} \in \big[C_0^\infty(\Omega)\big]^2\,. \tag{6.6}$$

Note that the functions $\mathbf{w}$ in (6.6) can have support across the interface, in contrast to (6.2). The equivalence is founded on the classical principle that a piecewise continuous solution is a valid weak solution if and only if it satisfies the Rankine-Hugoniot condition at discontinuities.

To obtain a conservative formulation of the two-fluid Euler equations, we must replace the nonconservative, advective form of the kinematic condition (6.4c) by a conservative equivalent. Under the conditions imposed by (6.6), an appropriate replacement for (6.4c) is:

$$\int_\Omega \lambda_t\,\rho g(\theta) + \lambda_x\,\rho g(\theta)\,v\,\mathrm{d}x\,\mathrm{d}t = 0\,, \qquad \forall \lambda \in C_0^\infty(\Omega)\,, \tag{6.7a}$$

with $\theta \mapsto g(\theta)$ a strictly monotone map with the property that for all $\lambda \in C_0^\infty(\Omega)$ and for all admissible $(\rho, \rho v)$ there exists a $w \in C_0^\infty(\Omega)$ such that

$$\int_\Omega w_t \rho + w_x \, \rho v \, \mathrm{d}x \, \mathrm{d}t = \int_\Omega \left(\lambda_t \, g(\theta) + \lambda \, g'(\theta) \, \theta_t\right) \rho + \left(\lambda_x \, g(\theta) + \lambda \, g'(\theta) \, \theta_x\right) \rho v \, \mathrm{d}x \, \mathrm{d}t \,. \tag{6.7b}$$

If g is a C^∞ map then $\lambda g(\theta) \in C^\infty(\Omega)$ and the identity (6.7b) follows by setting $w = \lambda g(\theta)$ and invoking partial differentiation. However, even if g is less regular, e.g., piecewise C^∞, then the condition can still be satisfied if the derivatives are understood in a generalized sense. To establish that (6.6) and (6.7a) imply (6.4c), we note that by (6.6) and (6.7b)

$$\int_\Omega \lambda_t \, \rho g(\theta) + \lambda_x \, \rho g(\theta) \, v \, \mathrm{d}x \, \mathrm{d}t + \int_\Omega \lambda_x \, \rho g'(\theta) \left(\theta_t + v \, \theta_x\right) \mathrm{d}x \, \mathrm{d}t = 0 \,, \qquad \forall \lambda \in C_0^\infty(\Omega) \,. \tag{6.8}$$

By virtue of (6.7a), the integrals in (6.8) must vanish separately. Therefore, Eq. (6.6) and (6.7a) imply (6.4c) weakly.

To conclude the setup of the two-fluid Euler equations, we note that the interface conditions (6.4) are identical to the continuity conditions for contact discontinuities; see, e.g., Refs. [63, 77]. Therefore, the two-fluid flow problem can be condensed into the variational statement

$$\int_\Omega \mathbf{w}_t \cdot \mathbf{q} + \mathbf{w}_x \cdot \mathbf{f}(\mathbf{q}) \, \mathrm{d}x \, \mathrm{d}t = 0 \,, \qquad \forall \mathbf{w} \in \left[C_0^\infty(\Omega)\right]^3 \,, \tag{6.9a}$$

where

$$\mathbf{q} := \begin{pmatrix} \rho \\ \rho v \\ \rho g(\theta) \end{pmatrix} \,, \quad \text{and} \quad \mathbf{f}(\mathbf{q}) := \begin{pmatrix} q_2 \\ q_2^2/q_1 + p \\ q_3 q_2/q_1 \end{pmatrix} \,, \tag{6.9b}$$

with the provision that θ can only change sign across a contact discontinuity, i.e., that the interface coincides with a contact discontinuity. In §6.4.2 we shall show that (6.9) indeed complies with the latter requirement.

Eq. (6.9) must be equipped with a compound equation of state of the form $p := p(\rho, \theta)$ with the property:

$$p(\rho, \theta) := \begin{cases} p_{\mathrm{p}}(\rho) & \text{if } \theta > 0, \\ p_{\mathrm{s}}(\rho) & \text{if } \theta < 0. \end{cases} \tag{6.10}$$

One may note that in (6.9)–(6.10), θ only acts as an intermediary between g and p. Therefore, θ does not have to appear explicitly in the formulation.

6.3 Pressure Oscillations

A common objection to interface capturing is the occurrence of *pressure oscillations*. These pressure oscillations expose the loss of the pressure-invariance property of the continuum problem under discretization. Below, we exemplify the pressure oscillations and we derive a pressure-invariance condition for discrete approximations to two-fluid flow problems. Furthermore, we construct a non-oscillatory conservative discretization for barotropic two-fluid flows.

6.3.1 Exemplification

The ensuing exemplification has appeared in similar form in, e.g., Refs. [2, 40, 57] and is merely included here for completeness.

To illustrate the pressure oscillations that are generally incurred by conservative discretizations of two-fluid flow problems, we consider (6.9) on $\Omega := \mathcal{L}\times]0,\infty[$, with $\mathcal{L}$ an open bounded subset of $\mathbb{R}$. We assign g as the primary volume fraction. In particular, this implies

$$g(\theta) := \begin{cases} 1 & \text{if } \theta > 0, \\ 0 & \text{otherwise}. \end{cases} \tag{6.11}$$

The compound equation of state is specified accordingly as

$$\rho(p,\theta) = g(\theta)\rho_{\mathrm{p}}(p) + \big(1 - g(\theta)\big)\rho_{\mathrm{s}}(p)\,, \tag{6.12}$$

with $\rho_{\mathrm{p}}(p)$ and $\rho_{\mathrm{s}}(p)$ the equations of state for the primary and secondary fluid. In fact, (6.12) provides a definition of the volume fraction in terms of p and ρ; see also §6.3.3. We allude to the fact that θ can be removed from the formulation and we suppress the dependence of g on θ below.

The spatial interval $\mathcal{L}$ is subdivided into open intervals $\mathcal{L}_j :=]x_j, x_{j+1}[$ with $j = 1,\ldots,n$ and (6.9)–(6.12) is supplemented with the initial conditions

$$\rho(x,0) = \rho_j^0\,, \quad v(x,0) = V\,, \quad g(x,0) = g_j^0\,, \quad x \in]x_j, x_{j+1}[\,, \quad j = 1,\ldots,n\,, \tag{6.13a}$$

with V an arbitrary positive constant and ρ_j^0 and g_j^0 constants such that

$$\rho_j^0 = g_j^0\,\rho_{\mathrm{p}}(P) + (1 - g_j^0)\,\rho_{\mathrm{s}}(P)\,, \tag{6.13b}$$

for some constant P. The equations (6.9)–(6.13) represent a two-fluid flow in which the velocity v is uniform and in which the density ρ and the primary volume fraction g are such that the pressure p is uniform as well.

The obvious solution to (6.9)–(6.13) is given by

$$\mathbf{q}(x,t) = \mathbf{q}(x - Vt, 0)\,. \tag{6.14}$$

The pressure $p(x,t)$ corresponding to (6.14) follows from the compound equation of state:

$$\rho(x,t) = g(x,t)\,\rho_{\mathrm{p}}(p(x,t)) + \big(1 - g(x,t)\big)\,\rho_{\mathrm{s}}(p(x,t))\,. \tag{6.15}$$

By (6.14)–(6.15),

$$\rho(x - Vt, 0) = g(x - Vt, 0)\, \rho_{\mathrm{p}}(p(x,t)) + \big(1 - g(x - Vt, 0)\big)\, \rho_{\mathrm{s}}(p(x,t))\,, \qquad (6.16)$$

and it follows that $p(x,t) = P$. In conclusion, if the initial velocity and pressure are uniform, then the pressure is invariant under (6.9).

To illustrate the loss of the pressure-invariance property, we consider the discretization of (6.9)–(6.13) on the grid $\{(x_j, t_k) : j = 1, \ldots, n, k = 1, 2, \ldots\}$ ($t_0 = 0$ and $t_k < t_{k+1}$) by means of the discontinuous Galerkin finite element method with piecewise constants:

$$\frac{\mathbf{q}_j^{k+1} - \mathbf{q}_j^k}{t_{k+1} - t_k} + \frac{\mathbf{f}\big(\mathbf{q}_j^k, \mathbf{q}_{j+1}^k\big) - \mathbf{f}\big(\mathbf{q}_{j-1}^k, \mathbf{q}_j^k\big)}{x_{j+1} - x_j} = 0\,, \qquad k = 0, 1, \ldots\,. \qquad (6.17)$$

This discretization is a first-order forward Euler finite-volume discretization. We specify the initial conditions $\mathbf{q}_j^0 = (\rho_j^0, \rho_j^0 V, \rho_j^0 g_j^0)^T$, in conformity with (6.13). In (6.17), $\mathbf{f}(\mathbf{q}_j^k, \mathbf{q}_{j+1}^k)$ refers to the *numerical flux* (see, e.g., Ref. [31]) between the elements $\mathcal{L}_j$ and $\mathcal{L}_{j+1}$. The grid function $\mathbf{q}_j^k$ is a piecewise constant approximation to $\mathbf{q}(x, t_k)$ according to (6.14) in the interval $\mathcal{L}_j$.

The states $\mathbf{q}_j^0$ and $\mathbf{q}_{j+1}^0$ ($j = 1, \ldots, n-1$) are connected by a contact discontinuity with velocity V. The corresponding Godunov flux becomes:

$$\mathbf{f}\big(\mathbf{q}_j^0, \mathbf{q}_{j+1}^0\big) = V \begin{pmatrix} \rho_j^0 \\ \rho_j^0 V \\ \rho_j^0 g_j^0 \end{pmatrix} + \begin{pmatrix} 0 \\ P \\ 0 \end{pmatrix}\,. \qquad (6.18)$$

Expression (6.18) is also valid for any approximate Riemann solver that features an exact representation of contact discontinuities, such as Osher's scheme. From Eqs. (6.17)–(6.18) it follows that

$$\mathbf{q}_j^1 = \mathbf{q}_j^0 - C\big(\mathbf{q}_j^0 - \mathbf{q}_{j-1}^0\big)\,, \qquad (6.19a)$$

with

$$C := V(t_1 - t_0)/(x_{j+1} - x_j)\,, \qquad (6.19b)$$

the local *CFL-number*. From Eqs. (6.19) and (6.13b) we obtain, successively,

$$\rho_j^1 = \rho_j^0 - C\big(\rho_j^0 - \rho_{j-1}^0\big) = g_j^*\, \rho_{\mathrm{p}}(P) + \big(1 - g_j^*\big)\, \rho_{\mathrm{s}}(P)\,, \qquad (6.20a)$$

with

$$g_j^* := g_j^0 - C\big(g_j^0 - g_{j-1}^0\big)\,. \qquad (6.20b)$$

Comparing (6.20) to (6.13b), we infer that a necessary and sufficient condition for pressure invariance of the discrete approximation is $g_j^1 = g_j^*$. However, conversely, from (6.13b) and (6.19) we obtain

$$g_j^1 = \frac{\Big((1-C)(g_j^0)^2 + C(g_{j-1}^0)^2\Big)\rho_{\mathrm{p}} + \Big((1-C)g_j^0(1-g_j^0) + Cg_{j-1}^0(1-g_{j-1}^0)\Big)\rho_{\mathrm{s}}}{\Big(g_j^0 - C(g_j^0 - g_{j-1}^0)\Big)\rho_{\mathrm{p}} + \Big(1 - \big(g_j^0 - C(g_j^0 - g_{j-1}^0)\big)\Big)\rho_{\mathrm{s}}}\,, \qquad (6.21)$$

with $\rho_{\mathrm{p/s}} := \rho_{\mathrm{p/s}}(P)$. In general, $g_j^1 \neq g_j^*$ and, hence, the discrete approximation from (6.17) lacks the pressure-invariance property of the continuum equations (6.9). Trivial exceptions are: $C = 0$ ($\Rightarrow \mathbf{q}_j^1 = \mathbf{q}_j^0$), $C = 1$ ($\Rightarrow \mathbf{q}_j^1 = \mathbf{q}_{j-1}^0$), $g_j^0 = g_{j-1}^0$ ($\Rightarrow \mathbf{q}_j^0 = \mathbf{q}_{j-1}^0$) and $\rho_{\mathrm{p}} = \rho_{\mathrm{s}}$.

It is noteworthy that if $(\rho g)_t + (\rho g v)_x = 0$ in (6.9) is replaced by

$$g_t + v g_x = 0\,, \qquad x \in \mathcal{L}, t \geq 0\,, \tag{6.22}$$

then, subject to the initial conditions (6.13), the first-order forward Euler discretization yields

$$g_j^1 = g_j^0 - C(g_j^0 - g_{j-1}^0)\,. \tag{6.23}$$

Hence, $g_j^1 = g_j^*$, and pressure invariance is maintained. However, Eq. (6.22) is in non-conservative form. The pressure invariance is in this case achieved at the expense of the conservative form of the equations.

6.3.2 Pressure-Invariance Condition

The implications of the above exemplification are restricted: The analysis does not imply that pressure oscillations are inherent to conservative discretizations of two-fluid flow problems. It merely implies that discrete approximations to two-fluid flow problems do not necessarily inherit the pressure-invariance property of the continuum equations.

To avoid pressure oscillations, discrete approximations of two-fluid flow problems must comply with a *pressure-invariance condition*. This condition is also mentioned in Ref. [57] in the context of a not-strictly-conservative method for multi-fluid flows with a stiffened-gas equation of state; see also [4, 59, 60]. Below we formulate the pressure-invariance condition for strictly conservative hyperbolic systems conform (6.9), provided with a compound equation of state of the form $p(\rho, \theta)$. We do not yet attach a specific connotation to g.

The pressure-invariance condition for discretizations of (6.9) is stated: If $v_j^k = V$, with V a constant, and ρ_j^k and θ_j^k satisfy

$$p(\rho_j^k, \theta_j^k) = P\,, \tag{6.24a}$$

for some constant P, then p is invariant under the characteristic mapping of the discretization, i.e.,

$$p\big(\rho_j^{k+1}, \theta_j^{k+1}\big) = P\,. \tag{6.24b}$$

In fact, $g_j^1 = g_j^*$ with g_j^* according to Eq. (6.20b) is an implementation of the pressure-invariance condition for a compound equation of state conform (6.12) and the first-order forward Euler discretization (6.17).

6.3.3 A Non-Oscillatory Conservative Scheme

To set up a pressure-invariant discretization for two-fluid flow problems, we consider two distinct compressible fluids with barotropic equations of state $\rho_{\mathrm{p}}(p)$ and $\rho_{\mathrm{s}}(p)$. For given density and pressure, the primary volume fraction α is implicitly defined by

$$\rho(x,t) = \alpha(x,t)\rho_{\mathrm{p}}(p(x,t)) + (1-\alpha(x,t))\rho_{\mathrm{s}}(p(x,t))\,. \tag{6.25}$$

Under the assumption $\rho_{\mathrm{p}}(p) \neq \rho_{\mathrm{s}}(p)$, Eq. (6.25) uniquely defines α. However, α does not appear in our final formulation and we do not rely on its unicity.

We also require the primary and secondary partial densities, defined as:

$$\rho'_{\mathrm{p}} := \alpha\rho_{\mathrm{p}}\,, \quad \text{and} \quad \rho'_{\mathrm{s}} := (1-\alpha)\rho_{\mathrm{s}}\,, \tag{6.26}$$

respectively. In terms of these partial densities, conservation of mass, for each fluid separately, is expressed by

$$(\rho'_{\mathrm{p}})_t + (\rho'_{\mathrm{p}}v)_x = 0\,, \quad \text{and} \quad (\rho'_{\mathrm{s}})_t + (\rho'_{\mathrm{s}}v)_x = 0\,. \tag{6.27}$$

Furthermore, the compound density satisfies $\rho = \rho'_{\mathrm{p}} + \rho'_{\mathrm{s}}$. Hence, if we assign g as the primary *mass fraction*,

$$g := \rho'_{\mathrm{p}}/\rho\,, \tag{6.28}$$

then conservation of mass, for each of the fluids separately, and conservation of momentum can be condensed into the form (6.9).

The compound equation of state associated with g according to (6.28) is implicitly given by

$$\rho g = \alpha\rho_{\mathrm{p}}(p)\,, \tag{6.29a}$$

$$\rho - \rho g = (1-\alpha)\rho_{\mathrm{s}}(p)\,. \tag{6.29b}$$

Eq. (6.29) follows from $\rho g = \rho'_{\mathrm{p}}$ and $\rho - \rho g = \rho'_{\mathrm{s}}$ and (6.26). Elimination of α yields the convenient form

$$\frac{1}{\rho} = \frac{g}{\rho_{\mathrm{p}}(p)} + \frac{1-g}{\rho_{\mathrm{s}}(p)}\,. \tag{6.30}$$

The first-order forward Euler discretization of (6.9) with the compound equation of state (6.29) or (6.30) satisfies the pressure-invariance condition. To corroborate this assertion, we note that if $v_j^k = V$ and $p\big(\rho_j^k, g_j^k\big) = P$, i.e.,

$$\rho_j^k g_j^k = \alpha_j^k \rho_{\mathrm{p}}(P)\,, \tag{6.31a}$$

$$\rho_j^k - \rho_j^k g_j^k = (1-\alpha_j^k)\rho_{\mathrm{s}}(P)\,, \tag{6.31b}$$

for all $j = 1,\ldots,n$, then the forward Euler discretization (6.17) with the numerical flux (6.18) yields

$$\rho_j^{k+1} = \rho_j^k - C\big(\rho_j^k - \rho_{j-1}^k\big)\,, \tag{6.32a}$$

$$\rho_j^{k+1} g_j^{k+1} = \rho_j^k g_j^k - C\big(\rho_j^k g_j^k - \rho_{j-1}^k g_{j-1}^k\big)\,, \tag{6.32b}$$

with C defined by (6.19b). From (6.31)–(6.32) it follows that

$$\rho_j^{k+1} g_j^{k+1} = \alpha_j^{k+1} \rho_{\mathrm{p}}(P)\,, \tag{6.33a}$$

$$\rho_j^{k+1} - \rho_j^{k+1} g_j^{k+1} = (1 - \alpha_j^{k+1}) \rho_{\mathrm{s}}(P)\,, \tag{6.33b}$$

with

$$\alpha_j^{k+1} := \alpha_j^k - C\big(\alpha_j^k - \alpha_{j-1}^k\big)\,. \tag{6.33c}$$

The compound equation of state (6.29) thus yields $p(\rho_j^{k+1}, g_j^{k+1}) = P$.

Summarizing paragraphs 6.3.1–6.3.3, we conclude that if g represents the primary volume fraction and the compound equation of state is specified accordingly as (6.12), then the discretization does not comply with the pressure-invariance condition. In contrast, if g is the primary mass fraction and the compound equation of state is given by (6.30), then the pressure-invariance condition is satisfied.

6.4 A Modified Osher Scheme for Two-Fluids

By virtue of its conservative form, the pressure-invariant formulation from §6.3.3 is ideally suited to treatment by Godunov-type methods. To avoid the computational expenses of solving the associated Riemann problems, below we set up an approximate Riemann solver for the two-fluid flow problem. The approximate Riemann solver is of Osher type. As a digression, we show that the interface indeed appears as a contact discontinuity, both in the exact Riemann solution and in the rarefaction-waves-only approximation that underlies Osher's scheme.

We emphasize that the choice of the approximate Riemann solver does *not* affect the pressure invariance; the invariance is ensured by the specific choice (6.28) for g and the corresponding compound equation of state (6.30). Any other approximate Riemann solver that resolves contact discontinuities exactly could have been selected here, e.g., Roe's scheme or the AUSM scheme.

6.4.1 The Two-Fluid Riemann Problem

We consider (6.9) provided with a compound equation of state of the form $p := p(\rho, g)$, e.g., Eq. (6.30). The formal dependence of g on θ in (6.9) can be ignored. The corresponding Riemann problem is defined on the half-space $\Omega := \{-\infty < x < \infty, 0 < t < \infty\}$ and is obtained by imposing the discontinuous initial conditions

$$\mathbf{q}(x,0) := \begin{cases} \mathbf{q}_L & \text{if } x < 0, \\ \mathbf{q}_R & \text{otherwise,} \end{cases} \tag{6.34}$$

for certain constant left and right states $\mathbf{q}_L$ and $\mathbf{q}_R$.

The properties of the Riemann problem and its solution are classical; see, e.g., [63]. This paragraph serves to collect the essentials for the ensuing presentation and contains the specifics for the two-fluid flow problem.

To obtain the Riemann solution for the two-fluid Euler equations, we need the Jacobian of $\mathbf{f}(\mathbf{q})$:

$$\mathbf{A}(\mathbf{q}) := \frac{\partial \mathbf{f}(\mathbf{q})}{\partial \mathbf{q}} = \begin{pmatrix} 0 & 1 & 0 \\ -(q_2^2 + c_2^2 q_3)/q_1^2 + c_1^2 & 2q_2/q_1 & c_2^2/q_1 \\ -q_3 q_2/q_1^2 & q_3/q_1 & q_2/q_1 \end{pmatrix}, \tag{6.35a}$$

with

$$c_1(\rho, g) := \sqrt{\partial p(\rho, g)/\partial \rho}\,, \quad \text{and} \quad c_2(\rho, g) := \sqrt{\partial p(\rho, g)/\partial g}\,. \tag{6.35b}$$

Its eigenvalues are

$$\lambda_1 := q_2/q_1 - c_1\,, \quad \lambda_2 := q_2/q_1\,, \quad \text{and} \quad \lambda_3 := q_2/q_1 + c_1\,, \tag{6.36}$$

and the corresponding eigenvectors are

$$\mathbf{r}_1 := \begin{pmatrix} 1 \\ q_2/q_1 - c_1 \\ q_3/q_1 \end{pmatrix}, \ \mathbf{r}_2 := \begin{pmatrix} q_1 \\ q_2 \\ -(c_1/c_2)^2 q_1^2 + q_3 \end{pmatrix}, \text{ and } \mathbf{r}_3 := \begin{pmatrix} 1 \\ q_2/q_1 + c_1 \\ q_3/q_1 \end{pmatrix}. \tag{6.37}$$

The eigenpairs $(\lambda_k, \mathbf{r}_k)$ are genuinely nonlinear for $k = 1, 3$ and linearly degenerate for $k = 2$ (cf. Ref. [43] for a definition of these classifications). The genuinely nonlinear eigenpairs are related to rarefaction waves and shock waves. The linearly degenerate eigenpair corresponds to a contact discontinuity.

For any admissible state $\mathbf{q}_A$ we associate two paths in state space with each eigenpair: the k-shock path and the k-rarefaction path. The k-shock path is defined as

$$\mathcal{S}_k(\mathbf{q}_A) := \left\{ \mathbf{q} \in \mathbb{R}^3 : s(\mathbf{q}, \mathbf{q}_A)(\mathbf{q} - \mathbf{q}_A) = \mathbf{f}(\mathbf{q}) - \mathbf{f}(\mathbf{q}_A),\, s(\mathbf{q}, \mathbf{q}_A) \to \lambda_k(\mathbf{q}_A) \text{ as } \mathbf{q} \to \mathbf{q}_A \right\}, \tag{6.38}$$

where $s(\mathbf{q}, \mathbf{q}_A)$ is referred to as the k-shock speed. The k-rarefaction path is defined as

$$\mathcal{R}_k(\mathbf{q}_A) := \left\{ \mathbf{q} \in \mathbb{R}^3 : \mathbf{q} = \mathbf{h}(\xi), \xi \in \mathbb{R} \right\}, \tag{6.39a}$$

with $\mathbf{h}(\xi)$ the solution to the ordinary differential equation

$$\mathbf{h}'(\xi) = \mathbf{r}_k(\mathbf{h}(\xi))/\beta(\mathbf{h}(\xi))\,, \quad \text{subject to} \quad \mathbf{h}\big(\lambda_k(\mathbf{q}_A)\big) = \mathbf{q}_A\,, \tag{6.39b}$$

with $\beta := \partial_{\mathbf{q}} \lambda_k(\mathbf{q}) \cdot \mathbf{r}_k(\mathbf{q})$ for the genuinely nonlinear eigenpairs and $\beta := 1$ for the linearly degenerate eigenpair. Note that $\lambda_k(\mathbf{h}(\xi)) = \xi$ for the genuinely nonlinear eigenpairs.

The Riemann solution can be constructed by means of the shock and rarefaction paths. The solution is constant in four (possibly empty) disjoint subsets of Ω. The constant states are denoted by $\mathbf{q}_{k/3}$, $k = 0, 1, 2, 3$. Furthermore, we set $\mathbf{q}_0 := \mathbf{q}_L$ and $\mathbf{q}_1 := \mathbf{q}_R$. We refer to $\mathbf{q}_{1/3}$ and $\mathbf{q}_{2/3}$ as *intermediate*

states. By connecting each pair of consecutive states by either a shock or a rarefaction path, we can connect $\mathbf{q}_0$ to $\mathbf{q}_1$. The unique sequence of paths that satisfies $\lambda_k(\mathbf{q}_{(k-1)/3}) > \lambda_k(\mathbf{q}_{k/3})$ if $\mathbf{q}_{(k-1)/3}$ and $\mathbf{q}_{k/3}$ are connected by $\mathcal{S}_k$ and $\lambda_k(\mathbf{q}_{(k-1)/3}) \leq \lambda_k(\mathbf{q}_{k/3})$ if $\mathbf{q}_{(k-1)/3}$ and $\mathbf{q}_{k/3}$ are connected by $\mathcal{R}_k$ corresponds to the Riemann solution. If $\lambda_k(\mathbf{q}_{(k-1)/3}) = \lambda_k(\mathbf{q}_{k/3})$ then the shock and rarefaction paths coincide and we opt for a rarefaction-path connection. This situation occurs for the contact discontinuity.

Recalling that the Riemann solution assumes the similarity form $\mathbf{q}(x,t) = \mathbf{q}(x/t)$ (see, e.g., Ref. [63]), we obtain

$$\mathbf{q}(x,t) := \mathbf{q}(x/t) = \begin{cases} \mathbf{q}_0 & \text{if } x/t < \sigma_0^+, \\ \mathbf{q}_{k/3} & \text{if } \sigma_k^- < x/t < \sigma_k^+, \\ \mathbf{h}_k(x/t) & \text{if } \sigma_{k-1}^+ < x/t < \sigma_k^-, \\ \mathbf{q}_1 & \text{if } x/t > \sigma_3^-, \end{cases} \tag{6.40a}$$

where $\mathbf{h}_k := \mathbf{h}$ according to (6.39b) with $\mathbf{q}_A := \mathbf{q}_{(k-1)/3}$ and

$$\sigma_k^+ = \begin{cases} \lambda_{k+1}(\mathbf{q}_{k/3}), & \text{if } \lambda_{k+1}(\mathbf{q}_{k/3}) \leq \lambda_{k+1}(\mathbf{q}_{(k+1)/3}), \\ s_{k+1}, & \text{otherwise,} \end{cases} \tag{6.40b}$$

$$\sigma_k^- = \begin{cases} \lambda_k(\mathbf{q}_{k/3}), & \text{if } \lambda_k(\mathbf{q}_{k/3}) \geq \lambda_k(\mathbf{q}_{(k-1)/3}), \\ s_k, & \text{otherwise.} \end{cases} \tag{6.40c}$$

An example of the solution (6.40) is presented in Figure 6.2.

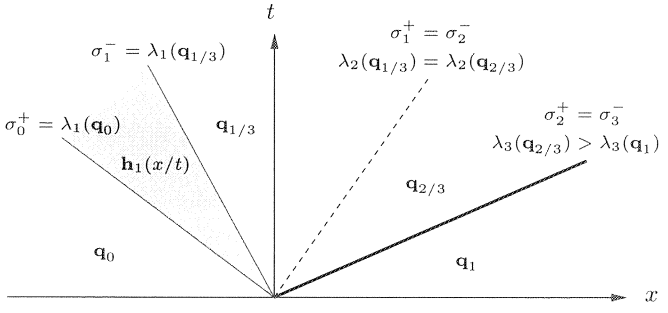

Figure 6.2: Illustration of a two-fluid Riemann solution: An expansion fan (*shaded*) connects $\mathbf{q}_0$ to $\mathbf{q}_{1/3}$, a contact discontinuity (*dashed*) connects $\mathbf{q}_{1/3}$ to $\mathbf{q}_{2/3}$ and a shock discontinuity (*solid*) connects $\mathbf{q}_{2/3}$ to $\mathbf{q}_1$.

6.4.2 Riemann Invariants

To each k-rarefaction path corresponds a set of *Riemann invariants*, i.e., functions which are invariant on $\mathcal{R}_k$. These Riemann invariants allow us to conveniently de-

termine the intermediate states in the rarefaction-waves-only approximation to the Riemann solution that underlies Osher's scheme. Moreover, by means of the Riemann invariants and a simple argument for shocks, we can show that the interface indeed appears as a contact discontinuity (cf. §6.2.3).

Consider the eigenvectors (6.37). A k-Riemann invariant for the two-fluid Euler equations (6.9) is any continuously differentiable function $\psi_k : \mathbb{R}^3 \mapsto \mathbb{R}$ with the property

$$\partial_{\mathbf{q}}\psi_k(\mathbf{q}) \cdot \mathbf{r}_k(\mathbf{q}) = 0\,. \tag{6.41}$$

There are at most two such k-Riemann invariants with linearly independent partial derivatives. Note that for the linearly degenerate eigenpair the eigenvalue is a Riemann invariant.

To derive the 1-Riemann invariants, we first solve the system of ordinary differential equations

$$\mathbf{h}'(\xi) = \mathbf{r}_k(\mathbf{h}(\xi))\,, \quad \text{subject to} \quad \mathbf{h}(0) = \mathbf{h}^0\,, \tag{6.42}$$

with $k = 1$:

$$h_1(\xi) = \xi + h_1^0\,, \tag{6.43a}$$

$$h_2(\xi) = h_1(\xi)\left(\frac{h_2^0}{h_1^0} - \int_{h_1^0}^{h_1(\xi)} \frac{c_1(\omega)}{\omega}\,\mathrm{d}\omega\right), \tag{6.43b}$$

$$h_3(\xi) = (h_3^0/h_1^0)\,\xi + h_3^0\,, \tag{6.43c}$$

with $c_1(\omega) := c_1\big(h_1(\omega), h_3(\omega)/h_1(\omega)\big)$. The 1-Riemann invariants can be obtained by constructing ξ-independent functions of $h_j(\xi)$, $j = 1, 2, 3$. The invariants thus obtained are presented in (6.48). Note that by virtue of the similitude of $\mathbf{r}_1$ and $\mathbf{r}_3$, the 3-Riemann invariants can be chosen identical to the 1-Riemann invariants with c_1 replaced by $-c_1$.

To derive the 2-Riemann invariants, we solve (6.42) for $k = 2$. Obviously,

$$h_1(\xi) = h_1^0 \mathrm{e}^{\xi}\,, \quad \text{and} \quad h_2(\xi) = h_2^0 \mathrm{e}^{\xi}\,. \tag{6.44}$$

To determine $h_3(\xi)$, we recall that c_1 and c_2 are defined by (6.35b). Therefore, Eq. (6.42) yields

$$h_3' D_2 p + D_1 p - h_3 D_2 p = 0\,, \tag{6.45}$$

where D_j denotes differentiation with respect to the j-th argument. Moreover, from $p := p(h_1, h_3/h_1)$ we obtain

$$\frac{\mathrm{d}p}{\mathrm{d}\xi} = h_1'\Big(D_1 p - \frac{h_3 D_2 p}{h_1^2}\Big) + h_3' \frac{D_2 p}{h_1}\,. \tag{6.46}$$

Eqs. (6.44)–(6.46) imply that $\mathrm{d}p/\mathrm{d}\xi = 0$, i.e., p is a 2-Riemann invariant and $h_3(\xi)$ is implicitly specified by

$$p\big(h_1(\xi), h_3(\xi)/h_1(\xi)\big) = p\big(h_1^0, h_3^0/h_1^0\big)\,. \tag{6.47}$$

From (6.44)–(6.47) we infer that p and q_2/q_1 are 2-Riemann invariants. Indeed, the linearly degenerate eigenvalue $\lambda_2 := q_2/q_1$ is a 2-Riemann invariant.

Summarizing, we can associate the following Riemann invariants with the two-fluid Euler equations (6.9) with a compound equation of state of the form $p := p(\rho, g)$:

$$\begin{aligned} &\psi_1^2 = v + \Psi(\rho, g)\,, \quad \psi_2^1 = v\,, \quad \psi_3^1 = v - \Psi(\rho, g)\,, \\ &\psi_1^3 = g\,, \qquad\qquad \psi_2^3 = p\,, \quad \psi_3^2 = g\,, \end{aligned} \tag{6.48a}$$

where

$$\Psi(\rho, g) := \int_{\rho^0}^{\rho} \frac{c_1(\omega, g)}{\omega}\, \mathrm{d}\omega\,, \tag{6.48b}$$

with ρ^0 an arbitrary positive real constant.

It is important to note that g is a Riemann invariant for the genuinely nonlinear eigenpairs ($k = 1, 3$) and that p and v are Riemann invariants for the linearly degenerate eigenpair ($k = 2$). In the absence of shocks, this implies that the change in g associated with the fluid transition at the interface can only occur across the contact discontinuity and, moreover, that the interface conditions (6.4) are indeed satisfied.

To demonstrate that g is also invariant across genuine (non-degenerate) shocks, we note that

$$s\,(\rho - \rho_A) = \rho v - \rho_A v_A \quad \Rightarrow \quad s\,(\rho g_A - \rho_A g_A) = \rho g_A v - \rho_A g_A v_A\,, \tag{6.49}$$

for any constant g_A. From (6.38) and (6.49) we can infer that there exist two shock paths on which g is invariant. Moreover, the shock path and rarefaction path of the degenerate shock ($k = 2$) coincide. Because g is not a 2-Riemann invariant, g can vary on the 2-shock path. Therefore, the shock paths on which g is invariant must be the 1- and 3-shock paths. These paths correspond to genuine shocks. The invariance of g on the 1- and 3-shock paths implies that the fluid transition at the interface cannot occur across a genuine shock.

6.4.3 Rarefaction-Waves-Only Approximation

In §6.4.1 it was shown that the intermediate states in the Riemann solution are connected by shock and rarefaction paths. A rarefaction-waves-only approximation is obtained by replacing the shock paths by rarefaction paths. Shock discontinuities in the Riemann solution are then approximated by so-called *overturned rarefaction waves*; see, e.g., Ref. [44].

The intermediate states in the rarefaction-waves-only approximation can be conveniently determined by means of the Riemann invariants. Supposing the approximate intermediate states $\tilde{\mathbf{q}}_{(l-1)/n}$ and $\tilde{\mathbf{q}}_{l/n}$ are connected by $\mathcal{R}_{k(l)}$, with $k : \{1, 2, 3\} \mapsto \{1, 2, 3\}$ a bijection,

$$\begin{gathered} \psi^m_{k(l)}\big(\tilde{\mathbf{q}}_{(l-1)/3}\big) = \psi^m_{k(l)}\big(\tilde{\mathbf{q}}_{l/3}\big)\,, \quad l, m = 1, 2, 3\,, \quad m \neq k(l)\,, \\ \text{with } \tilde{\mathbf{q}}_0 := \mathbf{q}_L \text{ and } \tilde{\mathbf{q}}_1 := \mathbf{q}_R\,. \end{gathered} \tag{6.50}$$

Usual choices for the ordering of the paths are the O-variant $k(l) := 4 - l$ (see Ref. [50]) and the P-variant $k(l) := l$ (see Ref. [30]). The O-variant and the P-variant have mutually reversed orderings. Throughout, we presume a P-variant ordering.

Eq. (6.50) represents a system of nonlinear equations, from which the approximate intermediate states $\tilde{\mathbf{q}}_{1/3}$ and $\tilde{\mathbf{q}}_{2/3}$ have to be extracted. Using the expressions for the Riemann invariants (6.48), it is easy to show that the Jacobian matrix corresponding to (6.50) is nonsingular. Therefore, by the inverse function theorem, Eq. (6.50) is indeed solvable.

To establish the accuracy of the approximate intermediate states from (6.50), we recall from [63] that the change in the k-Riemann invariants across a k-shock with strength μ is $O(\mu^3)$ as $\mu \to 0$, with the k-shock strength defined as the change in the eigenvalue λ_k across the shock. It follows that for sufficiently weak shocks, i.e., if $\mu := \sup_{k=1,3} \left(\lambda_k(\mathbf{q}_{(k-1)/3}) - \lambda_k(\mathbf{q}_{k/3})\right)$ is sufficiently small, the error in the approximate intermediate states is only $O(\mu^3)$ as well. Moreover, in the absence of shocks, the approximation according to (6.50) is even exact. If strong shocks impair the accuracy of the numerical solution, then an approximate Riemann solver which is suitable for shocks, or even an exact Riemann solver, should be applied.

From (6.48) and (6.50) we obtain

$$\tilde{g}_{1/3} = g_L\,, \quad \tilde{g}_{2/3} = g_R\,, \quad \text{and} \quad \tilde{v}_{1/3} = \tilde{v}_{2/3} =: \tilde{v}_{1/2}\,, \tag{6.51}$$

and, in turn,

$$\tilde{v}_{1/2} + \int_{\rho_L}^{\tilde{\rho}_{1/3}} \frac{c_1(\rho, g_L)}{\rho}\,\mathrm{d}\rho = v_L\,, \tag{6.52a}$$

$$\tilde{v}_{1/2} - \int_{\rho_R}^{\tilde{\rho}_{2/3}} \frac{c_1(\rho, g_R)}{\rho}\,\mathrm{d}\rho = v_R\,, \tag{6.52b}$$

$$p(\tilde{\rho}_{1/3}, g_L) = p(\tilde{\rho}_{2/3}, g_R)\,, \quad (=: \tilde{p}_{1/2}). \tag{6.52c}$$

For a compound equation of state of the form $\rho := \rho(p, g)$, e.g., Eq. (6.30), these conditions for the intermediate states can be cast in a convenient form. To derive this form, we use Eq. (6.35b) and the transformation $\rho := \rho(p, \theta)$ to obtain, successively,

$$\int_{\rho_a}^{\rho_b} \frac{c_1(\rho, g)}{\rho}\,\mathrm{d}\rho = \int_{\rho_a}^{\rho_b} \frac{1}{\rho}\sqrt{\frac{\partial p(\rho, g)}{\partial \rho}}\,\mathrm{d}\rho = \int_{p_a}^{p_b} \frac{1}{\rho(p, g)}\sqrt{\frac{\partial \rho(p, g)}{\partial p}}\,\mathrm{d}p\,, \tag{6.53}$$

for any $\rho_a, \rho_b \in \mathbb{R}_+$ and corresponding p_a, p_b. Eqs. (6.52)–(6.53) imply

$$\int_{p_L}^{\tilde{p}_{1/2}} \frac{1}{\rho(p, g_L)}\sqrt{\frac{\partial \rho(p, g_L)}{\partial p}}\,\mathrm{d}p + \int_{p_R}^{\tilde{p}_{1/2}} \frac{1}{\rho(p, g_R)}\sqrt{\frac{\partial \rho(p, g_R)}{\partial p}}\,\mathrm{d}p = v_L - v_R\,. \tag{6.54}$$

Equation (6.54) presents a concise condition for the intermediate pressure $\tilde{p}_{1/2}$. Once the intermediate pressure has been extracted from (6.54), the intermediate densities follow from the compound equation of state and $\tilde{v}_{1/2}$ is obtained from (6.52a) or (6.52b) in a straightforward manner.

It is noteworthy that (6.54) is well suited to treatment by numerical approximation techniques. In particular, the derivatives of the integrals with respect to $\tilde{p}_{1/2}$, which are required in Newton's method, are simply the integrands evaluated at $\tilde{p}_{1/2}$. Moreover, for a given approximation to $\tilde{p}_{1/2}$, the integrals can be evaluated by a standard numerical integration method (see, e.g., Ref. [34]).

6.4.4 The Modified Osher Scheme

The numerical flux in Osher's scheme [50], is determined by

$$\mathbf{f}_O(\mathbf{q}_L, \mathbf{q}_R) := \frac{1}{2}\mathbf{f}(\mathbf{q}_L) + \frac{1}{2}\mathbf{f}(\mathbf{q}_R) - \frac{1}{2}\sum_{l=1}^{3} \mathbf{d}_l \,, \tag{6.55a}$$

with

$$\mathbf{d}_l := \int_0^1 \big|\mathbf{A}\big(\mathbf{h}(\xi)\big)\big| \cdot \mathbf{r}_{k(l)}\big(\mathbf{h}(\xi)\big)\, \mathrm{d}\xi \,, \tag{6.55b}$$

where $\mathbf{h}(\xi)$ refers to a parametrization of the section of the $k(l)$-rarefaction path between $\tilde{\mathbf{q}}_{(l-1)/3}$ and $\tilde{\mathbf{q}}_{l/3}$ and

$$|\mathbf{A}(\mathbf{q})| := \big(\mathbf{r}_1, \mathbf{r}_2, \mathbf{r}_3\big) \cdot \mathrm{diag}\big(|\lambda_1|, |\lambda_2|, |\lambda_3|\big) \cdot \big(\mathbf{r}_1, \mathbf{r}_2, \mathbf{r}_3\big)^{-1} \,, \tag{6.55c}$$

with the eigenvalues and eigenvectors according to (6.36) and (6.37), their dependence on $\mathbf{q}$ being suppressed for transparency. The numerical flux (6.55) approximates $\mathbf{f}(\mathbf{q}(0))$, with $\mathbf{q}(x/t)$ the Riemann solution in similarity form according to (6.40).

From Eqs. (6.55b)–(6.55c) it follows that

$$\mathbf{d}_l = \int_0^1 \mathrm{sign}\big(\lambda_{k(l)}(\mathbf{h}(\xi))\big)\, \mathbf{A}\big(\mathbf{h}(\xi)\big) \cdot \mathbf{r}_{k(l)}\big(\mathbf{h}(\xi)\big)\, \mathrm{d}\xi \,. \tag{6.56}$$

If $\lambda_{k(l)}$ in (6.56) does not change sign on the integration interval, then the integral evaluates to

$$\mathbf{d}_l = \mathrm{sign}\big(\lambda_{k(l)}(\tilde{\mathbf{q}}_{(l-1)/n})\big)\, \big(\mathbf{f}(\tilde{\mathbf{q}}_{l/n}) - \mathbf{f}(\tilde{\mathbf{q}}_{(l-1)/n})\big) \,, \tag{6.57}$$

whereas if $\lambda_{k(l)}$ changes its sign once, say at $\tilde{\mathbf{q}}_*$ (i.e., $\lambda_{k(l)}(\tilde{\mathbf{q}}_*) = 0$), then

$$\mathbf{d}_l = \mathrm{sign}\big(\lambda_{k(l)}(\tilde{\mathbf{q}}_{(l-1)/n})\big)\, \Big(\big(\mathbf{f}(\tilde{\mathbf{q}}_*) - \mathbf{f}(\tilde{\mathbf{q}}_{(l-1)/n})\big) - \big(\mathbf{f}(\tilde{\mathbf{q}}_{l/n}) - \mathbf{f}(\tilde{\mathbf{q}}_*)\big)\Big) \,. \tag{6.58}$$

Under the condition $0 < \lambda_2(\tilde{\mathbf{q}}_{1/3}) = \lambda_2(\tilde{\mathbf{q}}_{2/3}) < \lambda_3(\tilde{\mathbf{q}}_{2/3}), \lambda_3(\tilde{\mathbf{q}}_1)$, we can then derive three generic cases

$$\mathbf{f}_O(\mathbf{q}_L, \mathbf{q}_R) = \begin{cases} \mathbf{f}(\tilde{\mathbf{q}}_*) & \text{if } \lambda_1(\tilde{\mathbf{q}}_0) < 0 < \lambda_1(\tilde{\mathbf{q}}_{1/3}), \\ \mathbf{f}(\tilde{\mathbf{q}}_{1/3}) & \text{if } \lambda_1(\tilde{\mathbf{q}}_0) < \lambda_1(\tilde{\mathbf{q}}_{1/3}) < 0, \\ \mathbf{f}(\tilde{\mathbf{q}}_0) + \mathbf{f}(\tilde{\mathbf{q}}_{1/3}) - \mathbf{f}(\tilde{\mathbf{q}}_*) & \text{if } \lambda_1(\tilde{\mathbf{q}}_0) > 0 > \lambda_1(\tilde{\mathbf{q}}_{1/3}). \end{cases} \tag{6.59}$$

Comparison to the corresponding $\mathbf{f}(\mathbf{q}(0))$ shows that $\mathbf{f}_O(\mathbf{q}_L, \mathbf{q}_R)$ is accurate in the first two cases, in particular, the error is then $O(\mu^3)$, and inaccurate in the third case, the error then being $O(\mu)$. This failure of Osher's scheme is exemplified by means of the Burgers equation in [44].

To avoid the aforementioned deficiency of Osher's scheme, we propose a modification of the scheme. The rarefaction-waves-only approximation is maintained. However, the overturned-rarefaction-wave representation of shocks in the approximate Riemann solution is avoided. Instead, the intermediate states from (6.50), with a presumed P-variant ordering of the subpaths, are used to construct the approximate Riemann solution:

$$\tilde{\mathbf{q}}(x/t) := \begin{cases} \tilde{\mathbf{q}}_0 & \text{if } x/t < \tilde{\sigma}_0^+, \\ \tilde{\mathbf{q}}_{k/3} & \text{if } \tilde{\sigma}_k^- < x/t < \tilde{\sigma}_l^+, \\ \mathbf{h}_k(x/t) & \text{if } \tilde{\sigma}_{k-1}^+ < x/t < \tilde{\sigma}_k^-, \\ \tilde{\mathbf{q}}_1 & \text{if } x/t > \tilde{\sigma}_3^-, \end{cases} \tag{6.60a}$$

where $\mathbf{h}_k := \mathbf{h}$ according to (6.39b) with $\mathbf{q}_A := \tilde{\mathbf{q}}_{(k-1)/3}$ and

$$\tilde{\sigma}_k^+ := \begin{cases} \lambda_{k+1}(\tilde{\mathbf{q}}_{k/3}) & \text{if } \lambda_{k+1}(\tilde{\mathbf{q}}_{k/3}) \le \lambda_{k+1}(\tilde{\mathbf{q}}_{(k+1)/3}), \\ \tilde{s}_{k+1} & \text{otherwise,} \end{cases} \tag{6.60b}$$

$$\tilde{\sigma}_k^- := \begin{cases} \lambda_k(\tilde{\mathbf{q}}_{k/3}) & \text{if } \lambda_k(\tilde{\mathbf{q}}_{k/3}) \ge \lambda_k(\tilde{\mathbf{q}}_{(k-1)/3}), \\ \tilde{s}_k & \text{otherwise,} \end{cases} \tag{6.60c}$$

$$\tilde{s}_k := \frac{1}{2}\lambda_k(\tilde{\mathbf{q}}_{(k-1)/3}) + \frac{1}{2}\lambda_k(\tilde{\mathbf{q}}_{k/3}). \tag{6.60d}$$

The numerical flux is subsequently computed as $\mathbf{f}_{OM}(\mathbf{q}_L, \mathbf{q}_R) := \mathbf{f}(\tilde{\mathbf{q}}(0))$.

Comparison of the approximate Riemann solution (6.60) with the exact Riemann solution (6.40) shows that $\tilde{s}_k$ acts as an approximation to the shock speed. In Ref. [63] it is proved that the speed of a shock with strength μ is equal to the average of the eigenvalues on either side of the shock and a remainder of $O(\mu^2)$, as $\mu \to 0$.

ρ_{p}^0	η_{p}	γ_{p}	ρ_{s}^0	η_{s}	γ_{s}
1	3000	7	10^{-3}	0	7/5

Table 6.1: Constants in Tait's equation of state (6.61).

6.5 Numerical Experiments and Results

To test the non-oscillatory conservative scheme from §6.3.3, equipped with the modified Osher scheme from §6.4.4 for the numerical fluxes, we consider two test cases. The first test case is a Riemann problem in which the initial velocity and pressure are uniform. Its solution corresponds to a translation of the interface. This test case serves to verify the pressure invariance of the method. The second test case concerns a Riemann problem associated with the collision of a shock with the interface. As a result of the interaction of the shock and the interface, both the conservation properties and the pressure invariance of the method are relevant in this case. Moreover, test case II is used to verify the asymptotic behavior of the error in the approximate intermediate states and in the shock-speed approximation, as the shock strength vanishes; refer to Sec. 6.4.

6.5.1 Test Case I

We consider the two-fluid Euler equations (6.9), provided with the compound equation of state (6.30). The primary and secondary fluid comply with Tait's equation of state (see, e.g., Ref. [72]):

$$\rho_{\mathrm{p/s}}(p) := \rho_{\mathrm{p/s}}^0 \left(\frac{(p/p^0) + \eta_{\mathrm{p/s}}}{1 + \eta_{\mathrm{p/s}}} \right)^{1/\gamma_{\mathrm{p/s}}}, \tag{6.61}$$

with p^0 (:= 1) an appropriate reference pressure, $\rho_{\mathrm{p/s}}^0$ the corresponding densities of the primary and secondary fluid and $\eta_{\mathrm{p/s}} \geq 0$ and $\gamma_{\mathrm{p/s}} > 1$ fluid-specific constants. The constants used in the numerical experiments are listed in Table 6.1. These constants are chosen such that the primary fluid models water and the secondary fluid models air in homentropic flow. Appropriate constants for other fluids are provided in [72].

Test case I concerns a Riemann problem with

$$\begin{pmatrix} \rho \\ v \\ g \end{pmatrix}_0 := \begin{pmatrix} 1 \\ 10^2 \\ 1 \end{pmatrix} \quad \text{and} \quad \begin{pmatrix} \rho \\ v \\ g \end{pmatrix}_1 := \begin{pmatrix} 10^{-3} \\ 10^2 \\ 0 \end{pmatrix}. \tag{6.62}$$

Hence, $p(x,0) = 1$ and $v(x,0) = 100$ for all x, i.e., the pressure and velocity are uniform. The solution then corresponds to a translation of the interface.

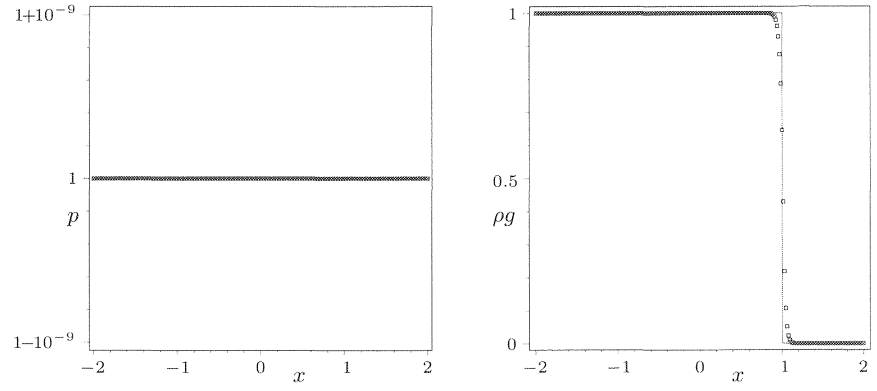

(a) pressure at $t = 0.01$.

(b) density at $t = 0.01$.

Figure 6.3: Test case I: Computed result (*markers only*) and exact solution (*solid line*).

The two-fluid flow problem is discretized by means of a Godunov-type finite volume method, with the numerical fluxes based on the modified Osher scheme from §6.4.4. Instead of a first-order discretization conform (6.17), we use a limited second order scheme with the minmod limiter (see, e.g., [77]). The intermediate pressure $\tilde{p}_{1/2}$ is solved from (6.54) by means of Newton's method. The integrals in (6.54) are approximated by 16-point Gauss quadrature. We use a uniform grid with mesh width $h = 2^{-6}$. The time step is set to $\tau = 2^{-9}h$.

Figure 6.3 plots the results for test case I. The initial position of the interface is set at $x = 0$. The results confirm the pressure invariance of the scheme.

6.5.2 Test Case II

Test Case II is illustrated in Figure 6.4 on the following page. The equation of state of the primary and secondary fluid is specified by (6.61), with the same constants as in Test Case I (Table 6.1 on the preceding page). The states $\mathbf{q}_0$, $\mathbf{q}_I$ and $\mathbf{q}_1$ are determined by

$$\begin{pmatrix}\rho\\ v\\ g\end{pmatrix}_0 := \begin{pmatrix}1.000427\ldots\\ 0.062042\ldots\\ 1\end{pmatrix}, \quad \begin{pmatrix}\rho\\ v\\ g\end{pmatrix}_I := \begin{pmatrix}1\\ 0\\ 1\end{pmatrix} \quad \text{and} \quad \begin{pmatrix}\rho\\ v\\ g\end{pmatrix}_1 := \begin{pmatrix}10^{-3}\\ 0\\ 0\end{pmatrix}. \tag{6.63}$$

The pressure corresponding to $\mathbf{q}_0$ is $p_{\mathrm{p}}(\rho_0) = 10$. The states $\mathbf{q}_0$ and $\mathbf{q}_I$ in the primary fluid (water) are connected by a 3-shock with speed $s_{\mathrm{p}} = 145.062002\ldots$ and $\mathbf{q}_I$ is connected to $\mathbf{q}_1$ by a steady contact discontinuity, representing the interface. At time $t = 0$, the shock collides with the interface, which is set at $x = 0$

(see Figure 6.4). The states $\mathbf{q}_0$ and $\mathbf{q}_1$ are then contiguous and, hence, the collision induces a Riemann problem. The corresponding Riemann solution assumes the form of a reflected rarefaction wave, a moving interface and a transmitted shock with speed $s_s = 37.491063\ldots (= \sigma_2^+ = \sigma_3^-)$.

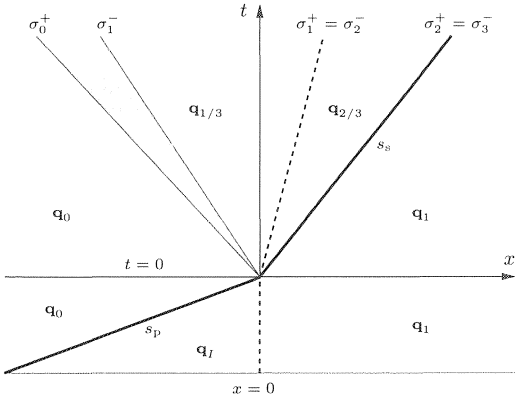

Figure 6.4: Test case II: The shock/interface collision at $t = 0$ induces a Riemann problem.

The details of the set up of the numerical experiment for test case II are identical to test case I. In figure 6.5 on page 97 we have plotted the results for test case II. The numerical results exhibit good agreement with the exact Riemann solution. We also monitored the mass-conservation errors for the two fluids separately and the momentum-conservation error for this test case: these errors are indeed of the order of the machine precision (results not displayed).

Furnished with different settings of the parameters, test case II can be used to verify the asymptotic behavior of the error in the intermediate states of the rarefaction-waves-only approximation and the error in the shock speed, as the shock strength vanishes (cf. §6.4.3 and §6.4.4). For this purpose, we consider different states $\mathbf{q}_0$ on the 3-shock path through $\mathbf{q}_I$. These states are characterized by the corresponding pressure. We then determine the intermediate states of the actual Riemann solution, $\mathbf{q}_{1/3}$ and $\mathbf{q}_{2/3}$, by means of the appropriate shock and rarefaction relations and, subsequently, the corresponding intermediate pressure $p_{1/2}$ and the shock strengths $\mu_\mathrm{p} := \lambda_3(\mathbf{q}_0) - \lambda_3(\mathbf{q}_I)$ and $\mu_\mathrm{s} := \lambda_3(\mathbf{q}_{2/3}) - \lambda_3(\mathbf{q}_1)$. The approximate intermediate pressure is extracted from (6.54). Furthermore, we determine the exact shock speeds s_p and s_s and their approximations according to $(\lambda_3(\mathbf{q}_0) + \lambda_3(\mathbf{q}_I))/2$ and $(\lambda_3(\mathbf{q}_{2/3}) + \lambda_3(\mathbf{q}_1))/2$, respectively. The results are listed in Table 6.2 on page 98. The entries in columns 4 and 6 confirm that $p' := \tilde{p}_{1/2} - p_{1/2} \propto \mu_\mathrm{p}^3$ as $\mu_\mathrm{p} \to 0$ and $s'_\mathrm{s} := s_\mathrm{s} - (\lambda_3(\mathbf{q}_{2/3}) + \lambda_3(\mathbf{q}_1))/2 \propto \mu_\mathrm{s}^2$ as $\mu_\mathrm{s} \to 0$, in accordance with the estimates in §6.4.3 and §6.4.4. Remarkably, column 5 indicates superconvergence of the approximation of the primary shock

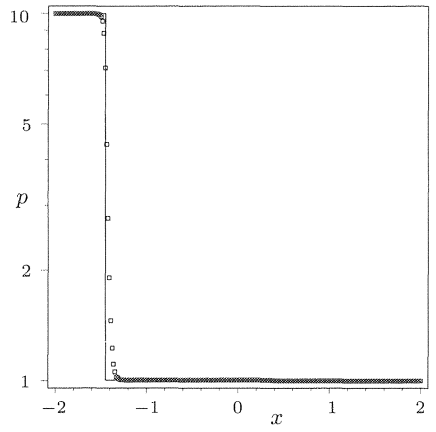

(a) pressure at $t = 0.01$ (*log-scale*).

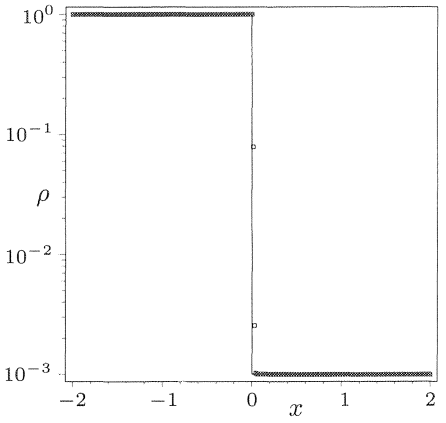

(b) density at $t = 0.01$ (*log-scale*).

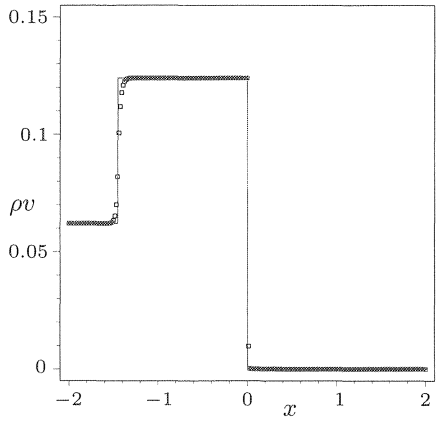

(c) momentum at $t = 0.01$.

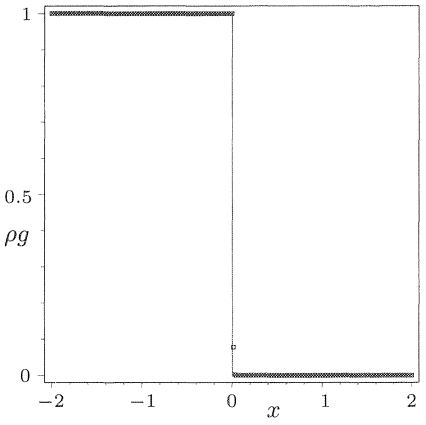

(d) primary partial density at $t = 0.01$.

Figure 6.5: Test case II: Computed result (*markers only*) and exact solution (*solid line*).

speed, in particular, $s'_{\mathrm{p}} := s_{\mathrm{p}} - (\lambda_3(\mathbf{q}_0) + \lambda_3(\mathbf{q}_I))/2 \propto \mu_{\mathrm{p}}^6$ as $\mu_{\mathrm{p}} \to 0$. A tedious asymptotic expansion analysis conveys that this superconvergence occurs exclusively for $\gamma_{\mathrm{p}} = 7$. A detailed exposition is beyond the scope of this work.

$p_{\mathrm{p}}(\mathbf{q}_0)$	μ_{p}	μ_{s}	p'	s'_{p}	s'_{s}
$1+10^{2}$	$2.73399\ 10^{0}$	$1.63994\ 10^{0}$	$4.24266\ 10^{-6}$	$1.09924\ 10^{-13}$	$6.96208\ 10^{-3}$
$1+10^{1}$	$2.75718\ 10^{-1}$	$1.65388\ 10^{-1}$	$4.21251\ 10^{-9}$	$1.19356\ 10^{-19}$	$7.10475\ 10^{-5}$
$1+10^{0}$	$2.75954\ 10^{-2}$	$1.65530\ 10^{-2}$	$4.20939\ 10^{-12}$	$1.20356\ 10^{-25}$	$7.11930\ 10^{-7}$
$1+10^{-1}$	$2.75978\ 10^{-3}$	$1.65544\ 10^{-3}$	$4.20907\ 10^{-15}$	$1.20456\ 10^{-31}$	$7.12075\ 10^{-9}$
$1+10^{-2}$	$2.75980\ 10^{-4}$	$1.65545\ 10^{-4}$	$4.20904\ 10^{-18}$	$1.20466\ 10^{-37}$	$7.12090\ 10^{-11}$
$1+10^{-3}$	$2.75980\ 10^{-5}$	$1.65545\ 10^{-5}$	$4.20904\ 10^{-21}$	$1.20467\ 10^{-43}$	$7.12091\ 10^{-13}$
$1+10^{-4}$	$2.75980\ 10^{-6}$	$1.65545\ 10^{-6}$	$4.20904\ 10^{-24}$	$1.20468\ 10^{-49}$	$7.12091\ 10^{-15}$

Table 6.2: Errors p', s'_{p} and s'_{s} for different shock strengths μ_{p} and μ_{s}.

6.6 Conclusions

We presented a non-oscillatory method for barotropic two-fluid flows, founded on a formulation of the two-fluid flow problem as a system of hyperbolic conservation laws. The conservative form of the two-fluid flow problem is well suited to treatment by a Godunov-type method. We considered an approximate Riemann solver for barotropic two-fluid flows, based on the rarefaction-waves-only approximation that underlies Osher's scheme. We established that the interface appears as a contact discontinuity, both in the exact solution and in the rarefaction-waves-only approximation. This implies compliance with the interface conditions.

Numerical results were presented for two Riemann problems, viz., a translating-interface test case and a shock/interface-collision test case. The first test case confirms the pressure invariance of the method. The second test case confirms its conservation properties. In both cases, the computed results agree well with the exact Riemann solution. Furnished with different settings, the second test case also confirmed the anticipated asymptotic behavior of the error in the approximate intermediate states and in the shock-speed approximation underlying the modified Osher scheme, as the shock-strength vanishes.

Bibliography

[1] R. Abgrall, *How to prevent pressure oscillations in multicomponent flow calculations: A quasi conservative approach*, J. Comput. Phys. **125** (1996), 150–160.

[2] R. Abgrall and S. Karni, *Computations of compressible multifluids*, J. Comput. Phys. **169** (2001), 594–623.

[3] B. Alessandrini and G. Delhommeau, *Simulation of three-dimensional unsteady viscous free surface flow around a ship model*, Int. J. Num. Meth. Fluids **19** (1994), 321–342.

[4] G. Allaire, S. Clerc, and S. Kokh, *A five-equation model for the numerical simulation of interfaces in two-phase flows*, C. R. Acad. Sci. Paris, Série I **331** (2000), 1017–1022.

[5] R. Aris, *Vectors, tensors and the basic equations of fluid mechanics*, Prentice-Hall, Englewood Cliffs, N.J., 1962.

[6] G.K. Batchelor, *An introduction to fluid dynamics*, Cambridge University Press, Cambridge, 1967.

[7] R. Becker, *An optimal control approach to a-posteriori error estimation for finite element discretizations of the Navier–Stokes equations*, Tech. Report IWR/SFB-Preprints 2000-34, Ruprecht-Karls-Universität Heidelberg, 2000, Available at `http://www.iwr.uni-heidelberg.de/sfb359/PP/Preprint2000-34.ps.gz`.

[8] R. Becker, M. Braack, and R. Rannacher, *Adaptive finite element methods for flow problems*, Tech. Report IWR/SFB-Preprints 2000-20, Ruprecht-Karls-Universität Heidelberg, 2000, Available at `http://www.iwr.uni-heidelberg.de/sfb359/PP/Preprint2000-20.ps.gz`.

[9] A. Brandt, *Multigrid techniques: 1984 guide with applications to fluid dynamics*, Tech. report, GMD, 1984.

[10] E.H. van Brummelen, *Numerical solution of steady free-surface Navier–Stokes flow*, Tech. Report MAS-R0018, ISSN 1386-3703, CWI, 2000, Available at `http://www.cwi.nl/ftp/CWIreports/MAS/MAS-R0018.ps.Z`.

[11] E.H. van Brummelen, H.C. Raven, and B. Koren, *Efficient numerical solution of steady free-surface Navier–Stokes flow*, J. Comput. Phys. **174** (2001), 120–137.

[12] J. Cahouet, *Etude numérique et experimentale du problème bidimensionnel de la résistance de vagues non-linéaire*, Ph.D. thesis, ENSTA, Paris, 1984, (In French).

[13] E. Campana, A. Di Mascio, P.G. Esposito, and F. Lalli, *Viscous-inviscid coupling in free surface ship flows*, Int. J. Num. Meth. Fluids **21** (1995), 699–722.

[14] T. Cebeci and A.M.O. Smith, *Analysis of turbulent boundary layers*, Academic Press, New York, 1974.

[15] Y.C. Chang, T.Y. Hou, B. Merriman, and S. Osher, *A level set formulation of Eulerian interface capturing methods for incompressible fluid flows*, J. Comput. Phys. **124** (1996), 449–464.

[16] U.T. Ehrenmark, *On viscous wave motion over a plane beach*, SIAM J. Appl. Math. **51** (1991), 1–19.

[17] B. Engquist and A. Majda, *Absorbing boundary conditions for the numerical simulation of waves*, Math. Comp. **31** (1977), 629–651.

[18] J. Farmer, L. Martinelli, and A. Jameson, *A fast multigrid method for solving the nonlinear ship wave problem with a free surface*, Proceedings of the 6th International Conference on Numerical Ship Hydrodynamics (Iowa, 1993) (W. Patel and F. Stern, eds.), National Academy Press, Washington D.C., 1994, pp. 155–172.

[19] R.P Fedkiw, T. Aslam, B. Merriman, and S. Osher, *A non-oscillatory Eulerian approach to interfaces in multimaterial flows (the ghostfluid method)*, J. Comput. Phys. **152** (1999), 457–492.

[20] C.A.J. Fletcher, *Computational techniques for fluid dynamics 2*, Springer, Berlin, 1988.

[21] A.V. Fursikov, M.D. Gunzburger, and L.S. Hou, *Boundary value problems and optimal boundary control for the Navier–Stokes system: the two-dimensional case*, SIAM J. Control Optim. **36** (1998), no. 3, 852–894.

[22] M.B. Giles and N.A. Pierce, *Adjoint equations in CFD: Duality, boundary conditions and solution behaviour*, AIAA **97-1850** (1997).

[23] J. Glimm, X.L. Li, Y. Liu, and N. Zhao, *Conservative front tracking and level set algorithms*, PNAS **98** (2001), no. 25, 14198–14201.

[24] S.K. Godunov, *Finite difference method for numerical computation of discontinuous solutions of the equations of fluid dynamics*, Mat. Sbornik **47** (1959), 271–306, (In Russian).

[25] M.D. Gunzburger and H. Kim, *Existence of an optimal solution of a shape control problem for the stationary Navier–Stokes equations*, SIAM J. Control Optim. **36** (1998), no. 3, 895–909.

[26] M.D. Gunzburger and H.K. Lee, *An optimization-based domain decomposition method for the Navier–Stokes equations*, SIAM J. Numer. Anal. **37** (2000), no. 5, 1455–1480.

[27] B. Gustafsson, H.-O. Kreiss, and J. Oliger, *Time dependent problems and difference methods*, Pure and Applied Mathematics, Wiley, New York, 1995.

[28] W.J. Harrison, *The influence of viscosity on the oscillations of superposed fluids*, Proc. Lond. Math. Soc. **6** (1908).

[29] R. Hartmann and P. Houston, *Adaptive discontinuous Galerkin finite element methods for nonlinear hyperbolic conservation laws*, Tech. Report IWR/SFB-Preprints 2001-20, Ruprecht-Karls-Universität Heidelberg, 2001, Available at `http://www.iwr.uni-heidelberg.de/sfb359/PP/Preprint2001-20.ps.gz`.

[30] P.W. Hemker and S.P. Spekreijse, *Multiple grid and Osher's scheme for the efficient solution of the steady Euler equations*, Appl. Num. Math. **2** (1986), 475–493.

[31] C. Hirsch, *Numerical computation of internal and external flows, volume i: Fundamentals of numerical discretization*, Numerical Methods in Engineering, Wiley, New York, 1995.

[32] M. Hoekstra, *Numerical simulation of ship stern flows with a space-marching Navier–Stokes method*, Ph.D. thesis, Delft University of Technology, Netherlands, 1999.

[33] P. Houston, B. Senior, and E. Süli, *hp-discontinuous Galerkin finite element methods for hyperbolic problems: error analysis and adaptivity*, Int. J. Numer. Meth. Fluids **40** (2002), 153–169.

[34] E. Isaacson and H.B. Keller, *Analysis of numerical methods*, Wiley, New York, 1966.

[35] P. Jenny, B. Müller, and H. Thomann, *Correction of conservative Euler solvers for gas mixtures*, J. Comput. Phys. **132** (1997), 91–107.

[36] S. Karni, *Multicomponent flow calculations by a consistent primitive algorithm*, J. Comput. Phys. **112** (1994), 31–43.

[37] ———, *Hybrid multifluid algorithms*, SIAM J. Sci. Comput. **17** (1996), 1019–1039.

[38] F.J. Kelecy and R.H. Pletcher, *The development of a free surface capturing approach for multidimensional free surface flows in closed containers*, J. Comput. Phys. **138** (1997), 939–980.

[39] J. Kevorkian and J.D. Cole, *Perturbation methods in applied mathematics*, Applied Mathematical Sciences, no. 34, Springer, Berlin, 1981.

[40] B. Koren, M.R. Lewis, E.H. van Brummelen, and B. van Leer, *Godunov and level-set approaches for homentropic two-fluid flow computations*, J. Comput. Phys. (2002), Accepted for Publication.

[41] H.-O. Kreiss, *Initial boundary value problems for hyperbolic systems*, Comm. Pure Appl. Math. **23** (1970), 277–298.

[42] H. Lamb, *Hydrodynamics*, 6th ed., Dover, New York, 1945.

[43] P.D. Lax, *Hyperbolic systems of conservation laws II*, Comm. Pure Appl. Math. **10** (1957), 537–566.

[44] B. van Leer, *On the relation between the upwind-differencing schemes of Godunov, Engquist-Osher and Roe*, SIAM J. Sci. Stat. Comput. **5** (1984), 1–20.

[45] M.J. Lighthill, *Introduction to Fourier analysis and generalised functions*, Cambridge University Press, Cambridge, 1958.

[46] ———, *Waves in fluids*, Cambridge University Press, Cambridge, 1978.

[47] H. Miyata, T. Sato, and N. Babo, *Difference solution of a viscous flow with free-surface wave about an advancing ship*, J. Comput. Phys. **72** (1987), 393–421.

[48] W. Mulder, S. Osher, and J.A. Sethian, *Computing interface motion in compressible gas dynamics*, J. Comput. Phys. **100** (1992), 209–228.

[49] D. Nguyen, F. Gibou, and R. Fedkiw, *A fully conservative ghost fluid method and stiff detonation waves*, Technical Papers of the 12th International Detonation Symposium, 12th International Detonation Symposium, San Diego, CA, 2002, Available at `http://www.sainc.com/onr/detsymp/PaperSubmit/FinalManuscript/pdf/Nguyen-37.pdf`.

[50] S. Osher and F. Solomon, *Upwind difference schemes for hyperbolic conservation laws*, Math. Comput. **38** (1982), 339–374.

[51] O. Pironneau, *Optimal shape design for elliptic systems*, Computational Physics, Springer, Berlin, 1984.

[52] H.C. Raven, *A solution method for the nonlinear ship wave resistance problem*, Ph.D. thesis, Delft University of Technology, Netherlands, 1996.

[53] R.D Richtmyer and K.W. Morton, *Difference methods for initial-value problems*, 2nd ed., Pure and Applied Mathematics, no. 4, Wiley, New York, 1967.

[54] P.A. Sackinger, P.R. Schuck, and R.R. Rao, *A Newton-Raphson pseudo-solid domain mapping technique for free and moving boundary problems: A finite element implementation*, J. Comput. Phys. **125** (1996), 83–103.

[55] H. Saito and L.E. Scriven, *Study of coating flow by the finite element method*, J. Comput. Phys. **42** (1981), 53–76.

[56] R. Saurel and R. Abgrall, *A multiphase Godunov method for compressible multifluid and multiphase flows*, J. Comput. Phys. **150** (1999), 425–467.

[57] ———, *A simple method for compressible multifluid flows*, SIAM J. Sci. Comput. **21** (1999), 1115–1145.

[58] L.E. Scriven, *Dynamics of a fluid interface*, Chem. Eng. Sc. **12** (1960), 98–108.

[59] K. Shyue, *A fluid-mixture type algorithm for compressible multicomponent flow with van der Waals equation of state*, J. Comput. Phys. **156** (1999), 43–88.

[60] ———, *A fluid-mixture type algorithm for compressible multicomponent flow with Mie-Grüneisen equation of state*, J. Comput. Phys. **171** (2001), 678–707.

[61] W.J. Silliman and L.E. Scriven, *Separating flow near a static contact line: Slip at a wall and shape of a free surface*, J. Comput. Phys. **34** (1980), 287–313.

[62] J. Simon, *Nonhomogeneous viscous incompressible fluids: Existence of velocity, density and pressure*, SIAM J. Math. Anal. **20** (1990), 1093–1117.

[63] J. Smoller, *Shock waves and reaction-diffusion equations*, Grundlehren der mathematischen Wissenschaften, Springer, New York, 1983.

[64] S. Spekreijse, *Multigrid solution of monotone second-order discretizations of hyperbolic conservation laws*, Math. Comput. **49** (1987), 135–155.

[65] J.J. Stoker, *Water waves: the mathematical theory with applications*, Pure and Applied Mathematics, Wiley, New York, 1992.

[66] P.K. Sweby, *High resolution schemes using flux limiters for hyperbolic conservation laws*, SIAM J. Numer. Anal. **21** (1984), 995–1011.

[67] S. Ta'asan, *Infinite dimensional preconditioners for optimal design problems*, Inverse Design and Optimization Methods (R.A. van den Braembussche and M. Manna, eds.), VKI Lecture Series, vol. 5, Von Karman Institute for Fluid Dynamics, 1997.

[68] ———, *Multigrid one-shot methods and design strategy*, Inverse Design and Optimization Methods (R.A. van den Braembussche and M. Manna, eds.), VKI Lecture Series, vol. 5, Von Karman Institute for Fluid Dynamics, 1997.

[69] ———, *Theoretical tools for problem setup*, Inverse Design and Optimization Methods (R.A. van den Braembussche and M. Manna, eds.), VKI Lecture Series, vol. 5, Von Karman Institute for Fluid Dynamics, 1997.

[70] R. Témam, *Navier–Stokes equations : theory and numerical analysis*, Studies in mathematics and its applications, vol. 2, North-Holland, Amsterdam, 1977.

[71] ———, *Navier–Stokes equations and nonlinear functional analysis*, CBMS Regional Conference Series in Applied Mathematics, vol. 41, SIAM, Philadelphia, 1983.

[72] P.A. Thompson, *Compressible fluid dynamics*, Advanced Engineering Series, McGraw-Hill, New York, 1972.

[73] E.C. Titchmarsh, *Introduction to Fourier integrals*, Oxford University Press, Oxford, 1937.

[74] W. Tsai and D.K.P. Yue, *Computation of nonlinear free-surface flows*, Annual Rev. Fluid. Mech. **28** (1996), 249–278.

[75] G.D. Tzabiras, *A numerical investigation of 2D steady free surface flows*, Int. J. Num. Meth. Fluids **25** (1997), 567–598.

[76] M. Vogt, *A numerical investigation of the level set method for computing free-surface waves*, Tech. Report CHA/NAV/R-98/0054, ISSN 1101-0614, Chalmers University of Technology, 1998.

[77] P. Wesseling, *Principles of computational fluid dynamics*, Springer Series in Computational Mathematics, vol. 29, Springer, Berlin, 2001.

[78] G.B. Whitham, *Linear and nonlinear waves*, Pure and Applied Mathematics, Wiley, New York, 1974.

[79] E. Zauderer, *Partial differential equations of applied mathematics*, 2nd ed., Pure and Applied Mathematics, Wiley, Chichester, 1989.

[80] S. Zhu and Y. Zhang, *On nonlinear transient free-surface flows over a bottom obstruction*, Phys. Fluids **9** (1997), no. 9, 2598–2604.

Author Index

Subject Index

CWI TRACTS

1 D.H.J. Epema. *Surfaces with canonical hyperplane sections.* 1984.
2 J.J. Dijkstra. *Fake topological Hilbert spaces and characterizations of dimension in terms of negligibility.* 1984.
3 A.J. van der Schaft. *System theoretic descriptions of physical systems.* 1984.
4 J. Koene. *Minimal cost flow in processing networks, a primal approach.* 1984.
5 B. Hoogenboom. *Intertwining functions on compact Lie groups.* 1984.
6 A.P.W. Böhm. *Dataflow computation.* 1984.
7 A. Blokhuis. *Few-distance sets.* 1984.
8 M.H. van Hoorn. *Algorithms and approximations for queueing systems.* 1984.
9 C.P.J. Koymans. *Models of the lambda calculus.* 1984.
10 C.G. van der Laan, N.M. Temme. *Calculation of special functions: the gamma function, the exponential integrals and error-like functions.* 1984.
11 N.M. van Dijk. *Controlled Markov processes; time-discretization.* 1984.
12 W.H. Hundsdorfer. *The numerical solution of nonlinear stiff initial value problems: an analysis of one step methods.* 1985.
13 D. Grune. *On the design of ALEPH.* 1985.
14 J.G.F. Thiemann. *Analytic spaces and dynamic programming: a measure theoretic approach.* 1985.
15 F.J. van der Linden. *Euclidean rings with two infinite primes.* 1985.
16 R.J.P. Groothuizen. *Mixed elliptic-hyperbolic partial differential operators: a case-study in Fourier integral operators.* 1985.
17 H.M.M. ten Eikelder. *Symmetries for dynamical and Hamiltonian systems.* 1985.
18 A.D.M. Kester. *Some large deviation results in statistics.* 1985.
19 T.M.V. Janssen. *Foundations and applications of Montague grammar, part 1: Philosophy, framework, computer science.* 1986.
20 B.F. Schriever. *Order dependence.* 1986.
21 D.P. van der Vecht. *Inequalities for stopped Brownian motion.* 1986.
22 J.C.S.P. van der Woude. *Topological dynamix.* 1986.
23 A.F. Monna. *Methods, concepts and ideas in mathematics: aspects of an evolution.* 1986.
24 J.C.M. Baeten. *Filters and ultrafilters over definable subsets of admissible ordinals.* 1986.
25 A.W.J. Kolen. *Tree network and planar rectilinear location theory.* 1986.
26 A.H. Veen. *The misconstrued semicolon: Reconciling imperative languages and dataflow machines.* 1986.
27 A.J.M. van Engelen. *Homogeneous zero-dimensional absolute Borel sets.* 1986.
28 T.M.V. Janssen. *Foundations and applications of Montague grammar, part 2: Applications to natural language.* 1986.
29 H.L. Trentelman. *Almost invariant subspaces and high gain feedback.* 1986.
30 A.G. de Kok. *Production-inventory control models: approximations and algorithms.* 1987.
31 E.E.M. van Berkum. *Optimal paired comparison designs for factorial experiments.* 1987.
32 J.H.J. Einmahl. *Multivariate empirical processes.* 1987.
33 O.J. Vrieze. *Stochastic games with finite state and action spaces.* 1987.
34 P.H.M. Kersten. *Infinitesimal symmetries: a computational approach.* 1987.
35 M.L. Eaton. *Lectures on topics in probability inequalities.* 1987.
36 A.H.P. van der Burgh, R.M.M. Mattheij (editors). *Proceedings of the first international conference on industrial and applied mathematics (ICIAM 87).* 1987.
37 L. Stougie. *Design and analysis of algorithms for stochastic integer programming.* 1987.
38 J.B.G. Frenk. *On Banach algebras, renewal measures and regenerative processes.* 1987.
39 H.J.M. Peters, O.J. Vrieze (eds.). *Surveys in game theory and related topics.* 1987.
40 J.L. Geluk, L. de Haan. *Regular variation, extensions and Tauberian theorems.* 1987.
41 Sape J. Mullender (ed.). *The Amoeba distributed operating system: Selected papers 1984-1987.* 1987.
42 P.R.J. Asveld, A. Nijholt (eds.). *Essays on concepts, formalisms, and tools.* 1987.
43 H.L. Bodlaender. *Distributed computing: structure and complexity.* 1987.
44 A.W. van der Vaart. *Statistical estimation in large parameter spaces.* 1988.
45 S.A. van de Geer. *Regression analysis and empirical processes.* 1988.
46 S.P. Spekreijse. *Multigrid solution of the steady Euler equations.* 1988.
47 J.B. Dijkstra. *Analysis of means in some non-standard situations.* 1988.
48 F.C. Drost. *Asymptotics for generalized chi-square goodness-of-fit tests.* 1988.
49 F.W. Wubs. *Numerical solution of the shallow-water equations.* 1988.
50 F. de Kerf. *Asymptotic analysis of a class of perturbed Korteweg-de Vries initial value problems.* 1988.
51 P.J.M. van Laarhoven. *Theoretical and computational aspects of simulated annealing.* 1988.
52 P.M. van Loon. *Continuous decoupling transformations for linear boundary value problems.* 1988.
53 K.C.P. Machielsen. *Numerical solution of optimal control problems with state constraints by sequential quadratic programming in function space.* 1988.
54 L.C.R.J. Willenborg. *Computational aspects of survey data processing.* 1988.
55 G.J. van der Steen. *A program generator for recognition, parsing and transduction with syntactic patterns.* 1988.
56 J.C. Ebergen. *Translating programs into delay-insensitive circuits.* 1989.
57 S.M. Verduyn Lunel. *Exponential type calculus for linear delay equations.* 1989.
58 M.C.M. de Gunst. *A random model for plant cell population growth.* 1989.

59 D. van Dulst. *Characterizations of Banach spaces not containing l^1*. 1989.

60 H.E. de Swart. *Vacillation and predictability properties of low-order atmospheric spectral models*. 1989.

61 P. de Jong. *Central limit theorems for generalized multilinear forms*. 1989.

62 V.J. de Jong. *A specification system for statistical software*. 1989.

63 B. Hanzon. *Identifiability, recursive identification and spaces of linear dynamical systems, part I*. 1989.

64 B. Hanzon. *Identifiability, recursive identification and spaces of linear dynamical systems, part II*. 1989.

65 B.M.M. de Weger. *Algorithms for diophantine equations*. 1989.

66 A. Jung. *Cartesian closed categories of domains*. 1989.

67 J.W. Polderman. *Adaptive control & identification: Conflict or conflux?*. 1989.

68 H.J. Woerdeman. *Matrix and operator extensions*. 1989.

69 B.G. Hansen. *Monotonicity properties of infinitely divisible distributions*. 1989.

70 J.K. Lenstra, H.C. Tijms, A. Volgenant (eds.). *Twenty-five years of operations research in the Netherlands: Papers dedicated to Gijs de Leve*. 1990.

71 P.J.C. Spreij. *Counting process systems. Identification and stochastic realization*. 1990.

72 J.F. Kaashoek. *Modeling one dimensional pattern formation by anti-diffusion*. 1990.

73 A.M.H. Gerards. *Graphs and polyhedra. Binary spaces and cutting planes*. 1990.

74 B. Koren. *Multigrid and defect correction for the steady Navier-Stokes equations. Application to aerodynamics*. 1991.

75 M.W.P. Savelsbergh. *Computer aided routing*. 1992.

76 O.E. Flippo. *Stability, duality and decomposition in general mathematical programming*. 1991.

77 A.J. van Es. *Aspects of nonparametric density estimation*. 1991.

78 G.A.P. Kindervater. *Exercises in parallel combinatorial computing*. 1992.

79 J.J. Lodder. *Towards a symmetrical theory of generalized functions*. 1991.

80 S.A. Smulders. *Control of freeway traffic flow*. 1996.

81 P.H.M. America, J.J.M.M. Rutten. *A parallel object-oriented language: design and semantic foundations*. 1992.

82 F. Thuijsman. *Optimality and equilibria in stochastic games*. 1992.

83 R.J. Kooman. *Convergence properties of recurrence sequences*. 1992.

84 A.M. Cohen (ed.). *Computational aspects of Lie group representations and related topics. Proceedings of the 1990 Computational Algebra Seminar at CWI, Amsterdam*. 1991.

85 V. de Valk. *One-dependent processes*. 1994.

86 J.A. Baars, J.A.M. de Groot. *On topological and linear equivalence of certain function spaces*. 1992.

87 A.F. Monna. *The way of mathematics and mathematicians*. 1992.

88 E.D. de Goede. *Numerical methods for the three-dimensional shallow water equations*. 1993.

89 M. Zwaan. *Moment problems in Hilbert space with applications to magnetic resonance imaging*. 1993.

90 C. Vuik. *The solution of a one-dimensional Stefan problem*. 1993.

91 E.R. Verheul. *Multimedians in metric and normed spaces*. 1993.

92 J.L.M. Maubach. *Iterative methods for non-linear partial differential equations*. 1994.

93 A.W. Ambergen. *Statistical uncertainties in posterior probabilities*. 1993.

94 P.A. Zegeling. *Moving-grid methods for time-dependent partial differential equations*. 1993.

95 M.J.C. van Pul. *Statistical analysis of software reliability models*. 1993.

96 J.K. Scholma. *A Lie algebraic study of some integrable systems associated with root systems*. 1993.

97 J.L. van den Berg. *Sojourn times in feedback and processor sharing queues*. 1993.

98 A.J. Koning. *Stochastic integrals and goodness-of-fit tests*. 1993.

99 B.P. Sommeijer. *Parallelism in the numerical integration of initial value problems*. 1993.

100 J. Molenaar. *Multigrid methods for semiconductor device simulation*. 1993.

101 H.J.C. Huijberts. *Dynamic feedback in nonlinear synthesis problems*. 1994.

102 J.A.M. van der Weide. *Stochastic processes and point processes of excursions*. 1994.

103 P.W. Hemker, P. Wesseling (eds.). *Contributions to multigrid*. 1994.

104 I.J.B.F. Adan. *A compensation approach for queueing problems*. 1994.

105 O.J. Boxma, G.M. Koole (eds.). *Performance evaluation of parallel and distributed systems - solution methods. Part 1*. 1994.

106 O.J. Boxma, G.M. Koole (eds.). *Performance evaluation of parallel and distributed systems - solution methods. Part 2*. 1994.

107 R.A. Trompert. *Local uniform grid refinement for time-dependent partial differential equations*. 1995.

108 M.N.M. van Lieshout. *Stochastic geometry models in image analysis and spatial statistics*. 1995.

109 R.J. van Glabbeek. *Comparative concurrency semantics and refinement of actions*. 1996.

110 W. Vervaat, H. Holwerda (ed.). *Probability and lattices*. 1997.

111 I. Helsloot. *Covariant formal group theory and some applications*. 1995.

112 R.N. Bol. *Loop checking in logic programming*. 1995.

113 G.J.M. Koole. *Stochastic scheduling and dynamic programming*. 1995.

114 M.J. van der Laan. *Efficient and inefficient estimation in semiparametric models*. 1995.

115 S.C. Borst. *Polling models*. 1996.

116 G.D. Otten. *Statistical test limits in quality control*. 1996.

117 K.G. Langendoen. *Graph reduction on shared-memory multiprocessors*. 1996.

118 W.C.A. Maas. *Nonlinear $\mathcal{H}_\infty$ control: the singular case*. 1996.

119 A. Di Bucchianico. *Probabilistic and analytical aspects of the umbral calculus*. 1997.

120 M. van Loon. *Numerical methods in smog prediction*. 1997.

121 B.J. Wijers. *Nonparametric estimation for a windowed line-segment process*. 1997.

122 W.K. Klein Haneveld, O.J. Vrieze, L.C.M. Kallenberg (editors). *Ten years LNMB – Ph.D. research and graduate courses of the Dutch Network of Operations Research*. 1997.

123 R.W. van der Hofstad. *One-dimensional random polymers*. 1998.

124 W.J.H. Stortelder. *Parameter estimation in nonlinear dynamical systems*. 1998.

125 M.H. Wegkamp. *Entropy methods in statistical estimation*. 1998.

126 K. Aardal, J.K. Lenstra, F. Maffioli, D.B. Shmoys (eds.) *Selected publications of Eugene L. Lawler*. 1999.

127 E. Belitser. *Minimax estimation in regression and random censorship models*. 2000.

128 Y. Nishiyama. *Entropy methods for martingales*. 2000.

129 J.A. van Hamel. *Algebraic cycles and topology of real algebraic varieties*. 2000.

130 P.J. Oonincx. *Mathematical signal analysis: wavelets, Wigner distribution and a seismic application*. 2000.

131 M. Ruzhansky. *Regularity theory of Fourier integral operators with complex phases and singularities of affine fibrations*. 2001.

132 J.V. Stokman. *Multivariable orthogonal polynomials and quantum Grassmannians*. 2001.

133 N.R. Bruin. *Chabauty methods and covering techniques applied to generalised Fermat equations*. 2002.

134 E.H. van Brummelen. *Numerical methods for steady viscous free-surface flows*. 2003.

MATHEMATICAL CENTRE TRACTS

1 T. van der Walt. *Fixed and almost fixed points.* 1963.

2 A.R. Bloemena. *Sampling from a graph.* 1964.

3 G. de Leve. *Generalized Markovian decision processes, part I: model and method.* 1964.

4 G. de Leve. *Generalized Markovian decision processes, part II: probabilistic background.* 1964.

5 G. de Leve, H.C. Tijms, P.J. Weeda. *Generalized Markovian decision processes, applications.* 1970.

6 M.A. Maurice. *Compact ordered spaces.* 1964.

7 W.R. van Zwet. *Convex transformations of random variables.* 1964.

8 J.A. Zonneveld. *Automatic numerical integration.* 1964.

9 P.C. Baayen. *Universal morphisms.* 1964.

10 E.M. de Jager. *Applications of distributions in mathematical physics.* 1964.

11 A.B. Paalman-de Miranda. *Topological semigroups.* 1964.

12 J.A.Th.M. van Berckel, H. Brandt Corstius, R.J. Mokken, A. van Wijngaarden. *Formal properties of newspaper Dutch.* 1965.

13 H.A. Lauwerier. *Asymptotic expansions.* 1966, out of print: replaced by MCT 54.

14 H.A. Lauwerier. *Calculus of variations in mathematical physics.* 1966.

15 R. Doornbos. *Slippage tests.* 1966.

16 J.W. de Bakker. *Formal definition of programming languages with an application to the definition of ALGOL 60.* 1967.

17 R.P. van de Riet. *Formula manipulation in ALGOL 60, part 1.* 1968.

18 R.P. van de Riet. *Formula manipulation in ALGOL 60, part 2.* 1968.

19 J. van der Slot. *Some properties related to compactness.* 1968.

20 P.J. van der Houwen. *Finite difference methods for solving partial differential equations.* 1968.

21 E. Wattel. *The compactness operator in set theory and topology.* 1968.

22 T.J. Dekker. *ALGOL 60 procedures in numerical algebra, part 1.* 1968.

23 T.J. Dekker, W. Hoffmann. *ALGOL 60 procedures in numerical algebra, part 2.* 1968.

24 J.W. de Bakker. *Recursive procedures.* 1971.

25 E.R. Paërl. *Representations of the Lorentz group and projective geometry.* 1969.

26 European Meeting 1968. *Selected statistical papers, part I.* 1968.

27 European Meeting 1968. *Selected statistical papers, part II.* 1968.

28 J. Oosterhoff. *Combination of one-sided statistical tests.* 1969.

29 J. Verhoeff. *Error detecting decimal codes.* 1969.

30 H. Brandt Corstius. *Exercises in computational linguistics.* 1970.

31 W. Molenaar. *Approximations to the Poisson, binomial and hypergeometric distribution functions.* 1970.

32 L. de Haan. *On regular variation and its application to the weak convergence of sample extremes.* 1970.

33 F.W. Steutel. *Preservations of infinite divisibility under mixing and related topics.* 1970.

34 I. Juhász, A. Verbeek, N.S. Kroonenberg. *Cardinal functions in topology.* 1971.

35 M.H. van Emden. *An analysis of complexity.* 1971.

36 J. Grasman. *On the birth of boundary layers.* 1971.

37 J.W. de Bakker, G.A. Blaauw, A.J.W. Duijvestijn, E.W. Dijkstra, P.J. van der Houwen, G.A.M. Kamsteeg-Kemper, F.E.J. Kruseman Aretz, W.L. van der Poel, J.P. Schaap-Kruseman, M.V. Wilkes, G. Zoutendijk. *MC-25 Informatica Symposium.* 1971.

38 W.A. Verloren van Themaat. *Automatic analysis of Dutch compound words.* 1972.

39 H. Bavinck. *Jacobi series and approximation.* 1972.

40 H.C. Tijms. *Analysis of (s,S) inventory models.* 1972.

41 A. Verbeek. *Superextensions of topological spaces.* 1972.

42 W. Vervaat. *Success epochs in Bernoulli trials (with applications in number theory).* 1972.

43 F.H. Ruymgaart. *Asymptotic theory of rank tests for independence.* 1973.

44 H. Bart. *Meromorphic operator valued functions.* 1973.

45 A.A. Balkema. *Monotone transformations and limit laws.* 1973.

46 R.P. van de Riet. *ABC ALGOL, a portable language for formula manipulation systems, part 1: the language.* 1973.

47 R.P. van de Riet. *ABC ALGOL, a portable language for formula manipulation systems, part 2: the compiler.* 1973.

48 F.E.J. Kruseman Aretz, P.J.W. ten Hagen, H.L. Oudshoorn. *An ALGOL 60 compiler in ALGOL 60, text of the MC-compiler for the EL-X8.* 1973.

49 H. Kok. *Connected orderable spaces.* 1974.

50 A. van Wijngaarden, B.J. Mailloux, J.E.L. Peck, C.H.A. Koster, M. Sintzoff, C.H. Lindsey, L.G.L.T. Meertens, R.G. Fisker (eds.). *Revised report on the algorithmic language ALGOL 68.* 1976.

51 A. Hordijk. *Dynamic programming and Markov potential theory.* 1974.

52 P.C. Baayen (ed.). *Topological structures.* 1974.

53 M.J. Faber. *Metrizability in generalized ordered spaces.* 1974.

54 H.A. Lauwerier. *Asymptotic analysis, part 1.* 1974.

55 M. Hall, Jr., J.H. van Lint (eds.). *Combinatorics, part 1: theory of designs, finite geometry and coding theory.* 1974.

56 M. Hall, Jr., J.H. van Lint (eds.). *Combinatorics, part 2: graph theory, foundations, partitions and combinatorial geometry.* 1974.

57 M. Hall, Jr., J.H. van Lint (eds.). *Combinatorics, part 3: combinatorial group theory.* 1974.

58 W. Albers. *Asymptotic expansions and the deficiency concept in statistics.* 1975.

59 J.L. Mijnheer. *Sample path properties of stable processes.* 1975.

60 F. Göbel. *Queueing models involving buffers.* 1975.

63 J.W. de Bakker (ed.). *Foundations of computer science.* 1975.

64 W.J. de Schipper. *Symmetric closed categories.* 1975.

65 J. de Vries. *Topological transformation groups, 1: a categorical approach.* 1975.

66 H.G.J. Pijls. *Logically convex algebras in spectral theory and eigenfunction expansions.* 1976.

68 P.P.N. de Groen. *Singularly perturbed differential operators of second order.* 1976.

69 J.K. Lenstra. *Sequencing by enumerative methods.* 1977.

70 W.P. de Roever, Jr. *Recursive program schemes: semantics and proof theory.* 1976.

71 J.A.E.E. van Nunen. *Contracting Markov decision processes.* 1976.

72 J.K.M. Jansen. *Simple periodic and non-periodic Lamé functions and their applications in the theory of conical waveguides.* 1977.

73 D.M.R. Leivant. *Absoluteness of intuitionistic logic.* 1979.

74 H.J.J. te Riele. *A theoretical and computational study of generalized aliquot sequences.* 1976.

75 A.E. Brouwer. *Treelike spaces and related connected topological spaces.* 1977.

76 M. Rem. *Associons and the closure statements.* 1976.

77 W.C.M. Kallenberg. *Asymptotic optimality of likelihood ratio tests in exponential families.* 1978.

78 E. de Jonge, A.C.M. van Rooij. *Introduction to Riesz spaces.* 1977.

79 M.C.A. van Zuijlen. *Empirical distributions and rank statistics.* 1977.

80 P.W. Hemker. *A numerical study of stiff two-point boundary problems.* 1977.

81 K.R. Apt, J.W. de Bakker (eds.). *Foundations of computer science II, part 1.* 1976.

82 K.R. Apt, J.W. de Bakker (eds.). *Foundations of computer science II, part 2.* 1976.

83 L.S. van Benthem Jutting. *Checking Landau's "Grundlagen" in the AUTOMATH system.* 1979.

84 H.L.L. Busard. *The translation of the elements of Euclid from the Arabic into Latin by Hermann of Carinthia (?), books vii-xii.* 1977.

85 J. van Mill. *Supercompactness and Wallmann spaces.* 1977.

86 S.G. van der Meulen, M. Veldhorst. *Torrix I, a programming system for operations on vectors and matrices over arbitrary fields and of variable size.* 1978.

88 A. Schrijver. *Matroids and linking systems.* 1977.

89 J.W. de Roever. *Complex Fourier transformation and analytic functionals with unbounded carriers.* 1978.

90 L.P.J. Groenewegen. *Characterization of optimal strategies in dynamic games.* 1981.

91 J.M. Geysel. *Transcendence in fields of positive characteristic.* 1979.

92 P.J. Weeda. *Finite generalized Markov programming.* 1979.

93 H.C. Tijms, J. Wessels (eds.). *Markov decision theory.* 1977.

94 A. Bijlsma. *Simultaneous approximations in transcendental number theory.* 1978.

95 K.M. van Hee. *Bayesian control of Markov chains.* 1978.

96 P.M.B. Vitányi. *Lindenmayer systems: structure, languages, and growth functions.* 1980.

97 A. Federgruen. *Markovian control problems; functional equations and algorithms.* 1984.

98 R. Geel. *Singular perturbations of hyperbolic type.* 1978.

99 J.K. Lenstra, A.H.G. Rinnooy Kan, P. van Emde Boas (eds.). *Interfaces between computer science and operations research.* 1978.

100 P.C. Baayen, D. van Dulst, J. Oosterhoff (eds.). *Proceedings bicentennial congress of the Wiskundig Genootschap, part 1.* 1979.

101 P.C. Baayen, D. van Dulst, J. Oosterhoff (eds.). *Proceedings bicentennial congress of the Wiskundig Genootschap, part 2.* 1979.

102 D. van Dulst. *Reflexive and superreflexive Banach spaces.* 1978.

103 K. van Harn. *Classifying infinitely divisible distributions by functional equations.* 1978.

104 J.M. van Wouwe. *GO-spaces and generalizations of metrizability.* 1979.

105 R. Helmers. *Edgeworth expansions for linear combinations of order statistics.* 1982.

106 A. Schrijver (ed.). *Packing and covering in combinatorics.* 1979.

107 C. den Heijer. *The numerical solution of nonlinear operator equations by imbedding methods.* 1979.

108 J.W. de Bakker, J. van Leeuwen (eds.). *Foundations of computer science III, part 1.* 1979.

109 J.W. de Bakker, J. van Leeuwen (eds.). *Foundations of computer science III, part 2.* 1979.

110 J.C. van Vliet. *ALGOL 68 transput, part I: historical review and discussion of the implementation model.* 1979.

111 J.C. van Vliet. *ALGOL 68 transput, part II: an implementation model.* 1979.

112 H.C.P. Berbee. *Random walks with stationary increments and renewai theory.* 1979.

113 T.A.B. Snijders. *Asymptotic optimality theory for testing problems with restricted alternatives.* 1979.

114 A.J.E.M. Janssen. *Application of the Wigner distribution to harmonic analysis of generalized stochastic processes.* 1979.

115 P.C. Baayen, J. van Mill (eds.). *Topological structures II, part 1.* 1979.

116 P.C. Baayen, J. van Mill (eds.). *Topological structures II, part 2.* 1979.

117 P.J.M. Kallenberg. *Branching processes with continuous state space.* 1979.

118 P. Groeneboom. *Large deviations and asymptotic efficiencies.* 1980.

119 F.J. Peters. *Sparse matrices and substructures, with a novel implementation of finite element algorithms.* 1980.

120 W.P.M. de Ruyter. *On the asymptotic analysis of large-scale ocean circulation.* 1980.

121 W.H. Haemers. *Eigenvalue techniques in design and graph theory.* 1980.

122 J.C.P. Bus. *Numerical solution of systems of nonlinear equations.* 1980.

123 I. Yuhász. *Cardinal functions in topology - ten years later.* 1980.

124 R.D. Gill. *Censoring and stochastic integrals.* 1980.

125 R. Eising. *2-D systems, an algebraic approach.* 1980.

126 G. van der Hoek. *Reduction methods in nonlinear programming.* 1980.

127 J.W. Klop. *Combinatory reduction systems.* 1980.

128 A.J.J. Talman. *Variable dimension fixed point algorithms and triangulations.* 1980.

129 G. van der Laan. *Simplicial fixed point algorithms.* 1980.

130 P.J.W. ten Hagen, T. Hagen, P. Klint, H. Noot, H.J. Sint, A.H. Veen. *ILP: intermediate language for pictures.* 1980.

131 R.J.R. Back. *Correctness preserving program refinements: proof theory and applications.* 1980.

132 H.M. Mulder. *The interval function of a graph.* 1980.

133 C.A.J. Klaassen. *Statistical performance of location estimators.* 1981.

134 J.C. van Vliet, H. Wupper (eds.). *Proceedings international conference on ALGOL 68.* 1981.

135 J.A.G. Groenendijk, T.M.V. Janssen, M.J.B. Stokhof (eds.). *Formal methods in the study of language, part I.* 1981.

136 J.A.G. Groenendijk, T.M.V. Janssen, M.J.B. Stokhof (eds.). *Formal methods in the study of language, part II.* 1981.

137 J. Telgen. *Redundancy and linear programs.* 1981.

138 H.A. Lauwerier. *Mathematical models of epidemics.* 1981.

139 J. van der Wal. *Stochastic dynamic programming, successive approximations and nearly optimal strategies for Markov decision processes and Markov games.* 1981.

140 J.H. van Geldrop. *A mathematical theory of pure exchange economies without the no-critical-point hypothesis.* 1981.

141 G.E. Welters. *Abel-Jacobi isogenies for certain types of Fano threefolds.* 1981.

142 H.R. Bennett, D.J. Lutzer (eds.). *Topology and order structures, part 1.* 1981.

143 J.M. Schumacher. *Dynamic feedback in finite- and infinite-dimensional linear systems.* 1981.

144 P. Eijgenraam. *The solution of initial value problems using interval arithmetic; formulation and analysis of an algorithm.* 1981.

145 A.J. Brentjes. *Multi-dimensional continued fraction algorithms.* 1981.

146 C.V.M. van der Mee. *Semigroup and factorization methods in transport theory.* 1981.

147 H.H. Tigelaar. *Identification and informative sample size.* 1982.

148 L.C.M. Kallenberg. *Linear programming and finite Markovian control problems.* 1983.

149 C.B. Huijsmans, M.A. Kaashoek, W.A.J. Luxemburg, W.K. Vietsch (eds.). *From A to Z, proceedings of a symposium in honour of A.C. Zaanen.* 1982.

150 M. Veldhorst. *An analysis of sparse matrix storage schemes.* 1982.

151 R.J.M.M. Does. *Higher order asymptotics for simple linear rank statistics.* 1982.

152 G.F. van der Hoeven. *Projections of lawless sequencies.* 1982.

153 J.P.C. Blanc. *Application of the theory of boundary value problems in the analysis of a queueing model with paired services.* 1982.

154 H.W. Lenstra, Jr., R. Tijdeman (eds.). *Computational methods in number theory, part I.* 1982.

155 H.W. Lenstra, Jr., R. Tijdeman (eds.). *Computational methods in number theory, part II.* 1982.

156 P.M.G. Apers. *Query processing and data allocation in distributed database systems.* 1983.

157 H.A.W.M. Kneppers. *The covariant classification of two-dimensional smooth commutative formal groups over an algebraically closed field of positive characteristic.* 1983.

158 J.W. de Bakker, J. van Leeuwen (eds.). *Foundations of computer science IV, distributed systems, part 1.* 1983.

159 J.W. de Bakker, J. van Leeuwen (eds.). *Foundations of computer science IV, distributed systems, part 2.* 1983.

160 A. Rezus. *Abstract AUTOMATH.* 1983.

161 G.F. Helminck. *Eisenstein series on the metaplectic group, an algebraic approach.* 1983.

162 J.J. Dik. *Tests for preference.* 1983.

163 H. Schippers. *Multiple grid methods for equations of the second kind with applications in fluid mechanics.* 1983.

164 F.A. van der Duyn Schouten. *Markov decision processes with continuous time parameter.* 1983.

165 P.C.T. van der Hoeven. *On point processes.* 1983.

166 H.B.M. Jonkers. *Abstraction, specification and implementation techniques, with an application to garbage collection.* 1983.

167 W.H.M. Zijm. *Nonnegative matrices in dynamic programming.* 1983.

168 J.H. Evertse. *Upper bounds for the numbers of solutions of diophantine equations.* 1983.

169 H.R. Bennett, D.J. Lutzer (eds.). *Topology and order structures, part 2.* 1983.